ATTILA CSOMOS

Design, Synthesis and Analysis of Novel Fluorescent Probes for Two-Photon Zinc Imaging

Dr. Zoltán Mucsi, Femtonics Ltd.
Dr. Ervin Kovács, Femtonics Ltd.
Consulent:
Dr. Gábor Durkó, Department of Organic Chemistry

———— Eötvös Loránd University ————
——— Faculty of Natural Sciences ———
—— Budapest, 2020 ——

Published on December 5th 2020.

Table of Contents

Acknowledgements

I would like to thank for all the support and help for everyone, who have been supporting me during this research. First of all, I would like to express my deepest appreciation for all the support and professional help for my supervisors, Dr. Zoltán Mucsi and Dr. Ervin Kovács. Their help could never be overestimated.

I would also like to extend my deepest gratitude for the funding and encouragement of the company, that made this research possible, Femtonics Ltd. I would like to express my sincere thanks for the help in the everydays to my colleagues in the laboratory, Anna Fülöp, Bence Kontra, Szandra Szilágyi and Csilla Haveland. I cannot begin to express my gratitude to Dr. Petra Dunkel, assistant professor of Semmelweis University for the great professional advice, opportunity to use their equipment and not least, for a good friendship. I would also like to thank for László Forgách and Dr. Domokos Máthé for the help with fluorescent spectroscopy.

I would like to specially honour my parents, Csaba and Ibolya Csomos and my whole family, who have made this hard period of the pandemic easier for me despite being separated from me by country borders. The success of this research would not have been possible without their support.

I want to say thanks for all the help, patience, good words and love coming from my girlfriend and all my best friends.

Finally, I thank God for the strength and health making me able to carry this research project out.

List of Abbreviations

Abbreviation	Explanation
MRI	magnetic resonance imaging
2P	two-photon
CNS	central nervous system
HTS	high-throughput screening
GFP	green fluorescent protein
MT	metallothionein
AA	amino acid
GABA	γ-aminobutyric
NMDA	N-methyl-D-asparaginate
Aβ	amyloid-β
APP	amyloid precursor proteins
RdRp	RNA dependent RNA polymerase
ACE2	angiotensin-converting enzyme 2
Pl^{pro}	papain-like protease
LASER	Light Amplification by Stimulated Emission of Radiation
UV	ultraviolet
NADH	Nicotinamide adenine dinucleotide
EDTA	ethylenediaminetetraacetic acid
ICT	Internal charge transfer
FRET	Förster resonance energy transfer
PET	photoinduced electron transfer
TSQ	6-methoxy-(8-p-toluenesulfonamido)quinoline
DMF	N,N-Dimethylformamide
8-HQ	8-hydroxyquinoline
8-AQ	8-aminoquinoline
DPA	dipicolylamine
DFT	density functional theory
G16	Gaussian 16
RT	room temperature
LCMS	liquid chromatography - mass spectrometry
ESI	electrospray ionisation
DCM	dichloromethane
TLC	thin layer chromatography
HEPES	(4-(2-hydroxyethyl)-1-piperazineethanesulfonic acid)
DMSO	dimethyl sulfoxide
HOMO	highest occupied molecular orbital
LUMO	lowest unoccupied molecular orbital
FEF	fluorescent enhancement factor

1. Introduction

Metal ions are undoubtedly essential components of any living organism. In fact, the human body contains on average a surprisingly high amount, 1–2 kilograms of metal ions. It is common knowledge, that they have several roles ranging from building up the structure of bones, through carrying breathing gases in our bloodstream, to taking part in cellular signalling processes and building up proteins.[1]

Despite trace metal elements being present only in small quantities in living tissue, their importance should not be underestimated. Many trace metals are essential, playing vital roles in transport processes, participating in redox reactions of the energy metabolism or catalysing enzyme systems.[2]

My recent research work, which is presented in this essay, discusses issues related to the second most abundant trace metal in the human body, zinc (Zn^{2+}).[3] There is no doubt, that zinc is the most frequently studied metal of the *d*-block, which can be accounted for its importance in biology.[4] First of all, there are more, than 300 metalloenzymes fulfilling specific functions in living organisms containing Zn^{2+}, so called zinc enzymes. Furthermore, catalytic, structural and signalling functions of zinc are present in all parts of the human body from the immune system to the nervous system.[3,5] I believe that understanding such complex systems of the body is one of the greatest challenges of our days, which could lead us to finding cures and therapies for diseases such as viral infections like COVID-19 or Alzheimer's disease, *etc*. Effective monitoring and tracking the concentration of Zn^{2+} in biological systems could be the key to overcome this challenge.

Yet, this task may be harder, than it sounds. To gather sufficient information, one needs techniques with outstanding submicrometer resolution and the capability of highly sensitive, 3D, real time measurements. Currently optical microscopy seems to be the most suitable technique for these measurements, as no other methods (*e.g.* MRI) can fulfil the criteria mentioned above. The current research was carried out at a Hungarian R&D company, Femtonics LTD., which has been developing and manufacturing two-photon (2P) microscopes, while doing internationally acknowledged research in the fields of neuroscience and biology for a decade.

Although 2P microscopes are superior in many aspects for these measurements, they unfortunately inherit a significant drawback of optical methods: they are unable to "see" the

ions on their own, as zinc has a valence shell electron configuration of $3d^{10}\,4s^2$ making it spectroscopically and optically "silent".[6] Compounds of Zn^{2+} are colourless, thus, to monitor them with an optical microscope one needs to visualize their presence. This is usually carried out by fluorescent molecular sensors. These basically nonfluorescent molecules are able to bind metal ions of choice in coordinative complexes and upon this process they become fluorescent when irradiated with light.[7] The emitted fluorescent light can be detected by the microscopes, this way the metal ions of choice are visualized. Or vice versa, some sensors turn off upon binding.

Even though our biologists have been keen on imaging zinc for a while in order to study the central nervous system (CNS), the main motivation of our work has been recent studies showing, that Zn^{2+} plays important role in cellular processes involved in COVID-19 disease.[3,8,9] We seek the possibilities in 2P Zn^{2+} imaging to find a potent, fast and convenient method for revealing the mechanism of the COVID-19 disease, to monitor the tissue damaging effects or to provide a test assay for drug development. Such method could lead to important discoveries or could be used in high throuput screening (HTS) experiments of potential drug candidates against the virus, getting us closer to a medicine resolving the current global crisis. Finally, application is not limited to viruses, but they can be used generally for neuroscientific research (*e.g.* studying possibilities of vision restoration, or curing Alzheimer's, *etc*.), or other scientific scopes.

From a chemical point of view, the goal is discover novel, efficient, 2P active fluorescent probes based on a completely new scaffold, in order to broaden the usable repertoire of fluorescent probes for scientists involved in 2P zinc imaging. The biological usability of a compound depends on many parameters, so offering a wider variety of probes differing radically in their scaffold could meet requirements of a larger scale of experiments.

This work presents the rational design of seven novel fluorescent probes for two-photon zinc imaging. Our concept is based on literature findings and own intuition, supported by computational results. I also demonstrate the synthesis of the probes on a 10 to ~300 mg scale and the analytical proof of their concept. Our sensor molecules were expected to improve the properties of currently known probes by combining the recent knowledge found in the literature with new discoveries of my colleagues.

The sensor molecules prepared are composed on a fine-tuned fluorescent scaffold discovered by the colleagues of our laboratory mimicking Green Fluorescent Protein (GFP)[10] and a Zn^{2+}

specific ligand. To my best knowledge, no fluorescent probes were made prior to this work involving the chosen scaffold.

2. Summary of the Literature

Before starting the research project, I have done a comprehensive study of the scientific literature on the topic. Firstly, I assessed the importance of Zn^{2+} in the human body focusing on the primary roles of Zn^{2+}, and I estimated the expected Zn^{2+} concentration in the relevant regions of interest. The research focuses on biological systems relevant for imaging, targeting mainly neuroscience. I have also investigated the relationship between Zn^{2+} and COVID-19 infections. In the current situation, finding links to COVID-19 should be considered a highly relevant aspect of any research, in order to stop the pandemic as soon as possible. Then I discuss the possibilities, advantages and disadvantages in 2P metal-ion imaging alongside with the principles behind it. Finally, an insight will be given into the field of the currently used and known sensor compounds and I will also focus on the background of new possibilities to create Zn^{2+} fluorescent probes.

2.1. Zn^{2+} in the human body: roles and abundance

2.1.1. General considerations, abundance and concentration

As referred in the introduction, zinc is considered a trace element. Nevertheless, it was proven in 1961 to be an essential element in living organisms by taking part in a surprizing number of processes.[11] In general, zinc is a redox-inert element in the body always being present in +2 oxidation state, mostly in colourless coordination complexes with coordination numbers of 2, 4 and 6.[6] According to the literature, the zinc content of a human body is *cca*. 2–3 g, while the concentration values in different parts of the body are highly varied.

Since the concentration of the analyte is one of the most important factors to consider, when designing sensor molecules, it is important to find out what concentration ranges can be expected during the application. However, measurement of the concentration of Zn^{2+} is problematic, since most of the ions are present bound to proteins and hidden in compartments of cells.[5] This is the reason, that even conservative estimates suggest, that more than 17-25% of the world population is zinc-deficient to some extent, altering their vital functions.[5,12,13]

Although different Zn^{2+} level values are reported in the human blood plasma, a concentration range of 10-25 μM can be accepted.[6,12,13] „Free", unbound cellular Zn^{2+} levels are also variable

and multiple values were reported. The reported concentrations range from tens of picomoles per litre to nanomolar and micromolar concentrations.[5,6] Higher concentrations covering mM ranges are localized in different parts of the body, such as the breasts, prostate, pancreas, the CNS and the brain.[6] A recent review published in 2019 by Johnson *et. al.* reports, that concentration in the presynaptic bouton of neurons can be as high as 300 mM.[6] This was a surprisingly high value. Nonetheless, reading the sources cited by the author revealed a value of only 300 μM.[14,15] These typos can be hazardous in the scientific literature, as an incorrect value may spread in publications citing each other leading to misconceptions. The amount of free ions is very important from the point of view of sensor molecules, as classically ionophores mainly bind to free, unbound ions. Consequently, these species are the ones, that can be indicated by fluorescent probes. However, the situation in case of Zn^{2+} is more complicated. While Zn^{2+} is rarely present in free form, the protein bound Zn^{2+} can be tightly bound (log K_d > 11), moderately (log K_d = 7-9) and loosely bound (log K_d < 7).[6] Since the binding of the ions follows an equilibrium (see *Chapter 2.2.2.1.*, *Eq. 8.*), an ionophore probe could be able to shift the equilibrium and release bound ions from proteins only to connect to them.[16] Moreover, if a protein does not bind to all the coordinative sites of Zn^{2+} and the ion is close to the surface of the complex, chelator fluorescent probes are often able to bind to the coordinative sites left free, this way turning on. Zn^{2+} in its free form is bound to water in $Zn(H_2O)_6^{2+}$ hexaaqua complexes, but exchanging water is not a problem for an ionophore. Finally, usually free Zn^{2+} is found in vesicles and compartments of cells, following a complex distribution. On top of vesicles, a special group of proteins are responsible for storing Zn^{2+}. These proteins are called metallothioneins (MTs). MTs are made up of 60-68 amino acids (AAs), among which 20-21 are cysteines (C). The sulphur atom of MTs are responsible for binding Zn^{2+}. It was shown that a maximum of 7 ions may be bound to a protein. MTs are redox-active, and upon oxidation, they can partially lose their ionophore character, consequently liberating Zn^{2+} as part of a modulation process of Zn^{2+}. MTs not only modulate cellular Zn^{2+} by redox mechanism, but their gene expression also helps in the modulation. The distribution of Zn^{2+} in cells is visualized on F*ig. 1.*[16]

All of this leads me to the conclusion, that fluorescent sensors for Zn^{2+} can work in concentrations ranging from nM to mM, depending on the type of usage. In addition, we must admit, that the dissociation constant (K_d) of a probe is the best parameter to quantify its usability based on its affinity for the analyte. In real life applications, however, a lot more parameters are important, that define the applicability of a probe such as its lipophilicity, and

ability to distribute into the regions of interest in the cells. Altogether, I concluded, that the complexity of Zn^{2+} distribution requires a wide range of different probes for different purposes and expanding the available set of fluorescent probes with completely new scaffolds could help broadening the possible investigations through microscopy, which could lead to answering new scientific questions.
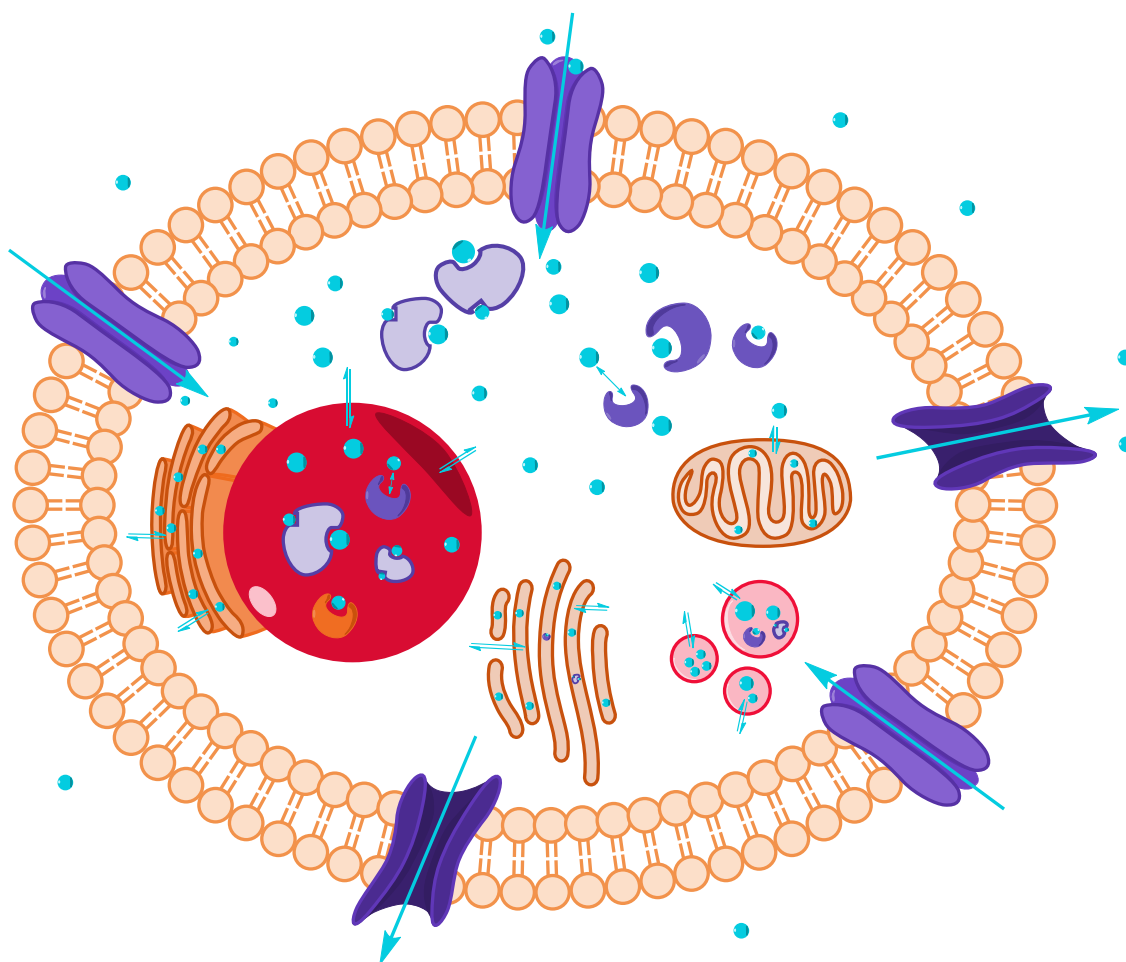
Figure 1. The distribution of Zn^{2+} in cellular medium. Blue dots represent Zn^{2+}, the red sphere represents the nucleus, pink circles are vesicles, while the orange items inside the cell represent organelles such as the ER. The purple tubes penetrating the cell wall represent ion channels. Arrows indicate, that ions can move in one, or both directions.

2.1.2. Role in biological systems

A great review published in 2013 by professor Wolfgang Maret gives a comprehensive picture about the importance of this element in biology.[5] I would like to highlight the idea of the author, that a more detailed understanding of the roles of zinc „became possible only with the development of new tools, in this case the advent of chelating agents that fluoresce when binding zinc ions and that allow measurement of zinc ions in cells with a sensitivity exceeding that of most other analytical techniques."[5]

Most importantly, zinc has been proven to take part in building up more, than 3000 human proteins.[3,5,6,17,18] Small protein domains formed mainly of cysteine (C) and histidine (H) in a few known arrangements called zinc fingers are able to bind one or more Zn^{2+} ions.[5] Binding Zn^{2+} ions mostly have a role of stabilizing the quaternary structure of the proteins, creating characteristic motifs. However, it was shown, that Zn^{2+} ions in proteins can have enzymatic, catalytic or inhibitory functions as well. To perceive the importance of Zn^{2+} ions in this regard, let us consider the prediction, that at least 10% of the human genome encodes zinc proteins.[5] These proteins fulfil different functions, being transcription factors, signalling proteins, hydrolases, *etc*.[5]

Anyhow, imaging proteins with zinc content does not carry any information. On the other hand, Zn^{2+} ions were also proved to act as second messengers in multiple cellular processes.[5] Zinc being involved in the function of so many proteins, it is easy to presume, that it needs to have roles in the intra- and intercellular communication. Tens of transporters for Zn^{2+} were identified, contrary to similar metals such as Fe^{3+}, which only have a few transporters, suggesting, that zinc homeostasis is involved in a complex signalling system.[17] Still, the specificity of these transporters is not always determined, while the scientific community have not reached to a consensus about the roles of Zn^{2+} in signalling. It is clear, that this fact further brings out the importance of zinc imaging and the need for novel fluorescent scaffolds for Zn^{2+} imaging.

In general, Zn^{2+} and its deficiency was connected to multiple diseases. It was shown, that zinc has anti- and proinflammatory properties at the same time,[3,9] anti-viral properties[3] and plays role in general in immunity, even though the mechanism of these effects is debated in the scientific milieu.[3] Furthermore, many signs show, that Zn^{2+} plays significant role in COVID-19, which I will discuss in the following chapters.[3,8,9,12] Besides this, originating from its role in signalling, zinc is an important element of neurological diseases, such as Alzheimer's disease, neuronal injury and amyotrophic lateral sclerosis.[3,6,8,9,12,17,19,20] The link between Zn^{2+} and the mentioned diseases also indicate the importance of our field of study.

2.1.2.1. The role of Zn^{2+} in the nervous system

Lately, zinc has been receiving special attention in the neuroscience community. This is one of the main reasons, we have started this research project. Zinc is omnipresent and mobile in the nervous system with evidence suggesting, that its effects in the CNS and the diversity of its signals in the brain may be comparable to those of Ca^{2+}.[17] Cognitive functions, like learning

and memory have been associated with the fact, that Zn^{2+} is actually not a trace element in the brain. Some parts of the brain, for example, the hippocampus, which is responsible for vision, contains Zn^{2+} in mM concentrations. In the grey matter, concentrations of Zn^{2+} are also on the level of 0.1-0.5 mM, which are comparable to the abundance of Mg^{2+}, one of the most prolific ions in cells. Neurons contain the highest concentration of Zn^{2+} in the human body, meaning, that the concentration of Zn^{2+} is 100-fold compared to neurotransmitters and can reach 10000-times larger concentrations, than neuropeptides.[17] Glutamatergic neurons can contain millimolar concentrations of labile Zn^{2+} in their vesicles, fascinating many neuroscientists.[17] It is widely accepted, that Zn^{2+} modulates synaptic transmission and the overall excitability of the brain trough Glutamate, *N*-methyl-*D*-asparaginate (NMDA) and γ-aminobutyric acid (GABA) neurotransmitters.[19]

In Alzheimer's disease, one of the most important pathological markers is the accumulation and deposition of amyloid-β (Aβ) peptides. Zn^{2+} has an important role in forming Aβ plaques too. With aging, the Cu^{2+} and Fe^{3+} levels in the brain increase, which promotes their binding to proteins. These metalloproteins easily get oxidized and get pushed out into synapses, where they can bind to Zn^{2+} due to its extraordinarily high concentration, consequently forming insoluble plaques. Another important interaction is present between Zn^{2+} and amyloid precursor proteins (APPs), which is suspected to also promote plaque formation. However, the complex mechanism is still not completely understood and there are more suspected other processes involving zinc.[17,19] Hopefully, scientists soon will be able to investigate these questions more in-depth, which would lead to fighting this disease.

2.1.2.2. Relations between Zn^{2+} and the novel coronavirus COVID-19

I feel, that in the times of the coronavirus-pandemic, every link and relation, that could lead to progress in resolving the global crisis is of high importance. There have been many news, rumours and tips, that taking zinc diet supplements help avoiding a serious COVID-19 disease. I went on to study the literature too see, whether there is any cellular biological process related to the novel coronavirus involving Zn^{2+}. It turns out, that there are a few reported recently in the literature.

As mentioned before, Zn^{2+} has a role in immunity in general, and it was also suggested to limit the cytokine storm happening[21] in severe COVID-19 patients due to its anti-inflammatory properties.[3,5,9,21] Higher ratio of zinc deficiency in elderly people was also connected to the fact, that the death ratio of the disease increases significantly with age. Taking Zn^{2+} combined

with a moderately strong zinc-ionophore was shown to increase cellular concentrations of the metal. The ionophore binds to the Zn^{2+} in the extracellular region, where the Zn^{+2} concentration is larger, then by crossing the cell membrane, it transports the ions into cells, where the complex dissociates due to the low local Zn^{2+} concentration.[3,8,9,12,21] It was shown before, that in the case of SARS-CoV-1, the RNA dependent RNA polymerase (RdRp) of the virus was inhibited by Zn^{2+}. It was suggested, that the RdRp may be inhibited in the case of SARS-CoV-2 as well by Zn^{2+}, consequently, multiple drugs, with zinc-ionophore properties are currently being tested with and without supplementary zinc intake in clinical tests.[3,8,9,12,21] Just to mention the most important ones, this is one of the suspected mechanisms of drugs known as chloroquine (**1a**), hydroxychloroquine (**1b**) (see *Fig. 2.*), which are also zinc-ionophores. In addition to these, a numerous amount of zinc-ionophores are known as antiviral agents.[8]

1a: R = H   chloroquine
1b: R = OH   hydroxychloroquine
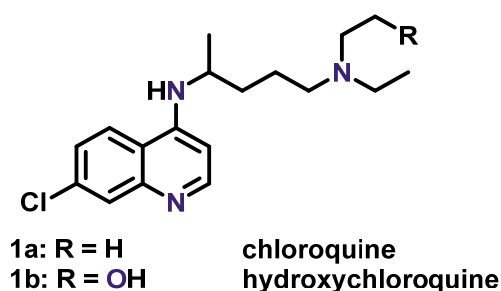
Figure 2. Structure of zinc-ionophores under clinical trial against COVID-19. Violet colour marks heteroatoms suggested to bind zinc.

Angiotensin-converting enzyme 2 (ACE2), which is the key entry point into cells for SARS-CoV-2 is also one of the many zinc-proteins and indirect evidence suggests, that Zn^{2+} may decrease its activity. Zinc-ionophores were shown to reduce the glycosylation of ACE2 receptor, and as a result, lower its affinity towards the viral spike proteins, therefore inhibiting viral access into the cells.[21]

Another possible target of zinc-ionophores may be the papain-like protease (PL[pro]) enzyme of SARS-CoV-2, which is stabilized by zinc fingers. It was suggested, that removing zinc with ionophores from this enzyme would destabilize it, therefore rendering it useless for viral reproduction, while the liberated zinc could inhibit the RdRp further inhibiting the reproduction of the virus.

Besides these, a multitude of relations were hypothesized in the scientific literature between zinc and the COVID-19. More sources include links between zinc and influenza, pneumonia, other infections and multiple cellular biological processes. I think that the mentioned

discoveries in this section are the most important ones, and the most plausible ones representing the relation between zinc and COVID-19. In my opinion, all the mentioned findings need to be treated with caution as presumptions, and not as proven facts. More research is needed in the field to clarify relations and reach consensus. Nonetheless, I think, that all these results confirm, that zinc plays important roles in this viral infection, accordingly, it should be taken into consideration, when looking for a possible cure. Again, all of this demonstrates the importance of research related to zinc and the importance of zinc imaging and the need for fluorescent probes for zinc. With a little optimism, we can even suggest, that screening our ionophores targeting zinc with a novel scaffold as drugs against the infection would not even be a bad idea.

2.2. Methods for measuring Zn^{2+} concentration

So, after I have demonstrated the findings in the scientific literature, that motivated us to address the development of zinc imaging, I collected the possible methods, that are applicable for measuring biological zinc-concentrations. Our main interest is focused on applicability in neuroscientific research, as our research team of biologists is keen in investigating mainly the hippocampus. The Zn^{2+} ion is thought to be one of the key elements in understanding Alzheimer's disease. In addition, recent results suggest that Zn^{2+} ions may also play key role in the neurobiology of vision and in restoring vision in blind people. In the current situation, our research offers possibilities for COVID-19 related research as well.

As I have mentioned in the introduction part, for the desired applications, sensitive, real time measurements are required, with large resolution, which does not destroy tissue in the meantime. Currently the only technique capable of this is optical, fluorescent microscopy. Femtonics LTD., the company I have done this research for is involved in the development and production of two-photon (2P) microscopes, which are the advanced types of fluorescent microscopes. In the next section, I will discuss the mechanism of working of these instruments and their advantages and disadvantages.

2.2.1. The mechanism of action of 2P microscopes and their advantages

2.2.1.1. Theory of the 2P effect

When Albert Einstein described the photoelectric effect, he proposed, that light has a dual nature, having wave and particle properties at the same time. He made this conclusion by observing, that excitation happens only, when the exciting light reaches a certain frequency

(energy), called *threshold frequency*. If illumination is made with lower frequency, but higher intensity light, no excitation happens. This is due to the quantized nature of energy levels in material and the fact, that energy is carried in small packets called *quantums*. If the energy content of a quantum cannot reach the difference in energy between the two levels (ΔE_{gap}), excitation is impossible. The energy „content" of quantums is of course related to the wavelength, or frequency of the light source as described in the well-known *Equation 1.*, where *h* represents Planck's constant (6.626×10^{-34} m$^2 \times$kg/s), *c* is the speed of light in vacuum (2.99×10^9 m/s), *λ* and *f* represent the wavelength and frequency respectively.[22]

$$E = \frac{h \times c}{\lambda} = h \times f \tag{1}$$

Not long after, in 1931, German-American physicist Maria Goeppert-Mayer predicted the existence of the two-photon effect on a theoretical basis.[23] Based on Heisenberg's uncertainty principle she predicted, that a short window of time exists in which short-lifetime "virtual energy levels" are created. If two photons under the threshold frequency hit one particle during this time window, their energy can be added, and if the sum of their frequencies reach the threshold frequency, the same excitation takes place. This means, that one can achieve excitation using a light that has double the wavelength compared to the exciting light needed in the normal single-photon case. Contrastingly, a very high photon density is needed in order to have statistical chance of two photons hitting one particle in a short time. This is the reason that the phenomenon was proved experimentally only in the 90's, when high power LASERs became available.

Simplifying the original theorem, let's investigate the consequences of Heisenberg's principle for the uncertainty of the measurements of lifetime and energy of an excited fluorophore in order to calculate the time in which two photons must hit the molecule to excite it. Let's consider *Equation 2.*:

$$\Delta E \times \Delta t = \frac{\hbar}{2} \tag{2}$$

ΔE represents the energy difference between the excited and ground state of the fluorophore, since it can be in either state, in the moment of the measurement. *Δt* represents the lifetime of the excited state. *ℏ* is the reduced Planck constant.

For a rhodamine molecule, the maximal absorption wavelength is 560 nm. In this case, ΔE_{gap} can be calculated from *Equation 1.* in the form represented by *equation 3.*

$$\Delta E = \Delta E_{gap} = \frac{h \cdot c}{\lambda_{abs}} = 3,31 \times 10^{-19} \text{ J} \tag{3}$$

If we express Δt from *Equation 2.* and replace the values of $\hbar$ and ΔE, we get *equation 4.*

$$\Delta t = \frac{\hbar}{2 \times \Delta E} = 1,593 \times 10^{-16} \text{s} = 0.159 \text{ fs} \tag{4}$$

Equation 4. shows us, that we have a statistical chance for a two-photon excitation only if two photons hit the fluorophore in a time period of 0.159 fs. This is an unimaginably short time period. The maximal allowed distance between the two consecutive photons can be calculated from *Equation 5.*, we just have to multiply Δt with the speed of the of the photons, which is known as the speed of light (c).

$$\Delta x = \Delta t \times c = 47.6 \, nm \tag{5}$$

To calculate the photon density let's assume, that the molecule has a width and height of 0.8 nm and 0.3 nm respectively. This means, that two photons are required to penetrate this plane in the mentioned timeframe. This is true only, if two photons having ΔE_{gap} are present in the volume created by the plane of the molecule and the maximal distance calculated in *Equation 5.* Considering this, the energy density (ρ_E) of the laser can be calculated from *Equation 6.*:

$$\rho_E = \frac{E}{V} = \frac{\Delta E_{gap}}{\Delta x \times h \times w} = \frac{3.31 \times 10^{-19} \text{J}}{47.7 \times 0.8 \times 0.3 \text{ nm}^3} = 2.89 \times 10^{-20} \frac{\text{J}}{\text{nm}^3} = 2.89 \times 10^7 \frac{\text{J}}{\text{m}^3} \tag{6}$$

When talking about lasers, it is common knowledge, that we are considering monochromatic, collimated light, in which all the photons carry the same amount of energy. Considering a 560 nm light, all photons have the energy calculated in *Equation 3.* The required photon density for 2P excitation can be calculated from *Equation 7.* using the calculated ρ_E value and the calculated energy of the photons ΔE_{gap}:

$$\rho_\Phi = \frac{\rho_E}{\Delta E_{gap}} = \frac{2,89 \cdot 10^7 \frac{\text{J}}{\text{m}^3}}{3,31 \times 10^{-19} \text{J}} = 8.73 \times 10^{25} \frac{1}{\text{m}^3} \tag{7}$$

$$C_\Phi = \frac{\rho_\Phi}{N_A} = \frac{8.73 \times 10^{25} \frac{1}{\text{m}^3}}{6.022 \times 10^{23} \frac{1}{\text{mol}}} = 145 \frac{\text{mol}}{\text{m}^3} = 0,145 \frac{\text{mol}}{\text{dm}^3}$$

This photon density is exceptionally high not even present in the collimated LASER beams. Achieving this high photon density is only possible in the focused beam of high-power pulsating LASERs.

2.2.1.2. Advantages of 2P microscopy

After the previous chapter has given an insight into the sophisticated mechanism of 2P microscopy, one can clearly see, that the technique requires extremely delicate mechanics, expensive and dangerous high-power LASERs. So, if these microscopes are so expensive and complicated, what advantages can they offer? Turns out, a lot. *Fig. 4.* represents the two-photon excitation and emission against the single-photon case, showcasing the differences between the two.

First of all, let's not forget, that in the case of two-photon excitation, the wavelength of the exciting light can be doubled versus the single-photon case for a given fluorophore. More exactly, the 2P excitation maximum is somewhat lower, than the double of the single-photon case, as 2P excitation tends to be an $S_0 \rightarrow S_2$ transition instead of the more common $S_0 \rightarrow S_1$. However, since S_1 and S_2 levels are not far in energy, the 2P absorption wavelength is almost the double compared to the 1P. In the mechanism, the excited S_2 state usually relaxes to S_1 on an irradiative path, then S_1 state relaxes radiatively to ground state by emitting a single fluorescent photon. Consequently, the emission wavelength is exactly the same as in the single-photon case. The possible processes are visible on *Fig. 3.*
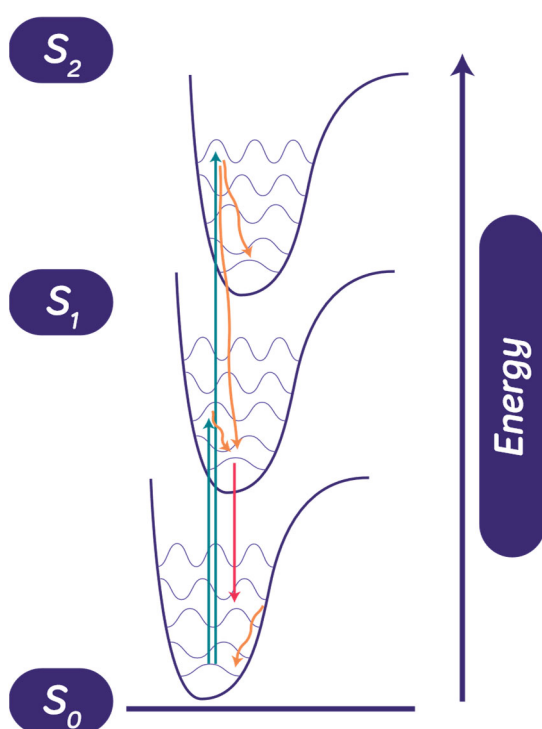
Figure 3. The possible excitation and relaxation processes visualised according to the Franc-Condon principle. Blue arrows represent excitation processes, orange arrows show nonradiative relaxations, while pink arrows indicate fluorescent relaxation processes.

This fact carries several advantages. In most cases this wavelength is rendered above 700 nm, in the infrared region, meaning, that the samples can be studied using infrared light instead of UV or visible light (represented by violet and pink lightpaths on *Fig. 4.*). The capability of near infrared light to penetrate any tissue is much higher compared to visible, or UV light, while it is significantly less destructive for tissue and avoids cellular autofluorescence caused by

NADH.[17] While the wavelength of excitation is almost the double compared to the single-photon case, the emission wavelength matches the single-photon case, which is an important advantage of 2P techniques. Having such a huge difference between the two wavelengths, we can apply filters before the detector to only detect the fluorescent light, as a result supressing the background and increasing the signal to noise ratio. As a consequence, the problem of stokes shift should not be addressed, when talking about 2P microscopy. Finally, the larger wavelength results in milder photobleaching, which is another important advantage.[24,25] A further advantage is, that the previously mentioned high photon density is not present in the collimated beam. To achieve the critical photon density, the high-power LASER beam must be focused. Therefore, excitation and emission takes place only in a small volume (~ 0.1 fl, with a diameter of 1.3 μm) near the focusing point, not in the whole lightpath as presented on *Fig. 4*.[26]. This enables measurement of well-established points in the sample, minimizing the background fluorescence, while keeping a high resolution. By moving the focus point, 3D scanning of the samples is made available. With fast and precise scanning movements, a 3D real-time monitoring of the region of interest is possible.[24,25]
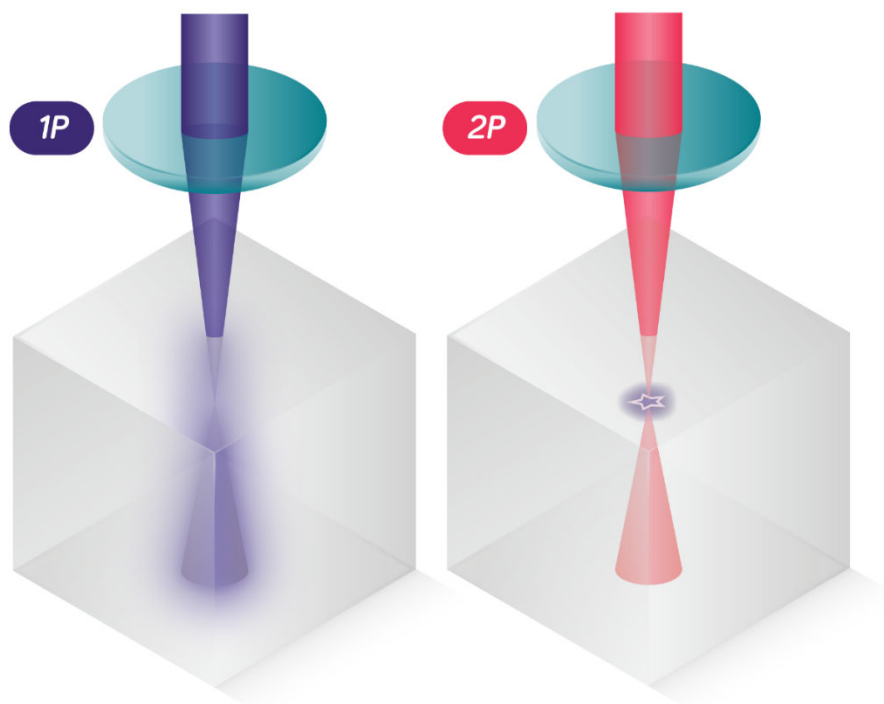
Figure 4. Visualization of single-photon microscopy (1P, left) versus two-photon microscopy (2P, right). The grey boxes represent the sample, while the purple and pink beams represent the light path. Purple represents UV-VIS light, pink represents IR light. The figure shows, that in the 2P case, excitation and emission happens only in the focus point of the beam.

In summary, despite being more expensive and complicated, 2P microscopy offers the possibility of high-resolution 3D real time measurements with great sensitivity thanks to the exceptional signal to noise ratio. Moreover, imaging deeper in the tissue, while minimizing the unwanted effects of UV and visible light, such as tissue destruction and photobleaching is also made possible.

2.2.2. About fluorescent probes

Despite all the discussed superiorities of these microscopes, the analytes, themselves (in our case, biological zinc) often do not emit fluorescent light, making the imaging impossible without indicator molecules.[7,20]

The most important features of sensor molecules are the following:

- it can get into cells and stays stable in cells during the measurement
- it can bind to the analyte in the studied concentration range (zinc, in our case)
- it is not fluorescent (or just weakly fluorescent) in free form and it gets fluorescent upon binding to the analyte (the higher the quantum yield, the better. Φ, the quantum yield is a number between 0 and 1 basically representing how strong fluorescence of a compound is. Φ expresses the percentage of absorbed energy, that is emitted in the form of fluorescence)
- it is selective towards the analyte (as much as possible)
- it is probably not toxic (enabling *in vivo* experiments)
- it absorbs 2P light in the spectrum emitted by most 2P lasers (~700-1100 nm)

Although fluorescent imaging is a relatively modern technique, the first "fluorescent sensor" got created millions of years before humanity. Photoprotein *aequorin* synthetized by a medusa *aequorea victoria* binds calcium and due to a conformational change it emits a photon without illumination based on a complex mechanism.[27–29] Despite this protein could be a good sensor for Ca^{2+}, its application was tried with only moderate success, since it cannot get into cells. Injecting with micropipettes or expression is a possible route, but the usage of this protein is not straightforward.[27]

A second group of fluorescent probes are getting larger and larger attention nowadays. These are genetically encoded proteins, having also a natural origin, that are usable as fluorescent sensors for different ions. Briefly, these probes often produce poor S/N ratio and are not always reliable, however, their potential in the future is outstanding.

Finally, small molecules have become the most successful, due to their large variability, reliability and tunability. Small molecules are also adjustable to get into specific regions of interest, and they have a great signal to noise ratio, usually without toxicity. This motivated me to choose these types of compounds for my development project.

Small molecule fluorescent probes usually consist of an ionophore part responsible for binding to the analyte and a fluorophore part. The ionophore usually binds to the analyte through a process called chelation, discussed in the next section. The fluorophore is a normally fluorescent moiety, that is quenched by the ionophore in free form and the quenching stops upon binding. The fluorophore and ionophore can be compactly linked together, even with the fluorophore taking part in the binding, but they can also be far, separated intramolecularly. The exact principles of operation will be interpreted in *section 2.2.2.2*.

2.2.2.1 Metal ion chelate complexes

Chelation has been a well-known effect in chemistry for a century used in multiple fields. The name itself comes from the Greek word "chela", which means "crab's claw". Chelate complexes often resemble a crab, which grabs the central ion with its claws. We talk about chelation, when a polydentate ligand binds to a metal ion trough the lone pairs of their heteroatoms.[30] In general, chelation results in highly stable complexes caused by multiple driving forces. An enthalpic effect (ΔH) is provided by the stable secondary bonds created between the chelator and the analytes, moreover, it is usually enhanced by the resulting stable heterocycles inside the complex. The empty d orbitals of the central ion getting filled with electrons is also a favourable enthalpic effect.[31] The other characteristic effect is an entropic one (ΔS), which is caused by the reaction, when the aquacomplexes of the metal ions turn into chelate complexes and release water. Taking a look at *Equation 8* one can observe, that from two initial particles during the chelation $n+1$ particles are being formed, where n represents the coordination number of the aquacomplex of the respective metal. Since this is usually larger, than 1 (6 in case of zinc), the number of particles are increasing during chelation, consequently, the entropy of the system is also increasing, which is highly favourable.[31]

$$M(H_2O)^{x+}_n + L = ML^{x+} + n \times H_2O \qquad\qquad \Delta H, \Delta S \qquad (8)$$

The number of conformational rotamers decreases, however, since the resulting complex is less flexible, but this effect is rather small compared to the others. I have to mention, that

many articles in the literature do not take this effect into account at all, which may be a mistake.

The stability of chelate complexes in general depend on the ionic radius, charge, polarizability of the metal ion and on the structure of the chelator. The stability of chelators is conventionally represented by their dissociation constant (K_d) or association/formation constant (K_f). Since these numbers are often very large or very small, the negative logarithm, so called „p" functions of the values are conventionally used. If we consider *Equation 8.* representing the process of chelation, the formation (K_f) and dissociation constants (K_d) can be calculated based on *Equation 9.* and *10.* respectively:

$$K_f = \frac{[ML^{x+}]}{[M^{x+}] \cdot [L]} \tag{9}$$

$$K_d = \frac{1}{K_f} = \frac{[M^{x+}] \cdot [L]}{[ML^{x+}]} \tag{10}$$

I think it is important to remark, that E*quations 9.* and *10.* can be used only if none of the binding heteroatoms is in protonated state, and if there is no competing effect present, such as a concurrent ionophore. The so-called apparent constants (K'_f, K'_d) represent complexes under the given circumstances, where competing phenomena with the chelation are present. Sensor molecules for imaging usually operate at physiological pH values within a complex matrix, where proteins and other ionophores are present. In these environments, values of these constants should be used with care. In spite of that, K_d values are the standard indicator of the affinity of a chelator to an ion, and it should be determined to characterize the compound of choice. A problem I have encountered in the literature is, that in many cases, for the biologically relevant chelators K_d values are measured at pH 7.4, which is physiologically relevant. This is completely correct, because for their scope, this is what represents them the best. The problem is that many authors forget to indicate this fact, which makes comparing K_d values of different compounds impossible. For example, K_d of classical chelators is usually determined at a basic pH, where the chelator is completely in free form. If the acid-base dissociation constants (K_a) of the compounds are determined, the real and the apparent dissociation constants relate to each other as *Equation 11.* shows (n is the number of protonatable heteroatoms):

$$K'_d = \frac{K_d}{\alpha_H} = \frac{K_d}{1 + \frac{[H^+]}{K_{a_n}} + \frac{[H^+]^2}{K_{a_n} \cdot K_{a_{n-1}}} + \cdots + \frac{[H^+]^n}{K_{a_n} \cdot K_{a_{n-1}} \cdots K_{a_1}}} \tag{11}$$

I would like to briefly mention, that the first chelator, ethylenediaminetetraacetic acid was introduced by Schwarzenbach in the '50s.[31] EDTA (**4a**) has found a wide range of applications since, such as chelatometric titrations, or medical uses against metal poisonings. EDTA is still the most used chelator of our days. The spectrum of chelating agents is very broad, with synthetic and natural representatives used for a wide array of purposes ranging from radiotherapy to immobilizing heavy metals in the soil.[31–38] *Figure 5.* shows the simplest synthetic chelators (top), alongside with a two natural representatives (middle). It also presents the binding of EDTA to a metal (bottom)

2a: R = H   iminodiacetate
2b: R = AcO⁻   nitrilotriacetate

3d: CyDTA

4: ethylene glycol tetraacetic acid (EGTA)

5: porphyrin

6:citrate

3a: *n* = 1 EDTA
3b: *n* = 2
3c: *n* = 3
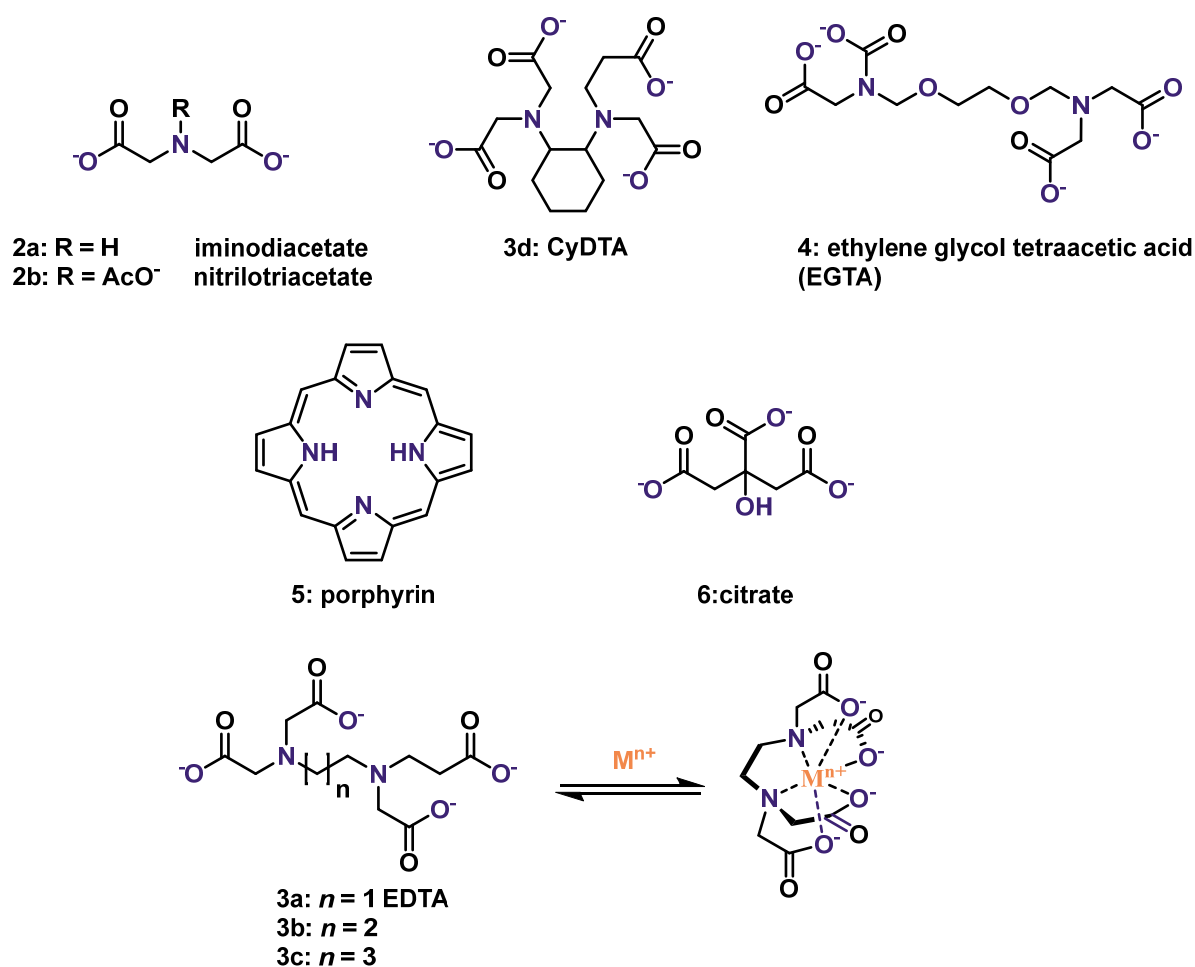
Figure 5. The most important representatives of chelators. Top: simple synthetic chelators. Middle: natural chelating molecules. Bottom: The structure of EDTA and its metal complexes. Violet colour marks metal binding heteroatoms.

2.2.2.2 General mechanisms of fluorescent probes

In general, different fluorescent sensor compounds operate by different principles presented in this section.

Internal charge transfer (ICT) is one of these principles[39]. In internal charge transfer sensors, the molecule must have an electron-rich part, which can donate electrons to an electron-poor region in the same molecule. During binding, the electron density of one part should change in order to achieve turn-on or turn-off effect. For example, if the probe has a chelator amine connected to a carbonyl via an aromatic scaffold, the probe emits fluorescent in the free state, since the amine moiety can donate electrons to the carbonyl. When the lone pairs of the amine are used up for binding, the ICT effect stops, and the sensor turns off. Another example would be a sensor, which has an electron-rich amine on one side and another electron-rich chelator on the other side.[40] This sensor would be turned off in free state, however, upon binding, the chelator side would lose its electron density and fluorescence could turn on. For cations, these kinds of sensors are rather rare. ICT sensors however are often used for detecting anions or other chemicals, since they can operate on the basis of reactivity. The inactive sensor may react with the analyte, or get oxidized by the analyte, while turning on. It is important, that reactive turn-on and turn-off effects are usually irreversible, which is a disadvantage. A good example for this are sensors for bisulphite anions[41], but ICT sensors were also made for cations like Ca^{2+}, Hg^{2+}, Fe^{3+}, *etc*. Mechanism of ICT sensors is illustrated on *Fig. 6.*
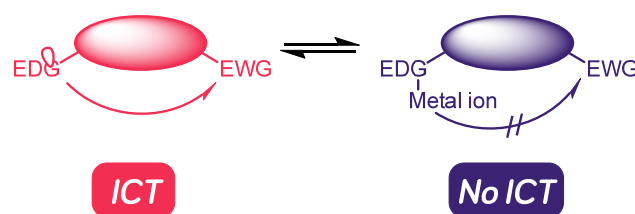
Figure 6. Illustration of the mechanism of ICT sensors.

Another group of sensors are based on the effect of Förster resonance energy transfer (FRET). In this case, the sensor consists of a donor and an acceptor part. The main criterium is, that the donor part must have its fluorescent emission wavelength very close to the absorption wavelength of the acceptor (*Fig. 7., right*), while the two parts also need to be close in space to each other(*Fig. 7., left*). If this happens, an energy transfer takes place between the two and fluorescent light bearing the fluorescent wavelength of the acceptor part is emitted. [40,42] The turn-on and turn-off effects can be controlled be an analyte altering the emission band of the donor/the absorption band of the acceptor upon binding or in protein sensors, by causing a large conformational shift upon which the two parts get separated in space blocking the FRET effect.[40] FRET sensors are mainly used as protein-based sensors, but small molecule FRET sensors also exist. They sometimes have limited signal to noise ratio and their signals may overlap if multiple sensors are used.[43]
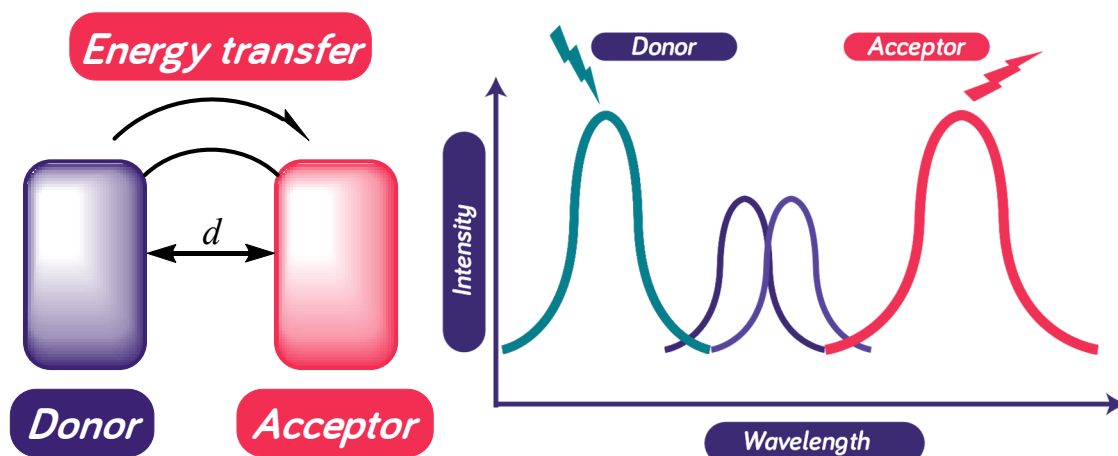
Figure 7. Illustration of the mechanism of FRET sensors.

Finally, the most popular and important mechanism of fluorescent probes are based on a principle called photoinduced electron transfer (PET) quenching. In this phenomenon, an ionophore containing donor heteroatoms is connected to a fluorophore, which is in itself fluorescent as visible in *Figure 8.* The ionophore in this case quenches the fluorescence of the fluorophore in a phenomenon called *photoinduced electron transfer* (PET). PET is a complex quantum chemical process. Taking simplifications into consideration to explain the mechanism of PET, let's propose, that the fluorophore and ionophore have separated molecular orbitals. When the probe is in free form, the ionophore contains heteroatoms with several lone pairs making its HOMO levels high in energy. Upon excitation, a vacancy is created on the HOMO of the fluorophore. In normal case, the excited electron relaxes into this vacancy radiatively. However, since the HOMO of the ionophore is on a higher energy level, than the vacancy, a HOMO electron can fill that for a period of time, as visible on *Fig. 8, bottom.* In this case, the excited electron can relax only in a longer time on an irradiative route. Basically this means, that the fluorescence is quenched.[7,40]

When the probe binds to ions, the lone pairs on the heteroatoms of the ionophore are used in the binding process, lowering the HOMO of the ionophore, making the transition of an electron to the vacancy impossible. By blocking PET, the fluorescence of the fluorophore is not quenched anymore (*see Fig. 8).*[7,40]
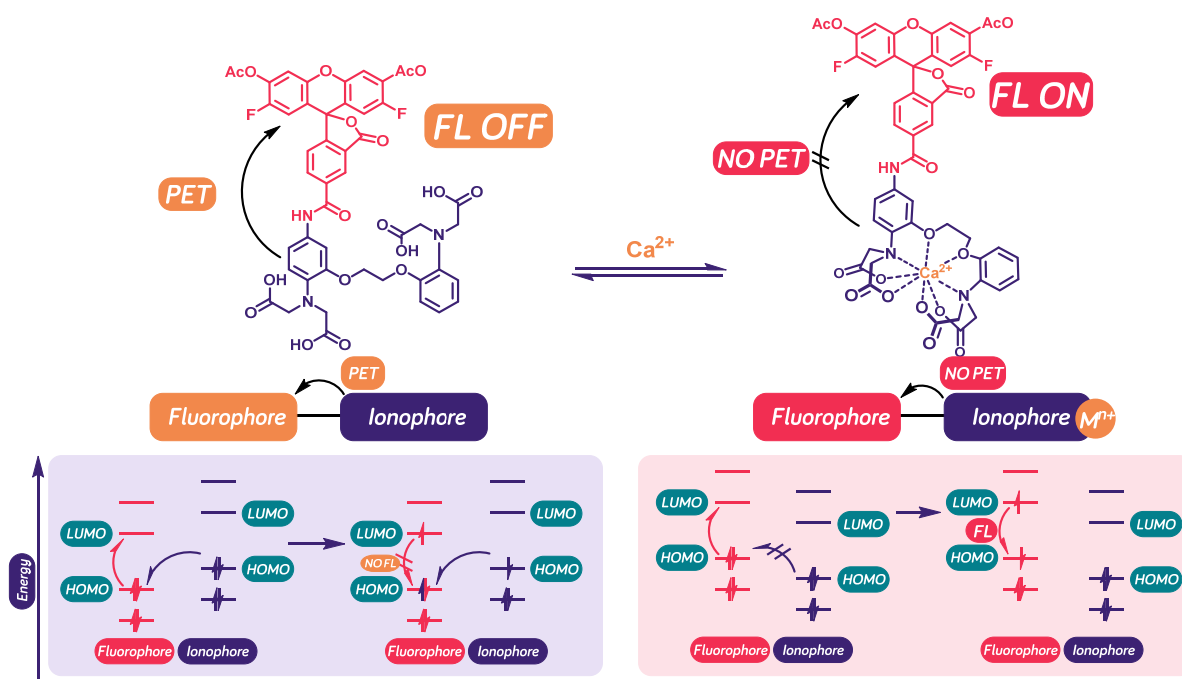
Figure 8. Illustration of the mechanism of PET sensors. (bottom) demonstration on the example of the most popular fluorescent probe, OGB-488-BAPTA, used in calcium imaging. (top).

PET sensors are the most widely used small molecular sensors with a reason. The combinations of fluorophores and ionophores enable large tunability. With combination of highly sensitive fluorophores and ionophores, these sensors can have high quantum yields and great signal to noise ratios even beside low analyte concentrations. Usually, multiple sensors are usable at the same time for detection in a wider concentration range or for detecting more than one ion simultaneously. PET sensors usually are able to penetrate cells and some contain ester groups, which get them into the cells and then enzymatically hydrolyse in the cytosol. PET sensors are relatively insensitive to matrix effects and have high stability. However, most of them contain protonatable heteroatoms (such as N).[7,40] Protonation of the ionophore on the physiological pH can unfortunately decrease the K_d as discussed in *Chapter 2.2.2.1.,* this way rendering the sensor unusable.

Since these are the most widely studied and applied sensors, we have decided to design our own compounds based on the principle of PET too.

2.2.3. Currently used sensor molecules for Zn^{2+} imaging.

There is a large number of already available fluorescent probes for zinc. However, the criteria required for these sensors in biology create serious problems at designing such molecules.[17] A successful sensor needs to have a fluorescent response for Zn^{2+}, while being selective for the most abundant competitive analytes in cells (Ca^{2+}, Mg^{2+}). The binding of the sensors must

be rapid and reversible. The criteria for K_d values vary depending on the region of interest, where the sensor is going to be used and the scope of the measurements. Tunability of K_d in a sensor family is also important, allowing it to be used in a larger number of experiments. Biocompatibility is also important, water-soluble, stable and nontoxic compounds are needed; however, lipophilic probes are also useful for monitoring zinc in vesicles. Insensitivity for pH is also an important design factor as discussed in the previous chapter.[17] Photophysical properties are also important, such as the wavelength of emission and excitation as well as the quantum yields (Φ), to achieve bright signals.[17] For 2P measurements, the wavelength of excitation should be at least above 350 nm, as otherwise, IR lasers will not be able to excite the molecule. In contrast, stokes shift is less important for 2P applications.

In order to be successful in fulfilling the strict criteria regarding the target compounds, I have made a comprehensive literature study to discover the most important probes for Zn^{2+} in the hope of finding inspiration for successful design of novel sensors.

2.2.3.1 Biological sensors

The literature presents a variety of biology-based sensors for zinc imaging. I will present these only marginally, as small molecule probes were my main interests.

Peptide sensors are usually FRET-based sensors, where zinc finger moieties are coupled with different fluorophores. Another group of peptide-based sensors are made of synthetic oxine (8-hydroxyquinoline, **7**) or dansyl (5-(dimethylamino)naphthalene-1-sulfonyl) containing amino acids. It turns out, as in further sections it will be visible, that oxine **7** is a good ionophore for zinc, which will be presented in the next section. Dansyl groups coupled to amino acids also work excellent for zinc binding.

Protein-based sensors operate on very similar basics as their peptide-based counterparts; however, they have an advantage in selectivity. In general, these proteins can be natural zinc binding proteins attached to synthetic fluorophores, but there are examples of proteins attached to both synthetic ionophores and fluorophores.

Finally, just to mention, a group of nucleic acid-based sensors also exist, but I do not consider them important enough for deeper presentation, which is done in review articles on the topic.[17]

In general, biological probes have their own advantages, that they usually have good properties in biological environments and some of them can be expressed in the cells, moreover, the natural zinc binding motifs have K_d values between 1 pM and 50 μM, which is

helpful in measurements, where the concentration change is happening between two very low values. However, their production is often complicated, their tunability is challenging and problems may arise originating from the large bioconjugate structures. The structures can be perturbated at the site of interest, large and complex conformational effects and interactions with the matrix need to be taken into account. These problems can be resolved by using small molecule chemical sensors, which will be discussed in the next sections.

2.2.3.2 Chemical sensors: quinoline derivatives

A large spectrum of quinoline derivatives are used as fluorescent Zn^{2+} probes. First of all, it is common knowledge, that the quinoline scaffold is fluorescent in general. One of first discovered fluorescent materials was *quinine*, an alkaloid found in the barks of *cinchona*. Quinine sulphate is even used as an analytical standard in fluorimetric measurements.[44]

The most important quinoline-based Zn^{2+} sensors are 8-aminoquinoline (**8-AQ, 7**) derivatives (see *Fig.9)*. The literature contains about 100 fluorescent sensors based on this scaffold according to a search on SciFinder. I am not going to attempt to present every one of them. The 8-amino group quenches the fluorescent quinoline scaffold during photoinduced proton/charge transfer to the aromatic nitrogen atom (ICT) and photoinduced electron transfer (PET) phenomena.[17] When the two N atoms (violet in *Figure 9.*) bind a metal ion, both effects are blocked and the fluorescence of the probe is turned on.

Many derivatives of **7** were prepared and described in the literature, most of which contain additional ionophore sidechains, such as in **8,9,10** to improve selectivity, K_d, solubility in water and other properties.[45–48] The selectivity and K_d values of sensors based on **8-AQ** are usually acceptable or good, however, Cd^{2+}, Cu^{2+} and Fe^{3+} ions sometimes can compromise these kinds of sensors. K_d values are on the μM range, which is good for many usages.

On the other hand, the main problem of **8-AQ**-based sensors is inherited from the quinoline scaffold as fluorophore itself, since quinolines can be excited mainly with UV-light of $\lambda = 300\text{-}380$ nm.[17] This excitation range is hardly good for 2P measurements, as it cannot be excited with most IR lasers, moreover, in 1P measurements it carries the negative effects of UV-irradiation. To avoid this unwanted effect, *Nolan et al.* linked **8-AQ** to fluorescein,[49] a well-known fluorophore, which has an excitation wavelength of $\lambda = 460$ nm.[50] The resulting compounds **12a** and **12b** have excitation wavelengths of 490-500 nm, almost no background fluorescence and $\Phi = 0.7\text{-}0.8$ values. Apparent K'_d values of the sensors were in

the μM range. In 1P and 2P experiments the compounds could get into the cells and has shown Zn^{2+}-response *in vivo,* however, these compounds are limited by their pH sensitivity.
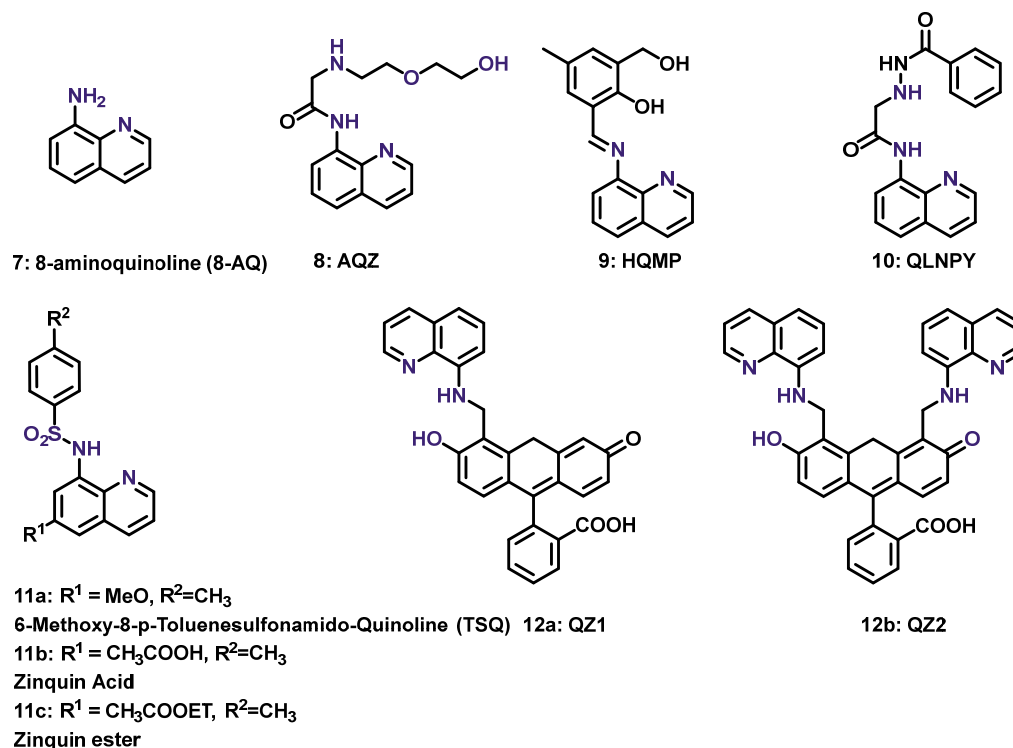
Figure 9. The most important representatives of 8-aminoquinoline-based (**8-AQ**) fluorescent probes for zinc. **7** represents the scaffold, **8.9.10** are modified ionophores, while **11** represents the **TSQ** family and **12** represents analogues linked to fluorescein.

Finally, another important group of chelators are the first and most popular fluorescent probes for detecting zinc are the derivatives of 8-p-toluenesulfonamido-quinolines. **TSQ (**6-methoxy-(8-p-toluenesulfonamido)quinoline**, 11a)** is presented on *Fig. 9.* along its optimized analogues, **11b** and **11c** called zinquin. The ester form of zinquin (**11c**) is capable of penetrating cells and then hydrolysing into the active acid form. TSQ is also membrane-permeable, pH-independent, non-toxic compound with small background-fluorescence. TSQ is applicable in concentrations as low as 0.1 nM and is selective against Ca^{2+} and Mg^{2+}. By forming a 2:1 (L:M) complex with zinc, its fluorescence increases by two orders of magnitude.[17] TSQ derivatives have a drawback: despite they are able to get into cells, their partition is instable, making longer *in vivo* experiments problematic. All molecules discussed are currently unavailable for order from the main chemical suppliers. Zinquin ester is only currently available at Sigma-Aldrich for a price of 153000 HUF / 5 mg. I think, that these facts support our idea to prepare novel fluorescent dyes with low production costs.

Another larger group of quinoline-based sensors are derivatives of 8-hydroxyquinoline (**8-HQ**, **13**) visible in F*igure 10.* These compounds share the limitations of previously mentioned probes, moreover, they are less selective for zinc, being rather considered universal chelators.[51] Their spectral properties were optimized by *Pearce et al.*[52] Although compounds with satisfactory excitation wavelengths, selectivity and quantum yield were made, none of them could successfully meet all three criteria.

13a: R^1 = H, R^2=H   13f: R^1 = SO$_3$H, R^2=SO$_3$H
13b: R^1 = NO$_2$, R^2=H   13h: R^1 = SO$_3$H, R^2=NO$_2$
13c: R^1 = NO$_2$, R^2=NO$_2$ 13i: R^1 = SO$_3$NMe$_2$, R^2=H
13e: R^1 = SO$_3$H, R^2=H   13j: R^1 = SO$_3$NBu$_2$, R^2=SO$_3$NBu$_2$

13: 8-hydroxyquinoline (HQ)
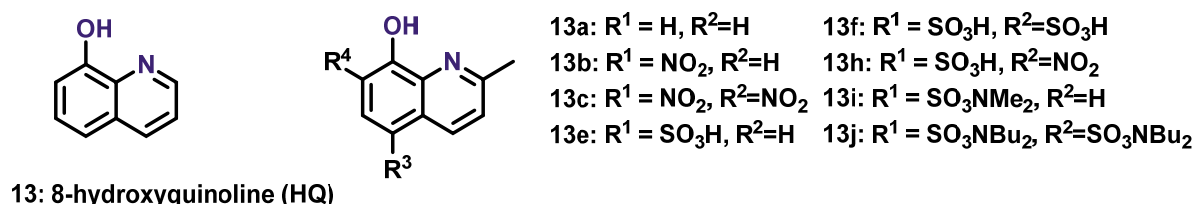
Figure 10. The most important representatives of 8-hidroxyquinoline-based (**8-HQ**) fluorescent probes for zinc.

More representatives of these compounds are denoted in the literature, but no great success have been earned on this field.[17]

2.2.3.4 Chemical sensors: dipicolylamine (DPA) and its derivatives

Dipicolylamine is an efficient chelator derived from the highly active chelator TPEN (N,N,N′,N′-tetrakis(2-pyridinylmethyl)-1,2-ethanediamine). I consider **DPA** (**14**) derivatives the second most important sensors for zinc after quinolines. It is straightforward, that **DPA** (**14**) is easily linkable to different fluorophores, while having three nitrogen atoms, that can bind to metals. Given the aliphatic nitrogen, which is usable as a linking point, it can act as a quencher based on PET and ICT mechanisms.[53] **DPA** (**14**) was shown to be selective and efficient chelator for Zn^{2+}, moreover, its affinity is tunable based on the electron donating or withdrawing property of the linked fluorophore. **DPA** (**14**) was linked with several fluorophores and promising results were achieved with it. The same research group at MIT, which created **QZ1** (**12b**) and **QZ2** (**12b**) also linked two **DPA** (**14**) molecules to fluorescein creating **ZinPyr-2** (**15**), the most basic representative of the **ZinPyr** (**ZP**) family of fluorescent probes.[17,49,53–56] This family of sensors consists of 20 derivatives containing one or two ionophores, and different combinations of substituents on the fluorophore and ionophore. The ionophore is also moderated in some cases by changing one of the methylpyridyl groups to aliphatic or other methyl-aromatic substituents. Other modifications involving the same scaffold were also carried out, and were presented in a comprehensive 28-page long review.[54]

14: DPA **15: ZinPyr-2**
The scaffold of ZP sensors **16: DPA linked to BODIPY**
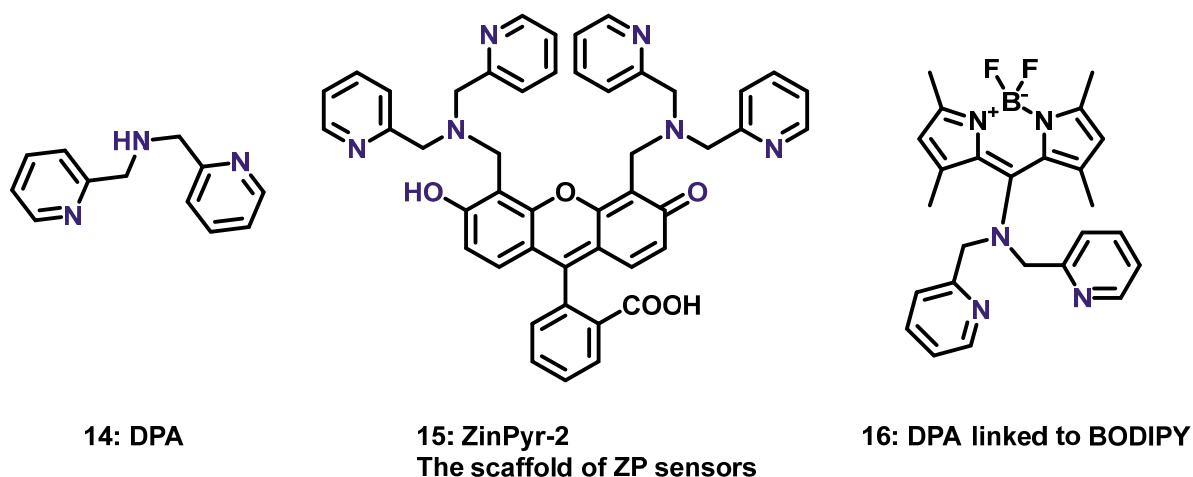
Figure 11. DPA and DPA linked with different fluorophores. The most important representatives.

Instead of trying to present these results here, I just sum up, that sensors with K_d values covering six orders of magnitude were created and successfully applied in real biological measurements, with up to 150-fold fluorescence increase in different wavelengths of the spectrum. Perhaps the most important moral of this family of sensors, is that **DPA** is a flexible, highly tuneable ionophore, by derivatization, or by exploiting electronic effects. Another important remark is, that in these compounds, **DPA** is not the only ionophore, but the hydroxy groups of the fluorescein also contribute to the binding.

In F*igure 11.* another example, **16** is also presented, in which **DPA** was bound to a **BODIPY** (boron-dipyrromethene) analogue moiety by the Peng group.[53] **16** has a high quantum yield, a 1 nM dissociation constant, high selectivity and a 7-fold fluorescence enhancement.

One could imagine, that hundreds of molecules were prepared by the combination of different analogues of **DPA** and different fluorophores. Some use extra chelator sidechains, while others include two ionophore sites, one being a **DPA**, the other being a quinoline-based site. It is not my goal in this essay to try to present all of them, as others did it in exceptional reviews available in the literature.[53] My goal was only to present, that **DPA** and its analogues are highly tuneable and efficient ionophores for zinc.

2.2.3.3 Chemical sensors: others

Presenting every aspect of the literature is hard and not a goal in this case, therefore, I present the other, less significant ionophores briefly in this section.

2,2'-bipyridine (BIPY) and its analogues were reported as zinc sensors in the literature, however, its use is far less popular with a reason. BIPY is rather a universal ionophore, it is

less selective and also has worse dissociation constants. Unhindered BIPY analogues in many cases form complexes with higher ligand to metal ratio spoiling the quantitative nature of measurements.[53]

Cyclic and acyclic polyamines are widely used metal chelators and large numbers of fluorescent probes are reported incorporating them. However, the selectivity of such ionophores depend on numerous factors, moreover, they are also pH sensitive. Despite some successful representatives, their use is rather limited.

Iminodiacetic acid and its analogues ethylene glycol-bis(2-aminoethylether)-*N,N,N',N'*-tetraacetic acid (EGTA) and bis(o-aminophenoxy) ethane-*N,N,N',N'*-tetraacetic acid (BAPTA) have been the most widely used fluorescent probes in calcium imaging.[57] These compounds were optimized for large selectivity towards Ca^{2+} against Mg^{2+}. A good observation is, that in fact, these compounds have larger affinity towards Zn^{2+}, than Ca^{2+},[58] however, due to the large excess of calcium compared to Zn^{2+} in biological samples, this is negligible during calcium imaging. Attempts were made to use iminodiacetate analogues and to optimize BAPTA analogues for Zn^{2+} imaging. By removing one or more chelator parts of BAPTA, selectivity towards zinc could be shifted. Similar results were achieved with iminodiacetate analogues. These compounds have shown nanomolar binding constants with zinc ions and their selectivity is not that bad either. However the achieved selectivity against Ca^{2+} is not enough due to its large concentration rendering these probes unusable for microscopy.[17,53]

In some cases, Schiff bases and triazoles were also employed as Zn^{2+} sensors with various success.[53] One top of these, the literature of the topic is broad mentioning a lot of unique sensors, immobilized sensors to polymers, nanoparticle sensors and probes, that employ two different ionophores, with different affinity towards Zn^{2+}. These sensors turn on at a low concentration and change colour at a higher concentration.[15,39,59,60]

2.2.4. Possibilities in the chromophore of Green Fluorescent Protein.

Green fluorescent protein (GFP, ca. 26.9 da, 238 AAs, $\Phi = 0.78$) is a protein, that emits green light upon excitation with UV or blue coloured light.[61,62] The protein was isolated from deep-sea organisms and it is routinely used in cellular biology as a reporter of expression.[63,64] The chromophore of GFP was identified decades ago and suggestions for its biosynthesis were made.[62] However, it was only last year, when the colleagues of our laboratory developed a chemical synthesis (*Scheme 1.*) for the chromophore,

p-HOBDI, ((5-(4-hydroxybenzylidene)-2,3-dimethyl-3,5-dihydro-4H-imidazol-4-one,

17, *Fig. 12*) and investigated the tunability of its fluorescence.[10] To their biggest surprise, the emission and excitation wavelength of **17** were similar to that of GFP, but its fluorescence was very weak ($\Phi_{rel} < 10^{-4}$).[10]

A hypothesis, that different steric and electronic effects present in the protein enhance the fluorescence of the fluorophore was made. To confirm this, 20 analogues employing different substituents were synthetized with success and characterized photophysically.[10] Compounds with best photophysical properties (**17a, 17b, 17c** on *Fig. 12.)* all involved an aminophenyl substituent on the 3,5-dihydro-4*H*-imidazol-4-one (abbreviated as imidazol-4-one from this point) ring system as well as a para substituents on the benzene ring of *p-HOBDI*. Although fluorescence was enhanced by a factor of 20, this is still orders of magnitude worse, than the one present in GFP.[10]

It can be hypothesized, that the nitrogen atoms of the imidazolone ring take part in intramolecular bonds when present in the protein. Contrary, when present in a free form in analogues of **17**, they could be able to quench the fluorescence by a PET mechanism.

17: p-HOBDI
The scaffold of ZP sensors

17a: R^1 = NHPh, R^2=4-AcNH Φ_{rel} = 27.5
17b: R^1 = NHPh, R^2=4-Cl Φ_{rel} = 23.0
17c: R^1 = NHPh, R^2=COOH Φ_{rel} = 23.1
17 more analogues Φ_{rel} = 2.5 to 22
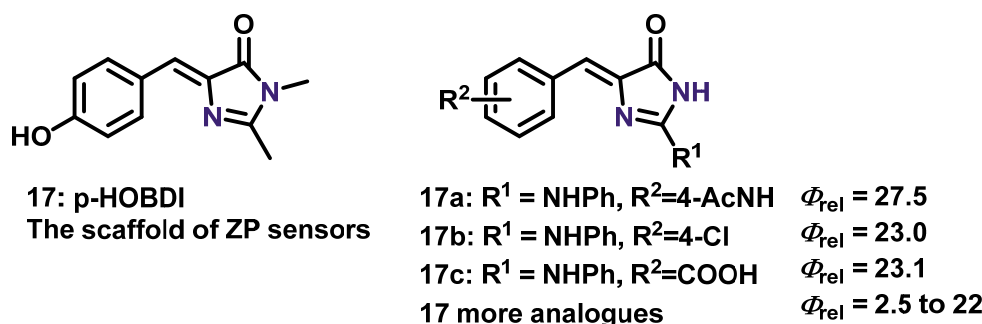
Figure 12. The minimal fluorescent scaffold of GFP (left) and its most successful synthetized analogues (right). Violet marks the nitrogen atom hypothesized as a PET quencher.

If this hypothesis is true, analogues of the GFP chromophore (**17**) containing additional chelator moieties could be successful fluorescent probes if the metal ion binding involves nitrogen atoms of the GFP scaffold. This fact makes this chromophore desirable in designing novel fluorescent probes, as it could yield in high fluorescent increases (cca. $\Phi = 0.01$ to $\Phi = 0.8$) based on the fluorescence of the scaffold observed in proteins, moreover, the extra chelator atom could provide increased selectivity. Absorption wavelengths of some analogues are also above 400 nm, which can be considered as the limit for 2P applications. On top, the new scaffold could present interesting partitions in cells, making more complex zinc-imaging available.

A new synthesis route for GFP analogues was also reported.[10] Although imidazol-4-one derivatives were published previously, the used synthetic procedures were inefficient.[10,65,66] The novel synthetic route in *Scheme 1.* starts from 2-thiohydantoin (**18**), which is treated with NaH in dry DMF (**18b**), and the deprotonated form is carried into a one-pot methylation by MeI to yield *S*-methylthiohydantoin (**19**). Although overmethylation to yield a dimethyl byproduct is a concern, the unwanted reaction can be supressed by careful addition of the reagents and control of temperature. This is followed by the one-pot addition of the desired amine compound resulting in the desired 2-amino substituted of imidazol-4-ones (**20**) after an aqueous work-up and purification. The resulting product **20** is then reacted with aromatic aldehydes in a Knoevenagel condensation to yield analogues of **17**. In some cases, the product is purified by simple filtration, otherwise further purification like chromatography is necessary.
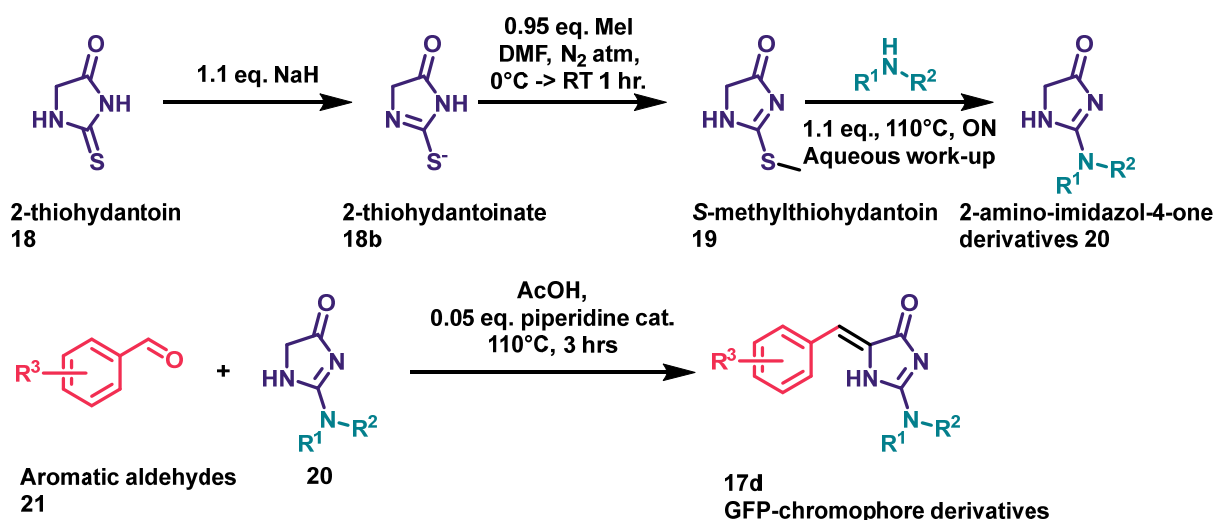
Scheme 1. Synthetic route to GFP-chromophore analogues reported by colleagues of our laboratory.[10]

Recent discoveries on the field of these compounds were also made, which are unpublished yet. Our colleagues recently discovered, that by reacting 2-hydroxy-benzaldehydes (**22**) with imidazole-4-one derivatives applying longer reaction times on elevated temperatures, a novel ring-closure reaction proceeds yielding chromeno[2,3-d]imidazole-2-amine derivatives (**23, 2nd gen. fluorophores**). Although exact measurements are in progress, it is visible to the naked eye, that these compounds exhibit much stronger fluorescence compared to analogues of *p-HOBDI* (**17**). The compounds are colourful powders from green to orange with intense fluorescence emitted in the green-red spectrum.

If benzaldehyde-2-boronic acid derivatives (**24**) were employed in the Knoevenagel reaction, a group of 3-amino-5-hydroxyimidazo[1,5-b][1,2]benzazaborinin-1-one

(**25, 3rd gen. fluorophores**) analogues were achieved with standard reaction conditions (**25**) upon another unpublished ring-closure. The pale coloured powders emitted bright fluorescence upon irradiation with cca. 400 nm light. Analogously benzaldehyde-2-trifluoroboronates (**26**) yield 5,5-difluorimidazo-[1,5-b][2,1]benzazaborine-3-amino-1-on (**27, derivatives 4th gen fluorophores**) in Knoevenagel reactions with derivatives of the GFP-chromophore **17**. These compounds show similar properties to analogues of **25**, even presenting brighter fluorescence.

These fluorophores exhibit desirable photophysical properties for imaging purposes. This fact indirectly supports our first hypothesis regarding the quenching effects of nitrogen atoms, since the electron structure of those atoms are highly different in the 2-4 generation chromophores.
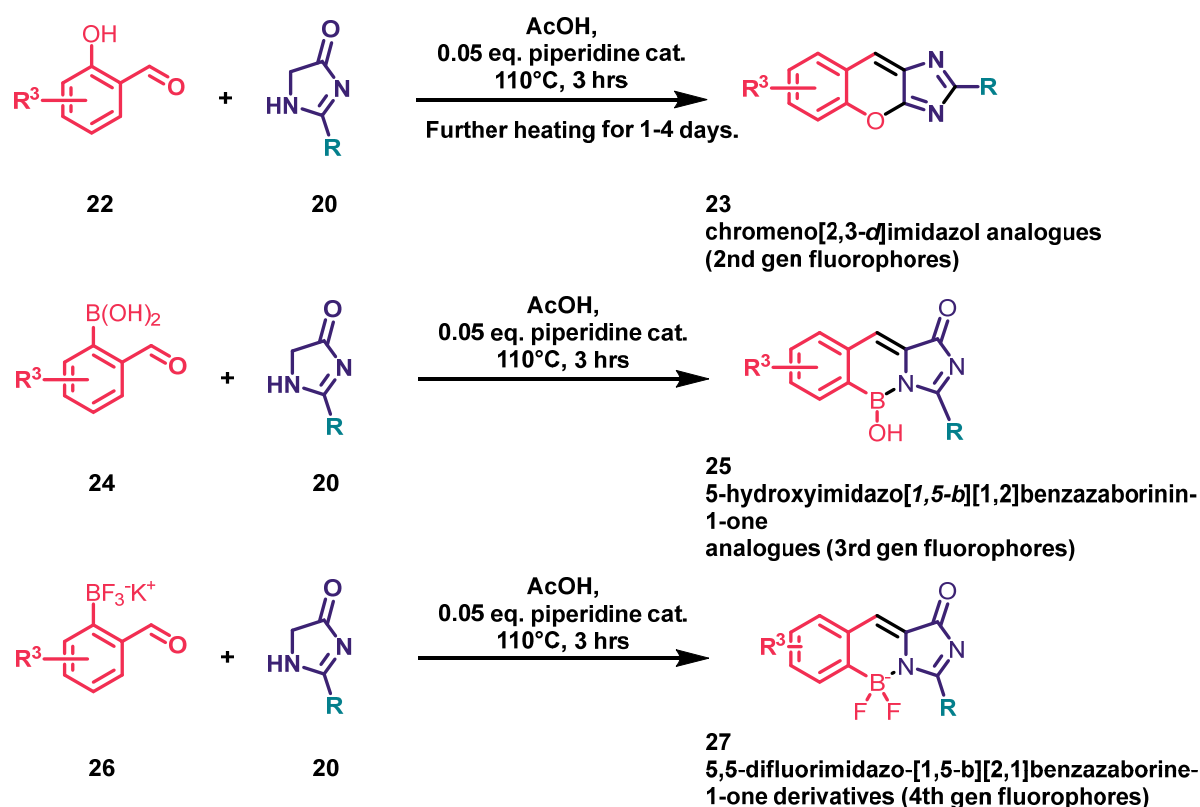
Scheme 2. Recent discoveries of our team.

Moreover, by substitution with chelators instead of aminophenyl derivatives on the 2 position of the imidazol-4-one ring, the fluorescence of compound families **23**,**25**,**27** may be quenched via a PET mechanism making them possible candidates for designing fluorescent PET sensors. It is true furthermore, that the nitrogen atoms of the imidazolone ring may even play a role in chelation further enhancing selectivity and K_d.

3. Aims and goals

Based of the available information in the literature, the current availability and high price of fluorescent sensors for zinc, I consider important to expand the repertoire of Zn^{2+} fluorescent probes. By having a novel fluorescent scaffold presented in *Chapter 2.2.4.* with promising qualities at hand, it was straightforward to attempt creating fluorescent probes on this platform. Using the analogue of a naturally occurring chemical moiety is also considered a good idea, as it can result in good toxicity and cell penetration properties.

I present the rationally planned compounds and experiments, that I was wishing to carry out in the next section.

3.1. Planned molecules

3.1.1. Quinoline-based compounds

We have decided to try two directions at designing novel probes. Firstly, we designed four novel sensors implementing quinoline-based ionophores visible in *Figure 13*. As mentioned in the literature, 8-aminoquinoline (**AQ, 7**) and 8-hydroxyquinonline (**HQ, 13**) were successfully used as selective sensors for Zn^{2+}. We expect, that upon conjugating them to the analogue of the chromophore of GFP, their main problem could be eliminated by achieving a bathochromic shift in the spectrum rendering the absorption wavelength into a region above 400 nm. Also, based on the bright fluorescence achieved by GFP, we were hoping, that our sensors will have good quantum yields as well. Moreover, we expected, that the nitrogen atoms of the GFP chromophore will improve selectivity and K_d values of the original **AQ** (**7**) and **HQ** (**13**) derivatives. As quinolines are aromatic moieties, they can be considered as an extension of the phenolic ring present in *p-HOBDI* (**17**). As a design principle, we have decided, to keep the aminophenyl substituent on the imidazolone ring, since previous in studies it always enchanced the quantum yield, moreover, it may even help in the chelation.

28 (GFPHQ1)   **29 (GFPAQ1)**   **30 (GFPAQ2)**   **31 (GFPAQ3)**
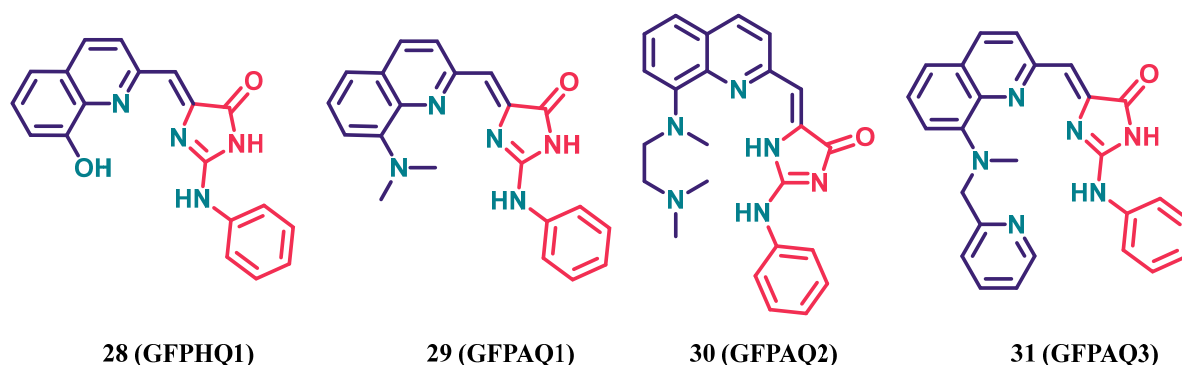
Figure 13. Novel quinoline-based fluorophores designed by us using derivatives of GFP. Violet marks the quinoline-part, while pink represents the fluorophore motif taken from GFP. Turquoise marks atoms predicted to be involved in the chelation process.

3.1.1.1 8-hydroxyquinoline derivative (GFPHQ1)

Sensor **GFPHQ1, 28** is our only sensor designed on the scaffold of 8-hydroxyquinoline (**13**). According to the literature**,** experiments were made to optimize the spectral properties and selectivity of **8-HQ** analogues (**13a-j**), but no compounds could combine good selectivity, brightness and acceptable excitation wavelength.[52] We hoped, that the modification introduced by our chromophore would provide a solution to these issues. Despite **8-HQ** being rather a universal ionophore, we were convinced, that the attached GFP analogue scaffold will optimize the affinity towards Zn^{2+}.

3.1.1.2 8-aminoquinoline derivatives (GFPAQ series)

A series of sensor candidates (**GFPAQ1-3; 29-31**) based on 8-aminoquinoline (**7**) were also considered as potentially successful probes for zinc ions. Our goal is again to earn positive changes in spectral properties similarly to the previous case, moreover, to optimize selectivity and K_d.

Compound **29, GFPAQ1** is a simple 8-dimethylaminoquinoline derivative, which has 3-4 binding arms marked in *Figure 13.* with turquoise.

In the hope of further optimizing the chelating properties, we introduced **30**, **GFPAQ2**, in which, we changed the dimethlyamino substituent to a chelating trimethyl-ethylenediamine substituent, which could further act as a quencher and an ionophore.

We were also fascinated by the possibility of combining the structures of aminoquinoline and dipicolylamine ionophores. Since in the cases of **ZinPyr** sensors (**15**) the most effective chelator was an N-methyl-N-picolyl derivative, we decided to use this moiety as a substituent on the position 8 of quinoline, when planning **GFPAQ3, 31.** Using two picolyl groups would

introduce too much steric hindrance, which is a disadvantage from the point of view of the synthesis and stability too. This molecule also has 4-5 binding spots, which all seemed to be selective for Zn^{2+}.

3.1.2. Sensors based on modified (2nd-4th generation) chromophores. (GFPDPA series)

The second group of chemical sensors designed by me involves the modified GFP-chromophores presented in the second part of *Chapter 2.2.4.* As discussed earlier, these compounds are fluorescent alone and have a more rigid framework consisting of condensed rings. This means, that it is not a good idea to incorporate them into the binding process, but rather to use them as efficient fluorophores linked to a chelating PET quencher. As an efficient PET quenching chelator usable for Zn^{2+} dipicolylamine (**DPA**) was chosen because of its successful applications in the past, which were explained in *Chapter 2.2.3.3.*

32 (GFPDPA1)   **33 (GFPDPA2)**   **34 (GFPDPA3)**
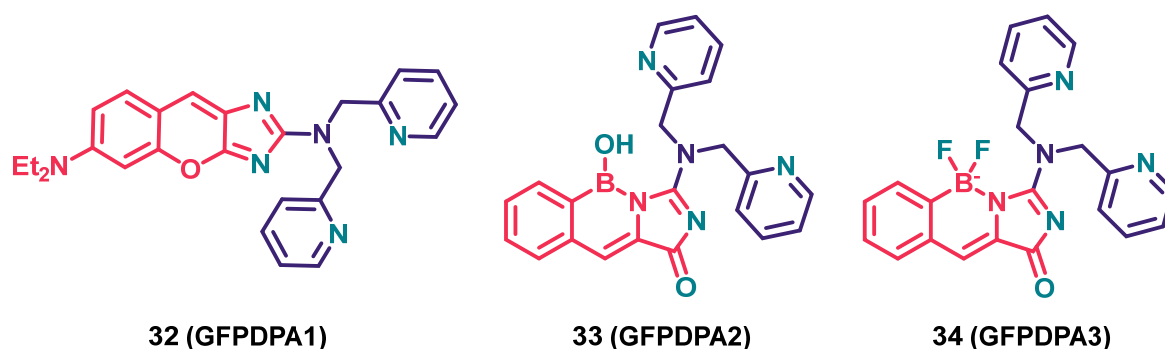
Figure 14. Novel DPA-based fluorophores designed by me using the advanced, 2nd, 3rd and 4th generation of GFP chromophore derivatives. Violet marks the DPA-part, while pink represents the fluorophore motif taken from GFP. Turquoise marks atoms predicted to be involved in the chelation process.

The **GFPDPA** series of compounds presented in *Figure 14.* (**32,33,34**) are based on linking the advanced chromophores on the imidazolone ring with dipicolylamine (**DPA**). These compounds are expected to have good affinity and selectivity for Zn^{2+} inherited from **DPA** and very weak fluorescence due to the quenching, which should be enhanced significantly upon binding to a metal ion. The brightness of these series is expected to be high, moreover, we hoped, that the different analogues will present different emission and excitation wavelengths. The possibly chelating heteroatoms were again marked by turquoise on *Fig. 14.* As one can observe, the heteroatoms of the fluorophore scaffold (marked with pink) could even contribute to the chelation similarly to what was observed in the case of **ZinPyr** (**15**) sensors. To make things simple, unsubstituted boronic derivatives were chosen, while a diethylamino-substituted derivative was chosen for **GFPDPA1** (**32**), since it has

commercially available precursors and the diethylamino group may enhance photophysical and solubility properties. Moreover, it gives a possibility for an eventual ITC quenching mechanism.

3.2. Experimental design

In the first turn, I made theoretical models of the planned molecules using DFT calculations. I aimed to model the free molecules as well as the complexes to propose a binding model. In previous works in which I tried to design efficient probes for Ca^{2+}, I attempted predicting the K_d values by calculations. The predicted values exhibited only moderate correlation to the measured values, thus the computation of the energy profile of the reaction was not included here and predictive calculations were not the goal. However, I must remark that the development new and efficient predictive methods would be very important, but it goes beyond the scope of this work.

As a synthetic chemist, my main goal was to prepare successfully the seven planned compounds (**28–34**) in 10 – 300 mg quantities with high chemical purity. After the preparation, I planned to determine the purity of compounds with HPLC-MS measurements and to confirm their structures using mass spectrum and NMR spectroscopy (1H, 13C).

I also planned to do analytical experiments in order to prove the applicability of the compounds. The first experiment I wanted to measure the fluorescent spectrum of the free compounds and the complexes to determine their relative brightness, wavelengths of excitation and emission. In the second experiment the goal is to estimate the K_d of the complexes and to determine the concentration range, where the prepared sensors are usable by fluorometric titration with Zn^{2+}. Finally, I wanted to determine the applicability of the compounds in 2P microscopy. In order to achieve this, I am planned to measure the fluorescence emitted upon 2P excitation of the free compounds and the complexes using a two-photon microscope.

In one word, my main goal is to design and synthetize two-photon applicable, selective fluorescent probes for Zn^{2+}, and characterize them to prove their usability. I am aware, that more measurements, such as selectivity, toxicity, *in vivo* applicability, M:L ratio determinations should be carried out, however, due to time constraints, this work includes only the previously mentioned experiments.

4. Results and discussion

4.1. Computational modelling

First and foremost, I started my work with modelling the planned molecules in order to prove the concept of their ion-binding capabilities and to propose binding models for each compound. The quantum chemical computations were carried out with the Gaussian 16 (G16)[67] software package, using DFT calculations. As the level of theory, M06-2X[68] was chosen, due to its high level of parametrization making it applicable for calculations in the field of transition-metal chemistry. The basis set was set as 6-31G(d,p), an implicit, polarized continuum model for THF (moderate polarity solvent) was used to model the effects of a common solvent. The structural models of the free molecules and the zinc complexes were created and optimization was done on with the mentioned methods. In cases, where multiple possible conformations were possible, all conformations were modelled and optimized. In this section, I present only the lowest energy conformers to propose a binding mechanism of the molecules. Although, energies and energy differences between the free and bound states were calculated, I am do not discuss them, as my previous experience shows, that their reliability for prediction is moderate.

In the next section I am going to present the optimized models of the complexes and the free form of the molecules.

4.1.1. Models of quinoline-based compounds

Models of quinoline-based compounds are presented in *Figure 15.* (**GBPHQ1**), *16.* (**GBPAQ1**), *17.* (**GBPAQ2**) and *18.* (**GBPAQ3**). First of all, in all cases the Z isomers were energetically more favourable, which is desired from the aspect of our rational design. This is not a surprise, the previous study confirmed the extra stability of Z isomers in several cases by NMR.[10] In some cases, an isomer mixture formed, with Z being the majority, however, the two isomers are distinguishable in NMR and HPLC-MS. Knoevenagel condensations usually yield the more stable isomers, therefore, it is expected, that Z isomers will be formed. Looking at the optimized structures, they show, that in all cases, the free structures prefer an open conformer (*Fig. 15-18 left*), which is not surprising. Upon binding, a conformational change happens in the molecules turning them into a "closed conformer" (*Fig. 15-18, right*).
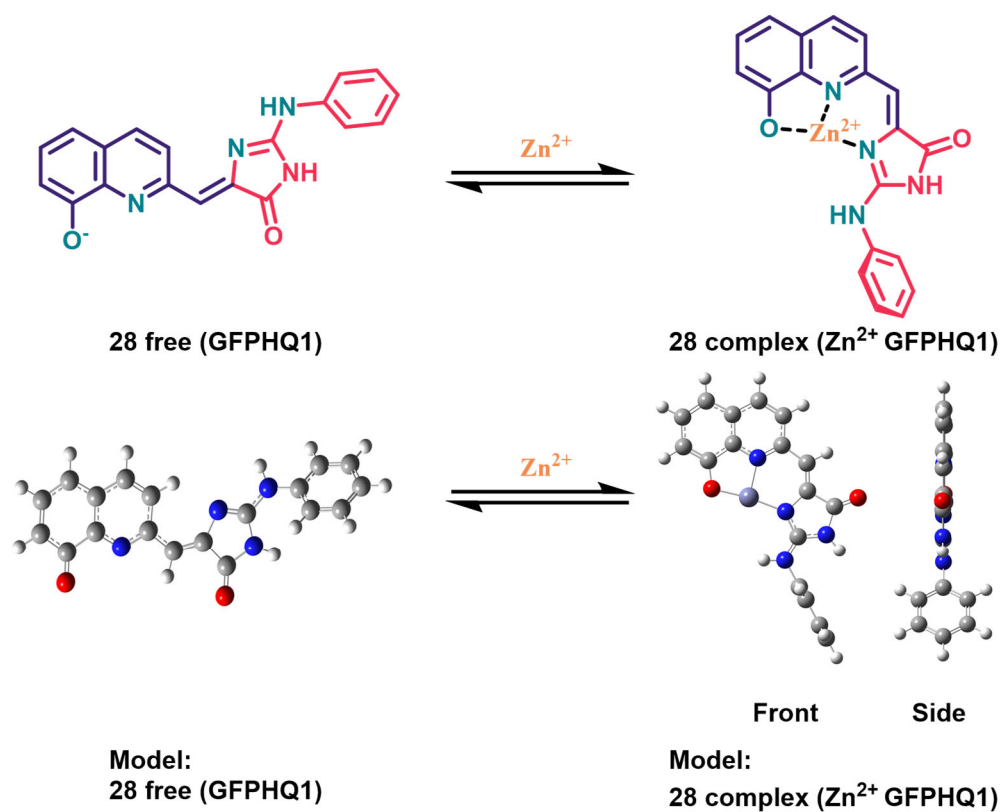
Figure 15. The free and complex forms of **GFPHQ1** (**28**). Top: schematic drawing of the structures based on the optimized models. Bottom: pictures of the optimized models of molecules. The deprotonated form of the molecule was considered.
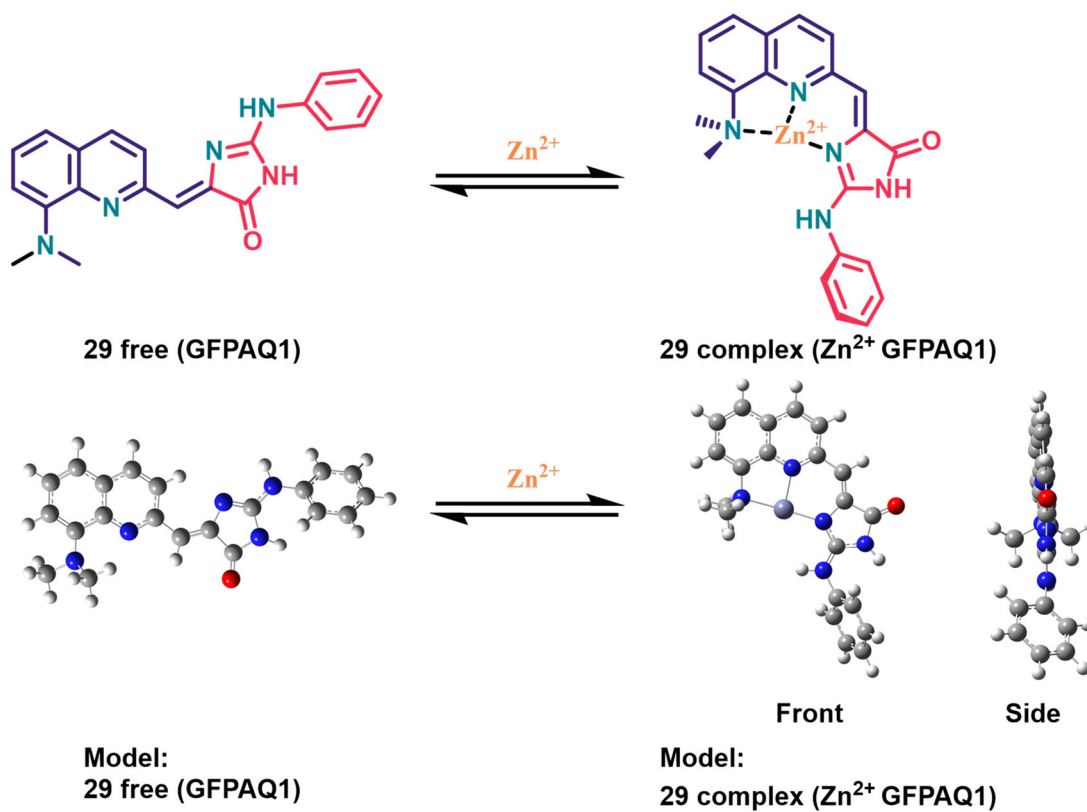
Figure 16. The free and complex forms of **GFPAQ1** (**29**). Top: schematic drawing of the structures based on the optimized models. Bottom: pictures of the optimized models of molecules.
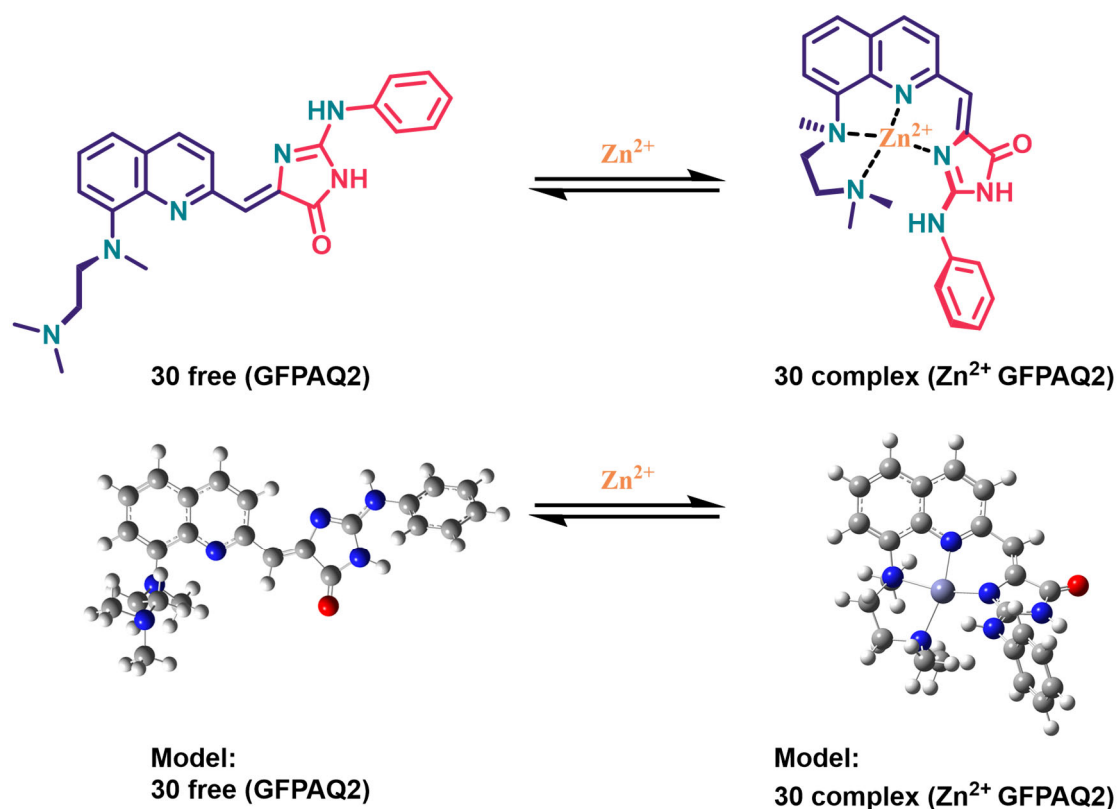
Figure 17. The free and complex forms of **GFPAQ2 (30)**. Top: schematic drawing of the structures based on the optimized models. Bottom: pictures of the optimized models of molecules.

Figure 18. The free and complex forms of **GFPAQ3 (31)**. Top: schematic drawing of the structures based on the optimized models. Bottom: pictures of the optimized models of molecules.

The models show that the 3D-structure of the free compounds is usually almost planar, only the aliphatic side-chains of **30** and **31** stand out of the plane and the -NHPh group on the imidazolone ring has a small torsion. The main scaffold of the complexes seems to show similar planarity, but -NHPh turns perpendicular to this plane. This may have on effect on optical properties. In **28** and **29** tridendate bindings show a possibly stable arrangement, while in the case of **30** and **31** the additional ligands contribute to form a tetragonal, tetracoordinate structure, which also looks stable. These calculations support our hypothesis, that the planned molecules will be able to bind to zinc ions in a favourable process.

4.1.2. Models of DPA-based compounds

Models of DPA-based compounds are shown in *Figure 19.* (**GBPDPA1**), *20.* (**GBPDPA2**) and *21.* (**GBPDPA3**). The models of the free scaffolds show, that the aliphatic nitrogen atom and methylene groups of DPA mostly stay in the plane defined by the scaffold of the fluorophore. The pyridyl groups stay perpendicular to this plane and stick out of the plane. In case of **32**, a stable, a tetradendate complex was stable, with a nitrogen of the GFP scaffold also binding to the metal. The complex of **33** has a tetracoordinate structure, the hydroxy group also plays a role in the coordination. Similar structural properties describe **34** too, however, in this case a tridendate coordination is observable.
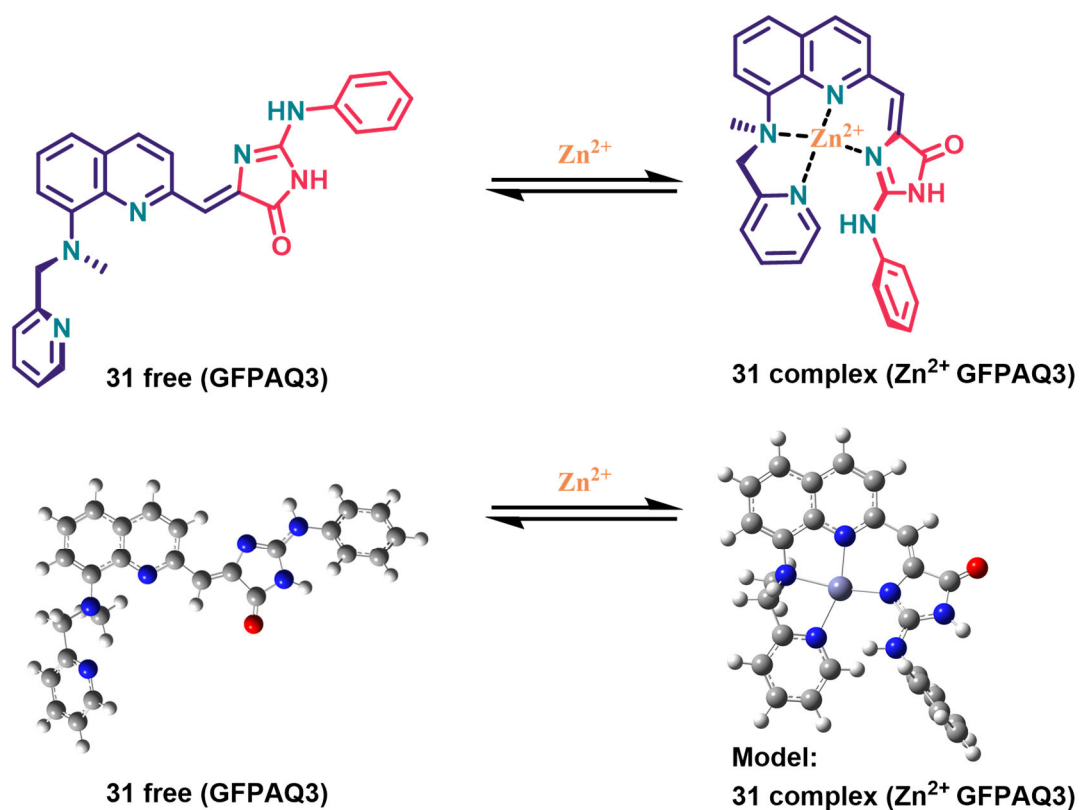

Figure 19. The free and complex forms of **GFPDPA1 (32)**. Top: schematic drawing of the structures based on the optimized models. Bottom: pictures of the optimized models of molecules. The diethylamino substituent was left out of the model to reduce the cost of calculations. The schematic drawing of the complex is exaggerated for better visibility.

33 free (GFPDPA2)

33 complex (Zn²⁺ GFPDPA2)

Model:
33 free (GFPDPA2)

Front

Side

Model:
33 complex (Zn²⁺ GFPDPA2)

Figure 20. The free and complex forms of **GFPDPA2** (**33**). Top: schematic drawing of the structures based on the optimized models. Bottom: pictures of the optimized models of molecules. The deprotonated form of the complex was considered.

34 free (GFPDPA3)

34 complex (Zn²⁺ GFPDPA3)

Model:
34 free (GFPDPA3)

Model:
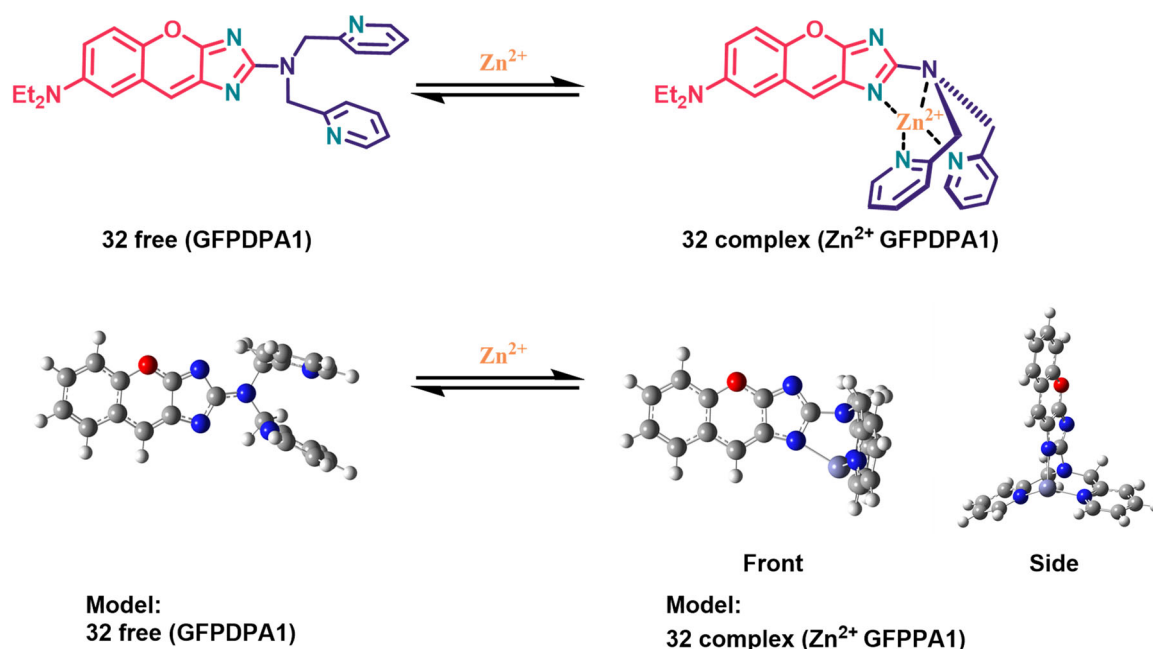**34 complex (Zn²⁺ GFPDPA3)**
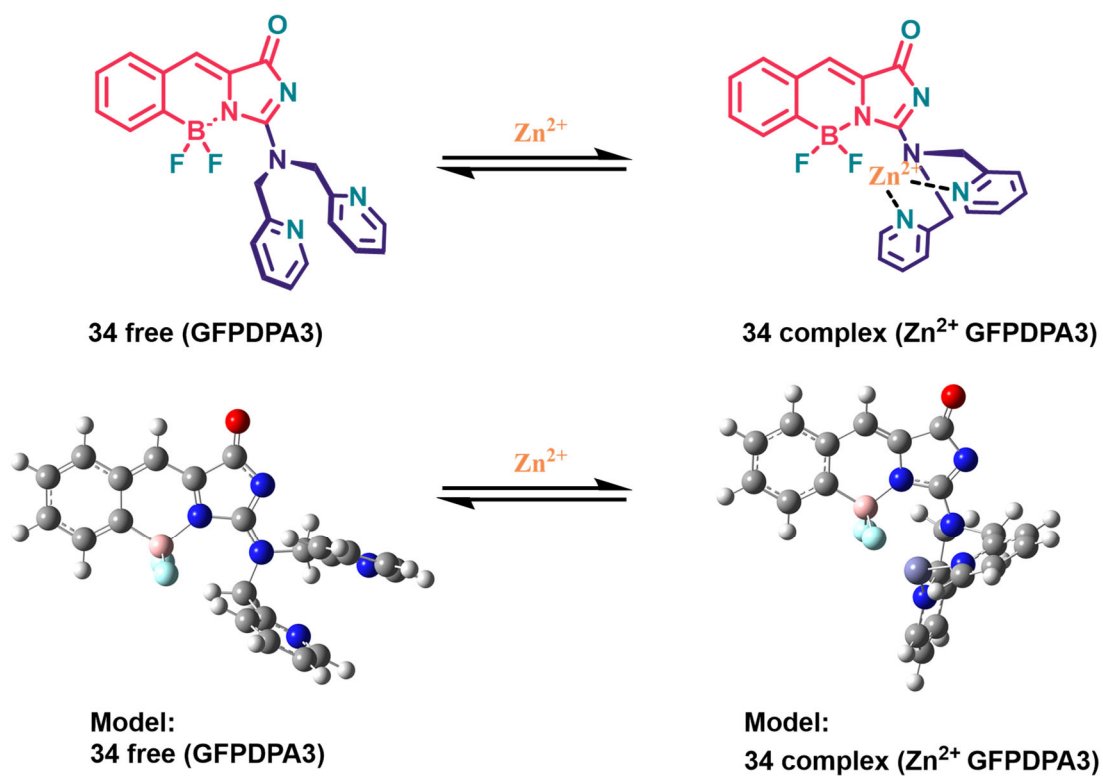
Figure 21. The free and complex forms of **GFPDPA3** (**34**). Top: schematic drawing of the structures based on the optimized models. Bottom: pictures of the optimized models of molecules.
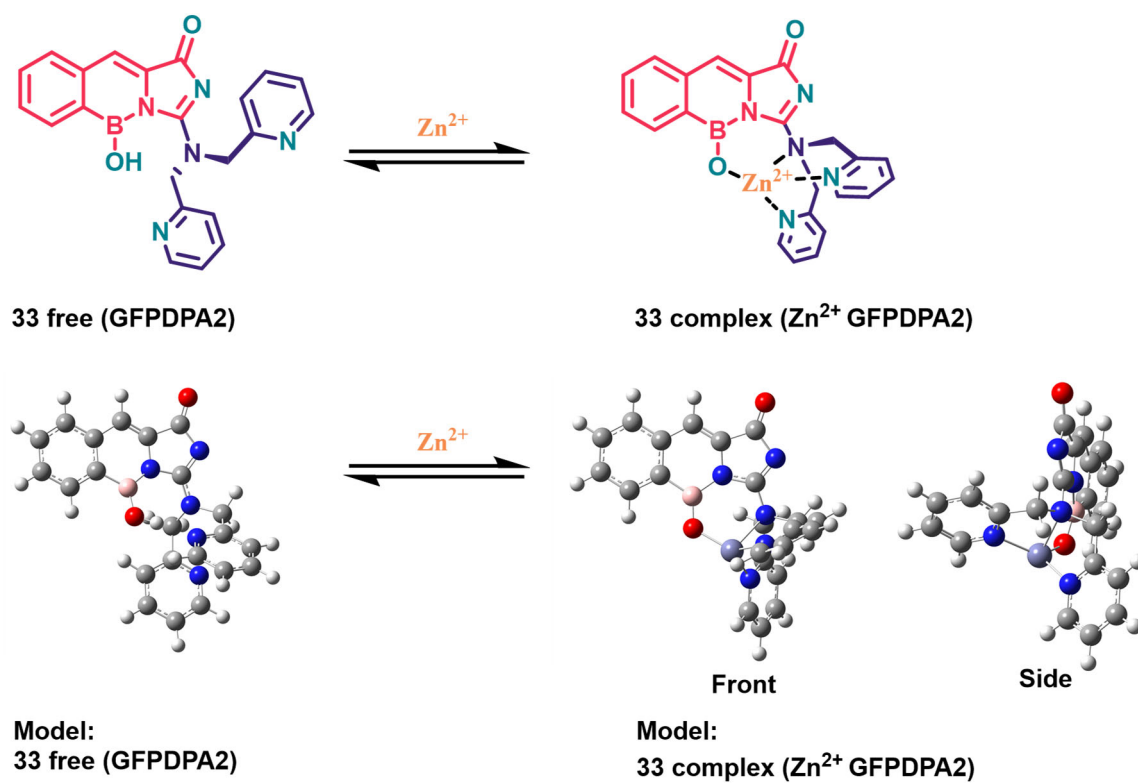
In summary, we modelled the free form and the complexes in all cases and chemically relevant structures were found to be stable, supporting the use of DPA. The aliphatic nitrogen of DPA always takes part in the binding, therefore, a PET or ITC quenching can be possible.

4.2. Synthetic work

In my synthetic work I prepared the target molecules in the most convenient way. Therefore, optimization and fine-tuning of the reactions were not the goal of the work, and no effort was made in this direction.

I have analysed the seven planned compounds from a retrosynthetic perspective, and I concluded, that the best strategy is to prepare the GFP chromophore analogue fluorophore scaffolds from 2-thiohydantoine and the desired amines as the first step, following the synthetic route discovered by our colleagues.[10] 2-Thiohydantoine (**18**), aniline (**35**) and dipycolylamine (**49**) are all commercially available, relatively inexpensive chemicals. After that, the most efficient way is to synthetize or purchase the aldehydes needed for the Knoevenagel reactions and then link the chromophores to the aldehydes in the final step.

Following this strategy, the synthesis of quinoline-based sensors (**28–31**) and DPA (**32–34**) sensors can be divided in two large sections. The whole synthetic plans are shown in *Scheme 4.* for quinoline-based sensors and *Scheme 10.* for DPA-based sensors in the respective chapters.

For sources of materials and the exact description of analytical and chromatographic methods see *Chapter 6. "Materials and methods"* and *Chapter 7. „Detailed description of the synthetic procedures".*

4.2.1. Synthesis of quinoline-based compounds

Since in the design of all quinoline sensors (**28-31**) the imidazol-4-one scaffold is connected to a phenylamino substituent, the transformation of thiohydantoin (**18**) into intermediate **36,** 2-phenylamino-imidazole-4-one was carried out as the first step according to *Scheme 3.*

Following the procedure described in the literature, I dissolved 2-thyohidantoine (**18**) in cold anhydrous dimethylformamide (DMF) under nitrogen atmosphere and slowly added it to a suspension of 1.1 eq. sodium hydride in DMF cooled to 0°C, in a three-necked flask equipped with a bubbler. Then, the solution was left to warm up to RT until deprotonation completed. Then, the solution was cooled again to 0°C, and 0.95 eq. of methyl iodide was added dropwise

under stirring, over the course of 30 minutes and then the solution was let to stir for an hour on room temperature. The reaction mixture turns into a pink suspension upon addition, which needs to be broken up from time to time. Multiple experiments show that the addition rate of MeI is the key to a successful reaction. LCMS samples show that faster addition leads to unreactive dimethyl intermediate **19b**, which makes work-up of the reaction mixture almost impossible. Slow addition results in 90% monomethyl (**19**) product ratio. In this case, the reaction mixture became a greenish suspension. The next step is the addition of 1.1 eq. aniline (**35**) without the isolation of intermediate **19** to. The reaction mixture is then heated to 110°C and left to stir overnight. This step needs to be carried out with great precautions, in a well-ventilated fume hood, as the leaving group in the S_N2 reaction is methyl mercaptan, which is an extremely repulsive smelling and toxic volatile gas. The reaction mixture is then poured onto crushed ice and the grey precipitate is filtered out and dried. A yield of 63% was achieved for the two-step procedure and the product contained practically no impurities. Purity and the structure were confirmed by LCMS and NMR (^{1}H, ^{13}C). The reaction was scaled up to yield 5 grams of product.
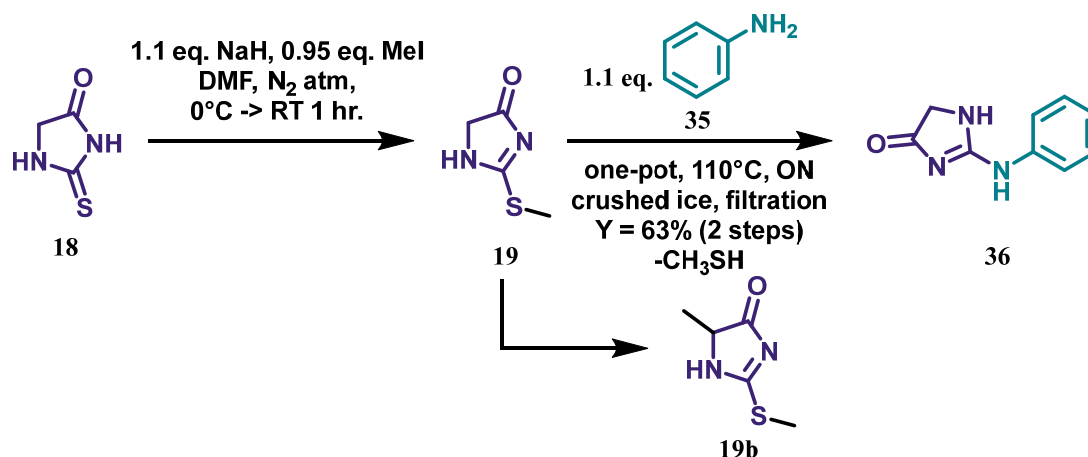
Scheme 3. Synthesis of common precursor 2-phenylamino-imidazole-4-one (**36**).

This product was then planned to get reacted in Knoevenagel condensation with the suitable aldehydes (**37,46,47,48**) to yield the desired quinoline-based sensor candidates (**28-31**). The synthetic plan to earn the quinoline-based sensors (**28-31**) is presented in *Scheme 4*. The transformations presented in the next sections were carried out according to this plan. When 2-formylquinoline derivatives were unavailable for the last, Knoevenagel step, they were all prepared from their 2-methylquinoline precursors, since these compounds were relatively easy to prepare.

An interesting observation was made, that although in the case of all final products (**28-34**) NMR spectra confirmed the structures, peaks in ^{1}H spectrum were broad, while ^{13}C spectrums could not be recorded. The bond between C2 of imidazolones and the nitrogens connected to them has a pseudo-double bond nature, resulting in a restricted rotation. We have found out, that measurements at room temperature do not give good spectra, however, tempering the sample to 80 °C results in sharp peaks and good ^{13}C spectra. Unfortunately, due to limited access to NMR spectrometers capable of sample temperation, only in a few, more complicated cases (**32, 33**) were spectra recorded at 80 °C.

After the Knoevenagel step, LCMS has shown one isomer in all cases, which is the Z isomer, based on previous experience. Further NMR measurements will be carried out to confirm this.
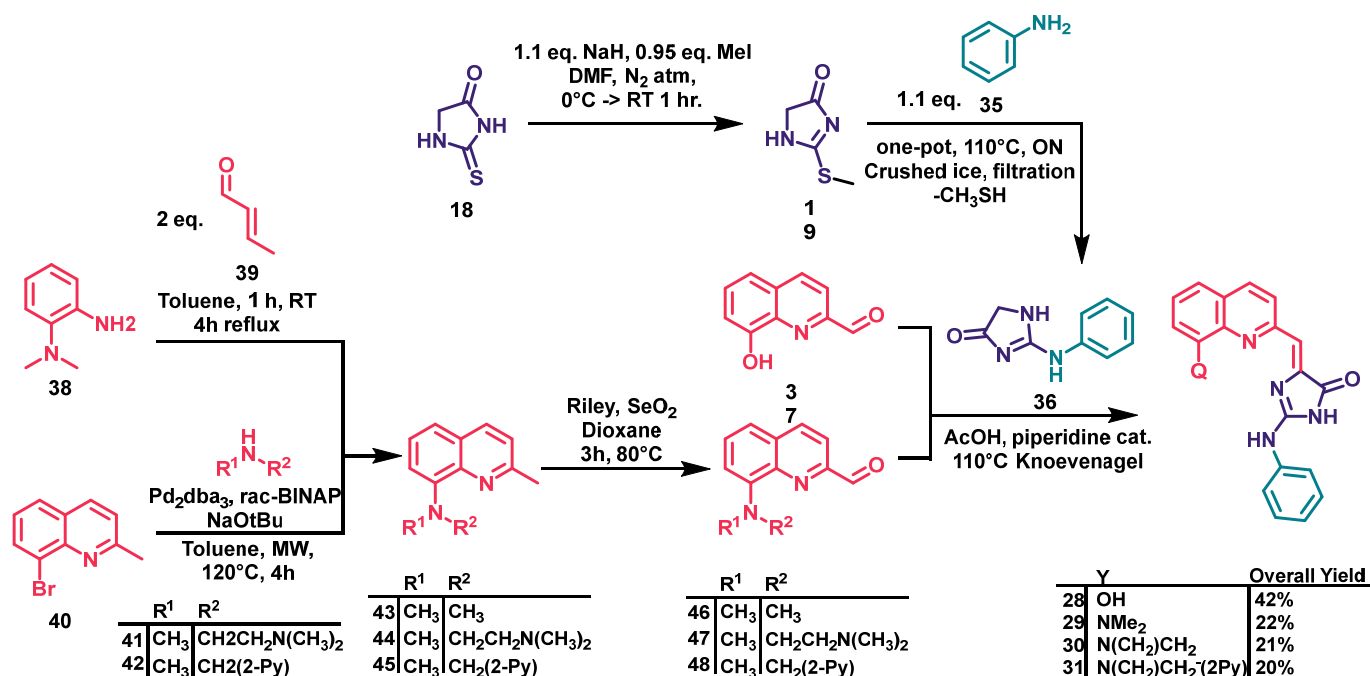
Scheme 4. presentation of the complete synthetic plan to earn quinoline based sensors. Violet marks the aldehydes used in the final Knoevenagel step and their precursors.

4.2.1.1 Preparation of GFPHQ1(28)

The first sensor, **GFPHQ1** (**28**) was the easiest and most convenient to prepare, since the needed aldehyde was commercially available for a reasonable price. The starting material, 2-phenylamino-imidazol-4-one (**36**) was dissolved in acetic acid and 1.05 eq. of 2-formyl-8-hydroxyquinoline (**37**) was added in solid form. Catalytic amount of piperidine was added and the mixture was heated to 110 °C in a closed tube. Based on LCMS, the Knoevenagel reaction seen on *Fig. 5.* was complete in 2 hours. After the evaporation of solvents, the product was purified with preparative HPLC (method A see *Chapter 6.2.3*). The

yield was 68% , purity was 99%. Purity and structure were confirmed by LCMS and NMR. The overall yield of the process is 42%. **GFPHQ1** (**28**) is a bright orange powder. The aqueous solution of the compound is orange coloured and shows no fluorescence. Upon addition of zinc salts, yellow fluorescence is visible under UV light.
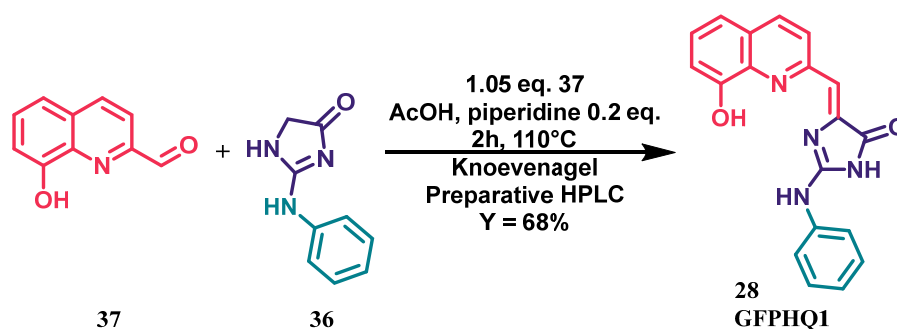
Scheme 5. Preparation of **GFPHQ1** (**28**).

4.2.1.2. Preparation of **GFPAQ1** (**29**)

The preparation of the simplest 8-aminoquinoline based sensor was more complicated. 2-formyl-8-dimethylaminoquinoline (**46**) is not commercially available. However, authors of an interesting publication[69] were investigating 8-dimethylaminoquinolines as "caging" scaffolds, which are also useful in microscopy. A method for preparation of 2-formyl-8-dimethylaminoquinoline was reported. We reproduced the Skraup-Doebner-Von Miller quinaldine synthesis as shown in *Scheme 6.*
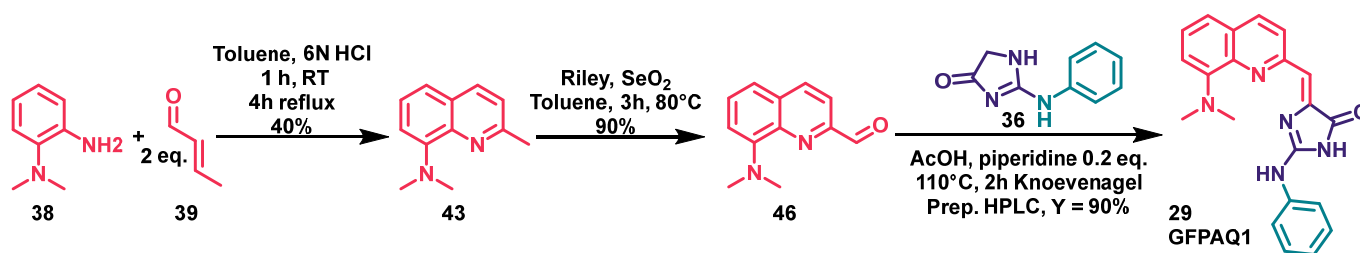
Scheme 6. Preparation of **GFPAQ2** (**29**).

To the commercially available 2-dimethylaminoaniline (**38**) 2 eq. of crotonaldehyde (**39**) was added. 6M HCl was added and the mixture was let to stir for one hour on RT, then toluene was added stirring was continued for 4 hours on 110°C. After removing the organic layer in vacuo, the aqueous layer was neutralized and extracted. The solvents were evaporated, and the product was purified by chromatography. A yellow oil was earned representing 8-dimethylaminoquinaldine (**8-DMAQ**, **43**, 97% purity, LCMS and NMR confirmed the purity and the structure).

The following step is a Riley oxidation also reported in the same publication. In this case SeO$_2$ was suspended in dioxane and heated to 80°C, then 1 eq. of **8-DMAQ** (**43**) was added to the reaction mixture. It was stirred for 3 hours at this temperature, until HPLC-MS has shown the completion of the reaction. The product was purified by chromatography to yield a dark oil (**46**) with 95% purity and 90% yield. Purity and structure were confirmed by LCMS and NMR.

Finally, the desired 8-dimethylaminoquinoline-2-carbaldehyde (**46**) was carried into Knoevenagel condensation in the same way as described in the previous case to yield the final product **29, GFPAQ-1**. Purification was also carried out on prep. HPLC (method A). The resulting bright red powder is >99% (LCMS) and its structure was also confirmed by NMR. The overall yield of the process was 22%. The aqueous solution of the compound is deep red coloured and shows no fluorescence. Upon addition of zinc salts, greenish fluorescence has become visible under UV excitation.

4.2.1.3. Preparation of **GFPAQ2 (30)**

The needed 8-(*N,N',N*"-trimethyl-ethylene diamine)-quinoline-2-carbaldehyde (**47**) is not commercially available, so we had to prepare it. Unfortunately, there was no usable synthesis reported in the literature. Since 8-bromoquinaldine (**40**) is a commercially available and affordable chemical, it looked rational to employ a Buchwald-Hartwig coupling with the similarly inexpensive *N*1,*N*1,*N*2-Trimethylethane-1,2-diamine (**41**) visible in *Scheme 7*. Standard conditions of Buchwald-Hartwig couplings were used, in presence of Bis(dibenzylideneacetone)palladium(0) (Pddba$_2$) as a catalyst and racemic BINAP (2,2′-bis(diphenylphosphino)-1,1′-binaphthyl) as a ligand. In the presence of NaOtBu base and argon atmosphere, the reaction took place in the course of four hours under microwave irradiation. Since the product did not elute well on silica gel TLC, solvents were removed, and the crude product was absorbed onto alumina then eluted on a plug of alumina with DCM/MeOH to earn intermediate **44**. NMR spectroscopy and MS confirmed the structure; however, purity was only 90%, but this was sufficient for the next step.

The next step was again a Riley oxidation carried out similarly to what was described in the previous section. However, to my surprize, after one hour of heating, no reactant (**44**) was present in the reaction mixture, but besides the desired aldehyde (**47**), a side-product (**47b**) formed, which had the molar weight of the overoxidated carboxylic acid derivative according to LCMS data (47/47b = 60/40%). After the evaporation of solvents, the solid residue was dissolved again and absorbed on alumina. After elution on an alumina plug, the desired

product (**47**) was only 50% pure and new impurities formed upon decomposition. This crude product was then repurified on preparative HPLC (method A). The lyophilized final product was 98% pure (LCMS), however, the yield of the step was only moderate (15%) due to the side reaction and decomposition upon purification. Upon waiting for NMR measurement, the sample was left out for days, in which the compound decomposed in DMSO.
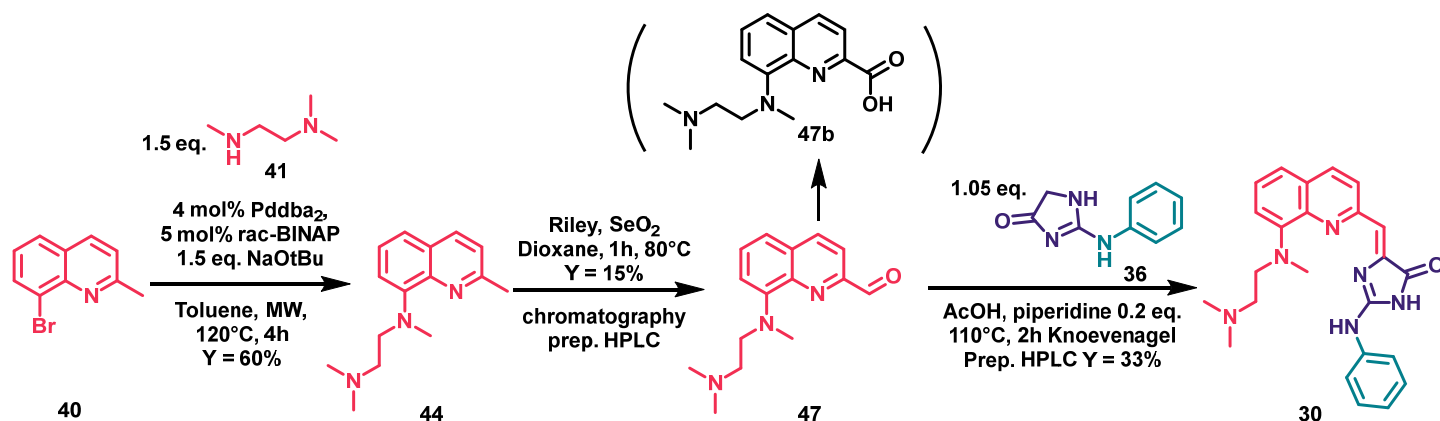
Scheme 7. Preparation of **GFPAQ2 (30)**.

Then the final Knoevenagel step was carried out as described in previous examples. Purification was made on prep. HPLC (method A). The product had 97% purity (LCMS) and was isolated in the form of an orange powder. The cumulative yield of the process is only 2.1 %. Unfortunately, the product decomposed in solution in the NMR sample too, while waiting for measurement, and due to our limited access under the current situation, it was not possible to record it again before the deadline of this essay.

4.2.1.4. Preparation of **GFPAQ3 (31)**

During the preparation of **GFPAQ3 (31)** I faced similar synthetic issues, since aldehyde **48** is not commercially available. However 2-(methylamino)pyridine (**42**) is also a very accessible chemical. An analogous strategy to the synthesis of **GFPAQ2 (30)** was applied as shown in *Scheme 8.*

A Buchwald-Hartwig cross-coupling reaction was employed analogously to the previous case. The substituted 8-aminoquinaldine product (**45**) was purified on silica gel column chromatography to achieve a yellow oil with 96% purity and a yield of 70% (LCMS, NMR).

The Riley oxidation was carried out again analogously to the previous case, however, in 3 hours the conversion complete and no overoxidated side-product was observable. After a filtration trough celite to remove the inorganic solids, the crude product was purified on silica

gel column chromatography. The product was an orange oil in 97% purity with a yield of 85%. (LCMS, NMR)
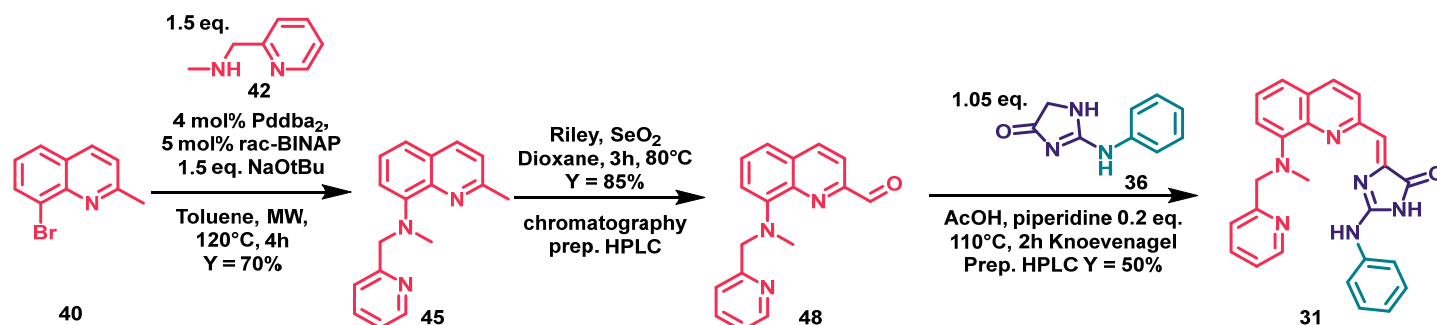
Scheme 8. Preparation of **GFPAQ3** (**31**).

Finally, this product was carried into the final Knoevenagel condensation step. This resulted in a bright orange powder after purification on prep. HPLC (method A), in >99% purity (LCMS, NMR), with a yield of 50%. This renders the overall yield of the process to 20%. The orange-coloured aqueous solution of the compound emits no fluorescence, however, upon addition of zinc ions a yellow fluorescent light can be observed under UV-lamp.

4.2.2. Synthesis of DPA-based compounds

The synthesis of DPA-based sensors (**32,33,34**) is based on their common precursor 2-(dipicolylamino)-imidazol-4-one (**50**) as shown in *Scheme 10.* summarizing the overall synthetic plan for preparing **GFPDPA** sensors.

Preparation of the common precursor was analogous to preparation of 2-phenylamino-imidazole-4-one (**36**) described in *Chapter 4.2.1,* but dipicolylamine (**DPA, 49**) was used instead of aniline (**35**). The process is illustrated in *Scheme 9.*
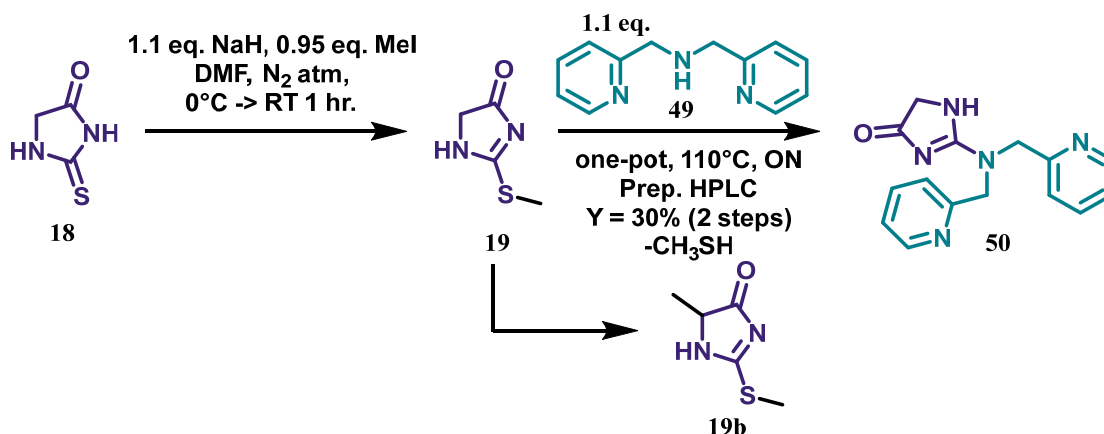
Scheme 9. Synthesis of common precursor 2-dipicolylamino-imidazole-4-one (**50**).

However, in this case the product did not precipitate upon pouring onto crushed ice in spite of the careful addition of iodomethane. Consequently, after evaporation of solvents, purification was carried out by the means of preparative HPLC. The standard acidic buffered method (LCMS method A) did not result in good chromatographic separation on analytical LCMS system, while a neutral buffer (NH$_4$HCO$_3$, (LCMS method B) was giving promising results on LCMS. Therefore, components were separated using this buffer on prep. HPLC. Good separation was earned, and the product was isolated in 100% purity, its structure was confirmed (LCMS, NMR). 2-Dipicolyl-imidazole-4-one (**50**) is a black sticky solid after lyophilization. This reaction gives a lower yield of only 29% for the two steps. This can be attributed to the larger steric hindrance of the nitrogen of **DPA** (**49**), its worse nucleophilicity and mostly to the need of chromatographic separation. Chromatography also limits the scalability of the reaction. A maximum of 400 mg of intermediate (**50**) was produced in one batch.

Precursor of **GFPDPA1** (**32**) for the Knoevenagel condensation is 4-(diethylamino)salicylaldehyde (**51**), which is commercially available and reasonably priced, therefore I did not bother synthetizing it. 2-formylphenylboronic acid (**52**), precursor aldehyde for **GFPDPA2** (**33**) is also a common chemical due to its frequent application in cross-couplings, thus it was purchased as well. Precursor of **GFPDPA3** (**34**), potassium (2-formylphenyl)trifluoroborate (**53**) is, however, not a common chemical and it is rather expensive. Although previous results were earned with purchased chemicals, I have tried preparing this precursor from 2-formylphenylboronic acid (**52**). The purification although was unsuccessful. The crude product was tried in the Knoevenagel reaction without success. Further attempts will be made for purification of potassium (2-formylphenyl)trifluoroborate (**53**) or its preparation on alternative route to synthetize **GFPDPA3** (**34**). At the moment of writing this essay, I could not successfully prepare my last planned sensor. Details of the syntheses will be presented in the next sections.

	Name	Overall Yield
32	GFPDPA1	2%
33	GFPDPA2	12%
34	GFPDPA3	–
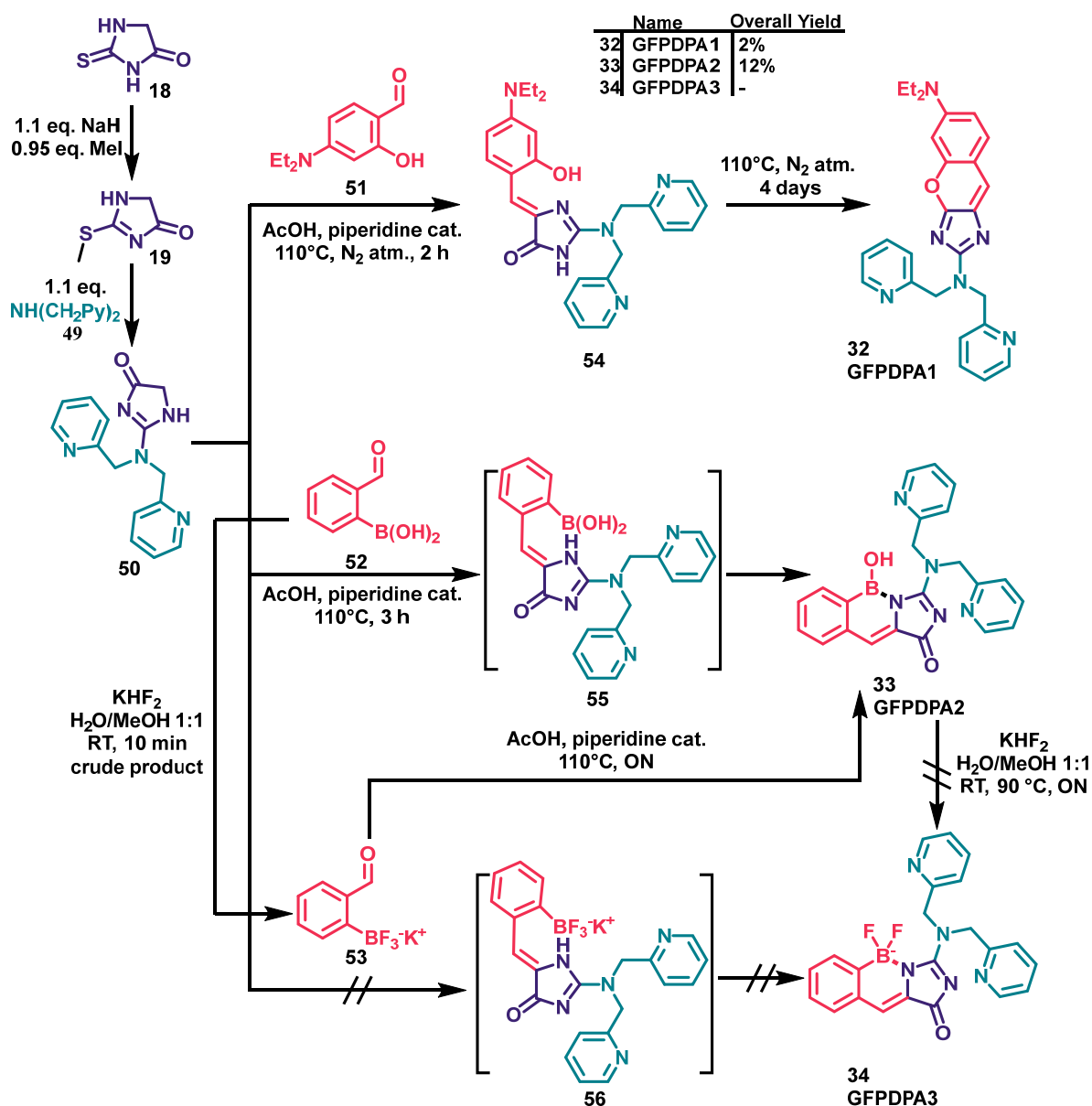
Scheme 10. presentation of the complete synthetic plan to earn DPA-based sensors. The plan shows unsuccessful and unwanted routes as well.

4.2.2.1. Preparation of **GFPDPA1** (**32**)

As simple as it may seem, the synthesis of **GFPDPA1** (**32**) hides challenges. A first trial was carried out in a normal flask according to the previously described Knoevenagel procedure employing 4-(diethylamino)salicylaldehyde as the aldehyde component. However, according to LCMS, instead of the expected intermediate 2-(dipicolyl)-5-(4-(diethylamino)-2-hydroxybenzylidene)-imidazol-4-one (**54**) mainly an other product was forming shown in *Scheme 11*. Based on the measured molecular weight, I concluded, that the reaction gave an oxidized product **57**.
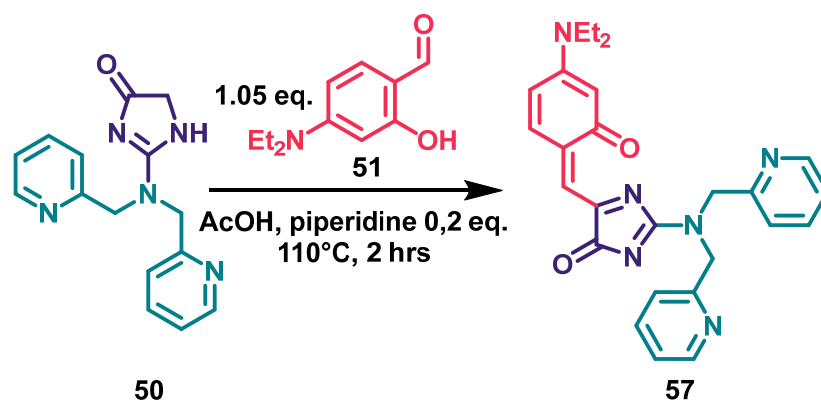
Scheme 11. results of the first experiment to synthetize GFPDPA1.

The oxidized side-product (**57**) do not participate in further ring-closure reaction. To avoid the undesired oxidation, I have tried the most convenient idea with success. A reaction was started with the same conditions, but under inert N_2 atmosphere, and it proceeded in 3 hours to the expected intermediate (**54**) as shown in *Scheme 12*.
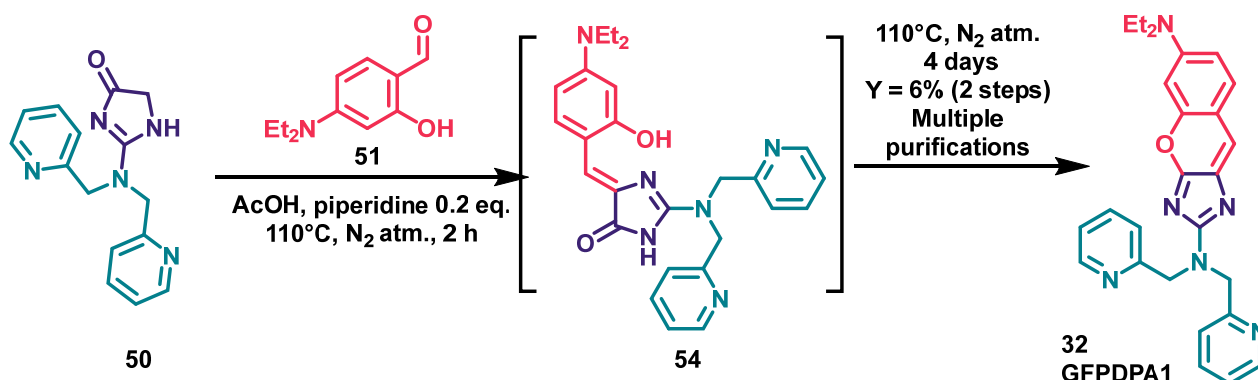
Scheme 12. Second, successful experiment on preparation of **GFPDPA1** (**32**).

The intermediate (**54**) was not isolated, but heating was continued for four more days. A final conversion of 33% to intermediate **54** and 66% to **GFPDPA1** (**32**) was achieved. The reaction mixture started to develop some decomposition products; therefore, acetic acid was removed *in vacuo* and the reaction mixture was purified on preparative HPLC (method A: 0.2% TFA in water 90% → MeCN 90%). Another challenge emerged at this point. The unified collected fractions were analysed with LCMS and based on the UV-VIS chromatogram and MS data; the solution contained 100% of **GFPDPA1** (**32**). After evaporating the MeCN, the solution was lyophilized. The lyophilized product was analysed again with LCMS. To my biggest surprise, 20% of the product (**32**) decomposed to the unwanted intermediate (**54**). I suspected, that the trifluoroacetic acid from the HPLC eluent, or the heat applied (40 °C) when removing MeCN could have led to the decomposition. On TLC I have observed two different spots, and

I attempted a further purification by flash chromatography, however, I could only partially purify the product. At this point I did not want to try another preparative HPLC run with the same eluents being afraid by achieving the same results. An LCMS run with neutral buffer (LCMS method B) was started and results were rather interesting: the main impurity (**54**) was well separated, and several other minor impurities were observed. Prep HPLC was employed in order to repurify the product in neutral buffered eluent (method B). The pure fractions were collected and analysed with LCMS. The MeCN was removed in high vacuum, on lower temperature (25 °C) in order to avoid decomposition. The aqueous residue was lyophilized and stored at -20 °C. LCMS and NMR spectroscopy confirmed the structure with >99% purity. The product is a bright yellow powder, which shows strong greenish fluorescence in aqueous solutions and a fluorescence shifted towards turquoise in less polar solvents. The fluorescence is visible even in daylight, which awoke concerns in me regarding the quenching effect of DPA on this scaffold.

Finally, the overall yield of the Knoevenagel step was only 6%, but this yield could be optimized in the future by applying microwave reactor and purifying right away with the neutral buffers on prep. HPLC. This way, I estimate, that a yield of 50-70% could be achieved. The yield of the complete process was 2%.

4.2.2.2. Preparation of **GFPDPA2** (**33**)

Synthesis of **GFPDPA2** (**33**) follows the same Knoevenagel procedure as described before. The reaction leads to complete conversion in one hour yielding the final product after the ring-closure (**GFPDPA2**, **33**). Open intermediate **55** visible in *Scheme 13.* is not detectable at any point in LCMS based on its molar mass, leading me to the conclusion, that it is a very reactive intermediate.
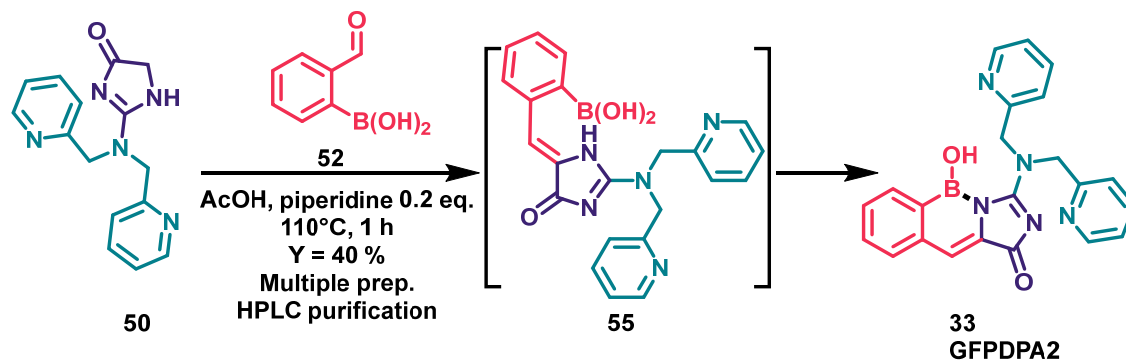
Scheme 13. Synthesis of **GFPDPA2** (**33**).

Purification of the reaction was hiding surprises again. Acetic acid was evaporated and purification on prep. HPLC was done with standard acidic buffer (method A). The NMR spectroscopy on elevated temperatures revealed, that the uniformly looking product on LCMS was impure. LCMS run on neutral buffer (LCMS method B) was carried out to reveal some minor impurities. A second preparative HPLC was carried out with neutral buffer (method B). The resulting product (**GFPDPA2**, **32**) was a completely pure beige coloured solid (LCMS). The yield was moderate, 40% after all the purifications. NMR measurements on elevated temperature were measured to determine the structure. Based on ^{1}H, ^{13}C, HMBC, HSQC, NOESY and TOCSY measurements, the structure was confirmed. Aqueous solution of the compound is almost colourless and emits no fluorescence under UV irradiation. Upon addition of zinc, a bright blue fluorescence can be observed under UV light. The yield for the complete process is 11.6%.

4.2.2.3. Experiments for the preparation of **GFPDPA3 (34)**

My main plan was, that I will produce the trifluoroborate precursor (**53**) of **GFPDPA3** (**34**) from the readily available boronic acid (**52**). The most convenient method for preparing organotrifluoroborates from organoboronic acids is by reacting them with KHF$_2$.[70] This method was reported in the literature in 1967. I tried to reproduce it and dissolved 2-formylphenylboronic acid (**52**) in 1:1 mixture of water and methanol, then added 4 eq. of potassium bifluoride to the mixture. According to HPLC, the reaction took place under 10 minutes at room temperature as seen in *Scheme 14*.
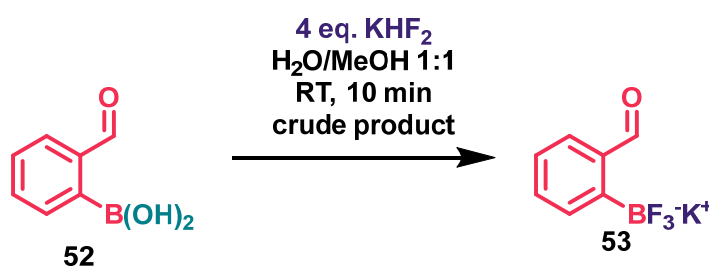
Scheme 14. Preparation of potassium (2-formylphenyl)trifluoroborate (**53**).

Purification the product on the other hand was much more challenging. The product is contaminated with inorganic salts such as KHF$_2$, KF, KOH. Unfortunately, the product co-precipitates with all salts. In theory, multiple extraction with acetone is able to purify the product to some extent. However, since I hypothesized, that the inorganic impurities will not affect the next Knoevenagel step, I did not put effort into further purification. An important

remark is, that precautions are needed, when working with KHF$_2$, since it produces in situ HF, which have etched the glassware I was working with.

The next step was tried with the impure reactant (**53**), but the reaction only yielded **GFPDPA2** (**33**) to my surprise (*Scheme 15.*). A subsequent hydrolysis of **34** may be a consequence of the impure starting material, but the topic was not further investigated. A book section from 2013 suggests an alternative method for preparing organic trifluoroboronate salts, with efficient purification methods[71]. However, in the lack of time, this was not yet tried.
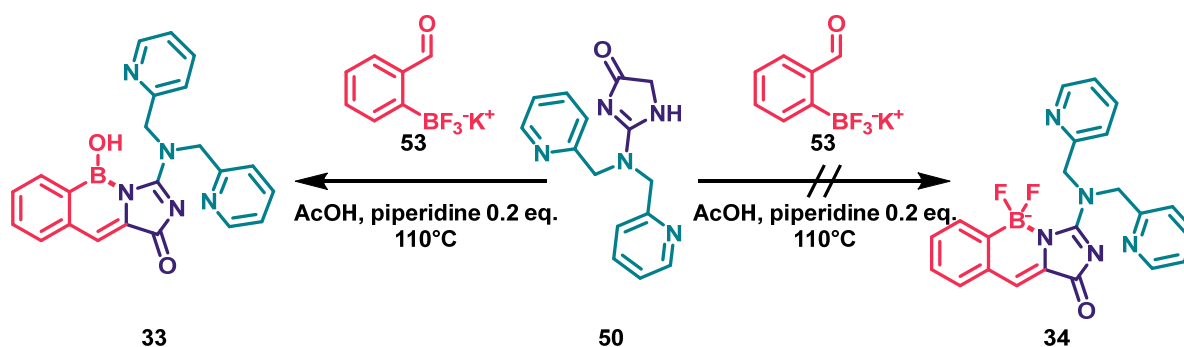
Scheme 15. Unsuccessful trial of the synthesis of **GFPDPA2** (**33**).

I have made one more experiment, in which I have tried transforming **GFPDPA2** (**33**) into **GFPDPA3** (**34**) directly (*Scheme 16.*). **GFPDPA2** (**33**) was dissolved in H$_2$O/MeOH and 4 eq. of KHF$_2$ was added. However, no conversion was observable either at room temperature, either upon heating up to 110°C for a night.

To this point, the synthesis of **GFPDPA3** (**34**) was unsuccessful, but more attempts will be made in the future with the alternatively prepared precursor (**53**) or by purchasing the precursor from commercial sources (available at TCI)

4.2.3. Summary of the synthetic work.

In summary, as a synthetic chemist, my goal was the production of the planned new compounds. An efficient retrosynthetic approach was employed, and synthetic routes were rationally created for all new compounds based on intuition and literature reports. In six out of seven cases, the target compounds were successfully prepared (**28**–**33**), and the emerging synthetic problems were resolved, therefore, I rate my work successful in this field.

4.3. Analytical experiments

The six successfully prepared sensors (**28-33**) were undertaken of experiments in order to determine their photophysical properties and the dissociation constants of their complexes with Zn^{2+}.

4.3.1. Determination of the photophysical properties of the produced probes

First of all, I intended to see whether the compounds show activity for Zn^{2+}. In order to investigate this, spectrofluorometric measurements were undertaken. Fluorescent spectra of the prepared sensors were measured in two buffer systems: HEPES (0.1M, pH 7.4) solutions containing no Zn^{2+} and ~1 mM Zn^{2+}. Concentration of the sensors were between 1 and 100 mM, and the iris of the instrument was configured in order to keep intensity in the linear range of the detector. The procedure I followed consisted of dissolving 1 mg (measured precisely, but not accurately) of the compounds in 2 ml of DMSO, then diluting 100 μl of this stock solution to 2 ml with each buffer. The UV-VIS spectra of the resulting solutions were recorded and the solutions were further diluted with buffers until the absorbance was below 0.1. This way, we earn a Zn^{2+} containing solution of the sensor and a metal-free solution. The two solutions contain the sensor compound in the same concentration. The spectra recorded in the maximum emission wavelength (determined by emission scan) of these solutions were recorded, spikes were removed, and the spectra were smoothed. The intensities were normalized to 1 mM sensor concentration and also with the area of the used iris. The spectra recorded this way is plotted on *Fig. 22.*

A number of conclusions can be drawn from these spectra. First, all prepared sensors show activity upon the addition of Zn^{2+} to the solution, except of **GFPDPA2 (32)** This means, that in the cases of (**28-31 and 33**) the PET / ICT quenching mechanism works, and the molecules are able to create complexes with Zn^{2+}. In the case of **33**, the most probable explanation to the lack of activity is, that DPA cannot quench the fluorescent scaffold. This may be due to the electron-rich fluorescent scaffold, that has a highly extended aromatic part with a high energy HOMO. The small intensity decrease observable on *Fig. 22., bottom left* can be attributed to the self-absorption of the inorganic ions.

It is also sinteresting to observe the intensities of the fluorescence in all cases. Although, the increase in fluorescence is significant in all cases, the absolute value of **GFPHQ1 (28)** is very low, while **GFPAQ1 (29)** shows one order of magnitude higher intensity. Although **GFPAQ2**

(**30**) and **GFPAQ3** (**31**) has the same aminoquinoline-based scaffold, they show a ten- and hundred-fold higher fluorescent intensity. In all cases, the concentration of Zn^{2+} was enough to be sure, that all molecules are in complexed form. Therefore, a conclusion can be drawn, that the ethylenediamine side-chain directs the complexation in such way, that it causes more efficient extinction of the PET-effect, while the side-chain containing a pyridyl group has a much stronger effect in this regard, maybe even acting as a part of the fluorophore.
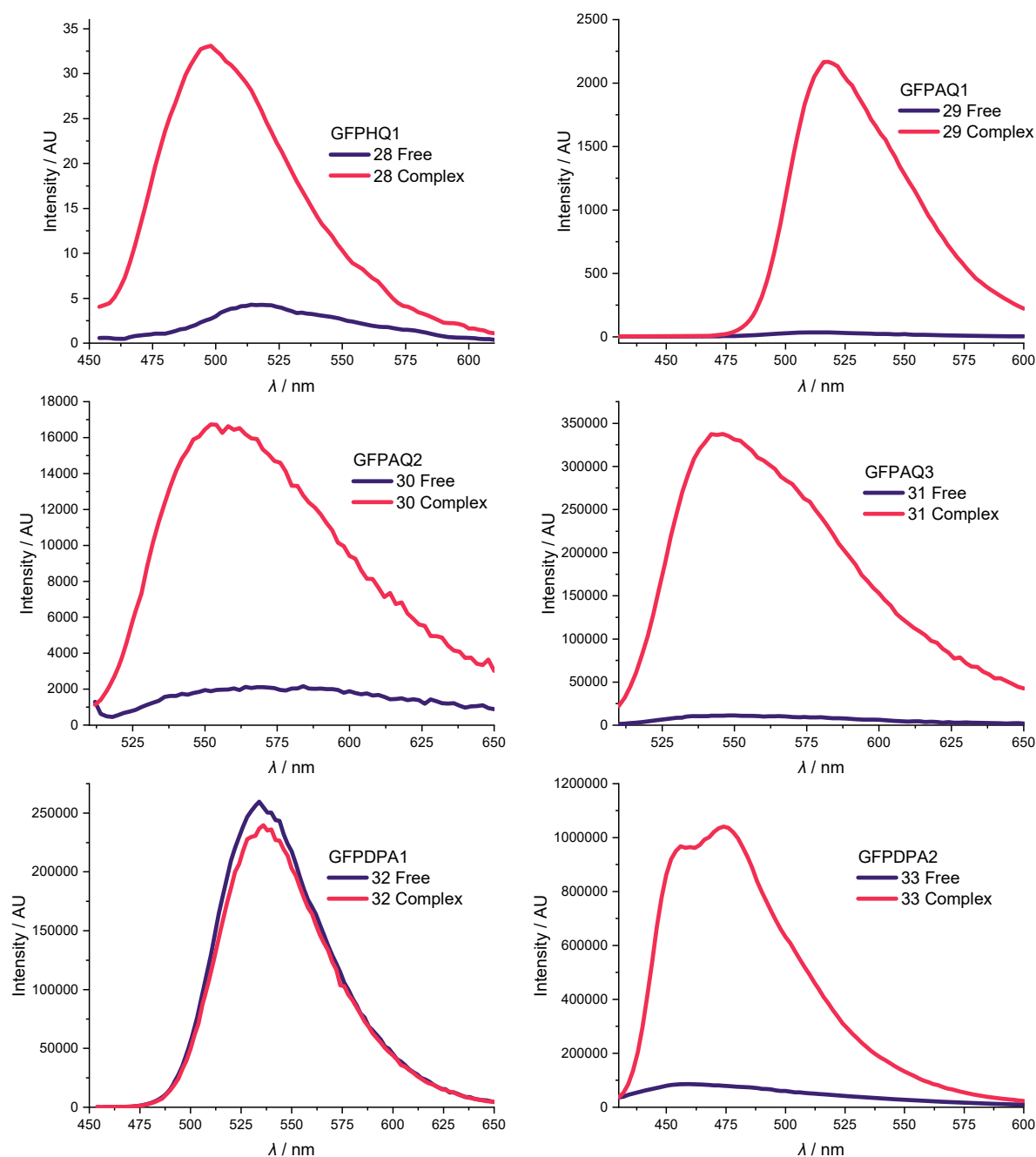
Figure 22. Fluorescence spectra of the prepared sensors in pH 7.4 (0.1 M) HEPES buffer normalized with concentration to 1 mM and slit area. Spectra were recorded at the maximum excitation wavelength. Violet represents the spectra of solutions containing no Zn^{2+}, while pink represents the spectra of solutions containing 1 mM Zn^{2+}.

It can be also observed, that while **GFPDPA1** (**32**) has shown no activity, it exhibits a very high fluorescent intensity. Finally, **GFPDPA2** (**33**) has the highest intensity of all prepared compounds, which makes it the most promising for the applications in microscopy. However, not only the absolute value of fluorescence is important, but rather the increase in the intensity. In the case of **GFPHQ1, GFPAQ2** and **GFPDPA2** (**28,30,33**) a moderate increase (7-12x) was observable in fluorescence, **GFPAQ3** increases a larger amount (30x) and finally **GFPAQ1** (**29**) has the largest amount of increase in fluorescence intensity (60x). All of the increment values suggest that these compounds could be used for fluorescent Zn^{2+} imaging based on their photophysical properties. This experiment has a very high value, as it confirmed my hypothesis and rational design. The calculated photophysical properties and fluorescent enhancement factors (FEF) are given in *Table 1*.

The wavelength of the emitted fluorescence is similar in all cases. Quinoline-based probes (**28-31**) emitted light between 500-575 nm, which is absolutely good for microscopy. **GFPDPA2** (**33**), the other promising probe has an emission wavelength around 480 nm, which can be lower, due to the radically different scaffold. This value is also completely acceptable for microscopy.

The UV-VIS absorptions spectra of the molecules were also measured in order to determine the absorption maxima, which are also given in *Table 1*. As it is shown, all absorption maxima are above 350 nm, which predicts, that all compounds may be applicable in 2P measurements, however, the value of **GFPAQ1** (**29**) and **GFPDPA2** (**32**) are under 360 nm, which may raise problems in the application.

4.3.2. Determination of apparent dissociation constant by fluorescent titration

Another important property of the fluorescent probes is their affinity to the analyte. In cellular medium this is represented by the apparent dissociation constant of the complex. In the next step I wanted to measure the value of K'_d for probes showing activity upon addition of Zn^{2+}.

To determine the K'_d for Zn^{2+} I followed a modified version of a procedure reported in the literature. [72] Into a cuvette, 3 ml of the previously mentioned zinc-free solution was added. Before every fluorimetric measurement, a small aliquot of the solution is discarded and refilled with the previously mentioned (1 mM) Zn^{2+} containing solution. The process is repeated until no more increase in fluorescence can be observed after increasing the Zn^{2+} concentration. This way, the Zn^{2+} concentration increases in every step. The actual concentration can be easily calculated using *eq. 12*.

$$[Zn^{2+}]_n = \frac{[Zn^{2+}]_{n-1} \times (V_{total} - V_{changed})}{V_{total}} + (V_{changed} \times C_{Zn\ solution})$$ (12)

$[Zn^{2+}]_n$ is the actual Zn^{2+} concentration after the nth change step, while $[Zn^{2+}]_{n-1}$ is the concentration of the previous step. $V_{changed}$ is obviously the volume, that we exchanged, while $c_{Zn\ solution}$ is the concentration of the Zn^{2+} containing solution (~ 1mM). The concentration of the sensor is the same in both solutions, therefore it is kept constant. The recorded fluorescent spectra with various Zn^{2+} concentrations are visible on *Fig. 24. left* (for **29**, **30**, **31**, **33**) and *Fig. 24* (for **28**).

By plotting the maximal fluorescence intensity of each spectrum against the actual concentration, we can get a titration curve, which can be used to determine the value of K'_d. For the determination of the K'_d we need to find the inflexion point of the titration curve. The easiest way to do this, is to use a so-called reversed Hill-plot. First, we calculate the value of $(F-F_{min})/(F-F_{max})$ for each concentration value, where F is the maximum fluorescent intensity measured for the given concentration, F_{min} is the maximum fluorescent intensity measured in the case of the lowest metal ion concentration, while F_{max} for the highest concentration. If the ratio is under 1, the concentration value is before the inflexion point, if the value is above 1, we are after the inflexion point. The inflexion point of the titration curve is found in the point, where this value is 1. To find this, we take the logarithm of the metal ion concentration and plot it against the logarithm of the mentioned ratio. In this case, the sign of $\log((F-F_{min})/(F-F_{max}))$ indicates the "position" on the titration curve. The inflexion point is in 0, so we only have to do a linear fitting on this plot and find the intercept of the fitted line with axis x. The calculated value is ($\log K'_d$). I made the Hill-plots and calculated the apparent stability constant of the prepared compounds in the case of **GFPAQ** sensors (**29-31**) and **GFPDPA2** (**33**). The Hill-plots are shown in *Figure 24., left.* The values (pK'_d) are found in *Table 1.* Based on the titration curve, a range of applicability is also suggested in *Table 1.*

Unfortunately, as visible in *Figure 23.*, **GFPHQ1** did not only show relatively weak photophysical properties, but it also behaved strangely, when I tried to titrate it with Zn^{2+}. Measuring the compound in absence of Zn^{2+} gave the expected small background fluorescence, while the solution containing 1 mM Zn^{2+} has shown a seven-fold fluorescent intensity increase. To my surprise, the solution containing 330 μM of Zn^{2+} emitted less fluorescence, than the solution containing no metal ions, and the fluorescence further decreased, when the Zn^{2+} level was increased to 660 μM. This made the titration impossible,

and it is indeed, a very interesting observation. The experiment was reproduced only to give the same results.
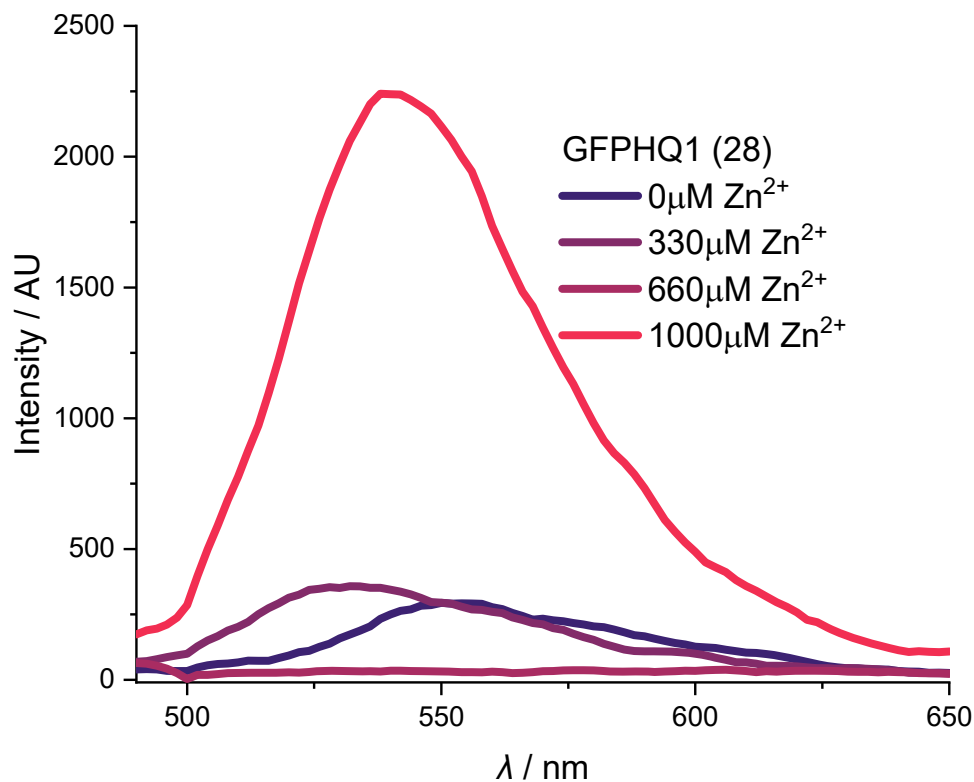
Figure 23. Fluorescence spectra of **28** pH 7.4 (0.1 M) HEPES buffer containing different amounts of Zn^{2+}. Values are not normalized, spectra were recorded at the maximum excitation wavelength.

Table 1. Photophysical characterisation of the prepared compounds, apparent dissociation constants of their complexes with Zn^{2+} and the proposed concentration range of application.

Compound	FEF*	Norm. free fl.int / AU	Norm. complex fl.int / AU (λ_{em} / nm)**	λ_{abs} / nm	Stokes shift / nm	p(K'_d***/M)	K'_d, (Concentration range of applicability) / µM
GFPHQ1(28)	6.73	4.3	33.1 (496)	385	111	-	-
GFPAQ1(29)	59.37	35.9	2166.3 (514)	357	132	4.32	47 (20-500)
GFPAQ2(30)	6.76	2155.1	16740.1 (558)	377	181	5.44	3.6 (1-100)
GFPAQ3(31)	28.8	11317.0	337599.8 (472)	382	90	5.27	5.4 (1-30)
GFPDPA1(32)	~ 0	259784.9	239569.9 (534)	490	44	-	-
GFPDPA2(33)	11.1	86066.9	1040747 (425)	358	67	3.46	347 (100-500)

* FEF: Fluorescence enhancement factor: $(F_{complex} - F_{free})/F_{free}$
** maximal value measured at the excitation maximum
*** at pH 7.4 (0.1 M) HEPES

Figure 24. Left: Fluorescence spectra of **29,30, 31** and **33** pH 7.4 (0.1 M) HEPES buffer containing different amounts of Zn²⁺. Values are not normalized,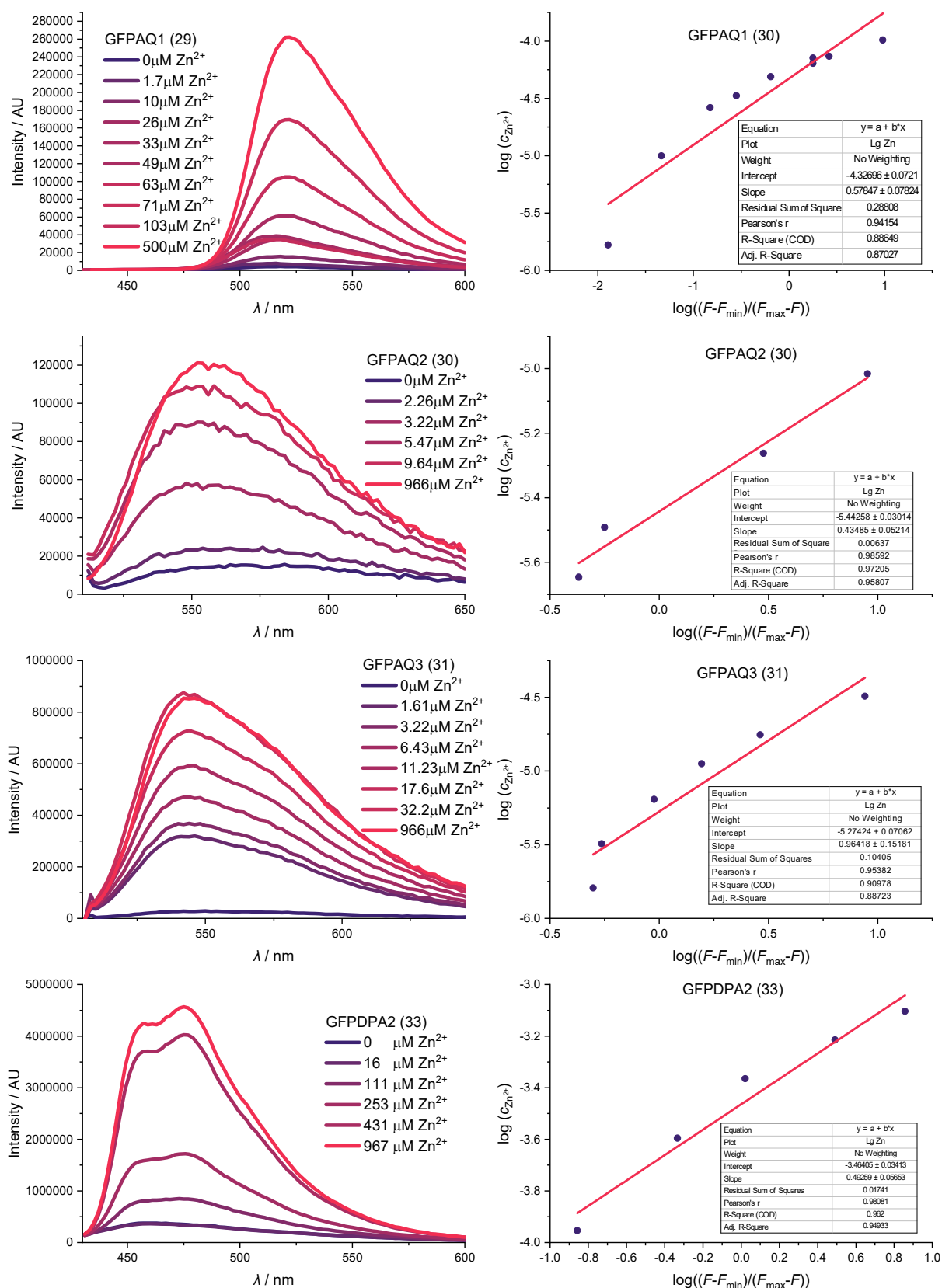 spectra were recorded at the maximum excitation wavelength.. Right: reversed Hill-plots for determination of the K'ₐ values for **29,30, 31** and **33**.

It is interesting to observe, that the additional ionophore side-chains on **31** and **31** indeed increased the stability constant of aminoquinoline probes by an order of magnitude. It is also observable, that DPA has one order of magnitude lower binding constant to Zn^{2+} in these compounds.

Looking at the achieved results, I was very satisfied, as four sensors seem to fulfil all the precaused criteria for the usability in the fields of microscopy. The K'_d values are all in the optimal 3-300 µM range, which is the most useful concentration range for biology related applications. As mentioned in *Chapter 2.*, the lower, 3–50 µM range could be useful for detecting signalling processes, while the range of 100–500 µM is fitted for investigating synaptic vesicles, the grey matter and other neurobiological regions of interest. Moreover, the compounds will be tested in research related to the SARS-CoV-2 virus by a partner research group.

An additional positive highlight is, that the four sensors cover a wide range of concentrations, and the difference in their emission wavelengths make a simultaneous use theoretically possible. This means, that these sensors could make a high dynamic range measurement possible.

4.3.3. Determination of two-photon applicability of the promising probes

The four promising sensors (**GFPAQ1,2,3, GFPDPA2; 29-31,33**) were selected to be undertaken into two-photon suitability measurements. The same Zn^{2+} free and 1mM Zn^{2+} containing stock solutions used for the determination of single photon photophysical properties were used in this case as well. Capillaries were immersed into the solutions and filled, then the ends of the capillaries were sealed by immersion into hot wax. The capillaries were put onto a glass slide under the lens of a two-photon microscope. A water-immersion lens was used, thus, a droplet of water was carefully put onto above the capillary and the lens was immersed into the droplet. The top edge of the capillary was pulled into focus every time and then the focal point of the lens was shifted downwards with 50 mm to measure in the middle of the capillary. In these measurements, I basically measured excitation scans, as the wavelength of the laser was changed between 700 nm and 1040 nm and the intensity of the emitted light was measured. Unfortunately, microscopes cannot take a spectrum, the PDA detector only records the sum of the collected photons as a signal. A filter was used before the detector letting in only light between 450 and 600 nm. Images were recorded of the capillary

in every 10 nm step. The average brightness of the capillary was calculated and corrected with the brightness of the background.

The measured normalized excitation scan spectrums were normalized based on the concentration and plotted in *Figure 25*. It was clearly visible, that no probes emitted detectable fluorescence in the absence of Zn^{2+}. Contrastingly the fluorescence of solutions with Zn^{2+} content was clearly visible on the captured images.
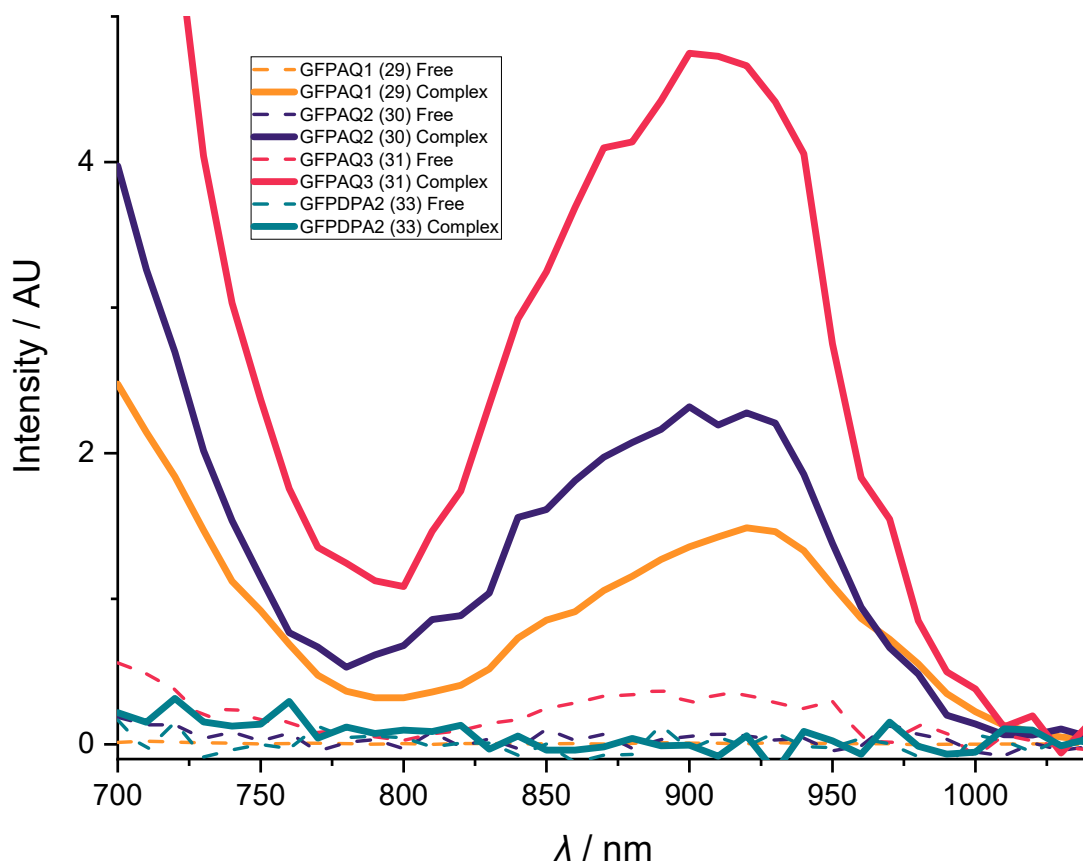
Figure 25. The measured two-photon excitation scan spectrums. The spectra were normalized based on the concentration of the sensors. Dotted lines represent the ion-free solutions, while the bold continuous lines represent the solutions containing Zn^{2+}.

Table 2. Photophysical characterisation of the promising probes for 2P applicability.

Compound	2P FEF	Norm. free 2P fl.int / AU	Norm. complex 2P fl.int / AU	$\lambda_{abs, max}$ / nm
GFPAQ1(29)	108	0.0135	1.48	920
GFPAQ2(30)	32	0.0725	2.31	910
GFPAQ3(31)	12.64	0.346	4.72	910
GFPDPA2(33)	~ 1	0.15	0.30	720

By looking at the data summarized in *Table 2.*, we can see, that the most intense fluorescence is emitted by **GFPAQ3 (31)** among the quinoline-based probes, just as in the single-photon case, followed by **GFPAQ2 (30)** and **GFPAQ1 (29)**. However, The fluorescent enhancement

factors are somewhat changed. The best in this regard is still **GFPAQ1** (**29**), like in the single-photon case, but in 2P, **GFPAQ2** (**30**) shows better FEF, than **GFPAQ3** (**31**), unlike in the single-photon case. The most efficient excitation wavelengths are at 910 nm, but looking at *Figure 25.* we can conclude, that another, even more intense excitation can be done at around 700 nm. With a laser emitting from 650 nm, this peak would be clearly visible and usable.

In conclusion, the 2P measurements lead us to the conclusion, that the novel aminoquinoline-based probes (**29,30,31**) have the desired proberties for 2P imaging uses,while my DPA-based sensor is usable only in single-photon fluorescent microscopy.

5. Summary

At the beginning of my work, I set a goal to develop novel fluorescent sensors for Zn^{2+} usable in fluorescent and two-photon microscopy.

The reported ionophores and fluorescent probes for Zn^{2+} in the literature were studied, and reports on the structure and properties of the fluorescent scaffold present in the Green fluorescent protein (GFP) were considered before starting the work. Based on these pieces of information, I rationally designed seven novel scaffolds (**28-34**) containing analogues of the GFP-fluorophore. Four designed sensors (**28-31**) contained a quinoline-moiety, while three sensors were based on dipicolylamine (**32-34**).

All designed compounds were studied using computational chemistry to successfully propose a binding model.

After this, a viable synthetic route was developed for the synthesis of six out of the seven planned compounds (**28**-**33**) from commercially available reagents. Structure of the successfully prepared compounds were confirmed, fulfilling the first main goal of the project.

Single-photon and two-photon photophysical characterization of the prepared compounds were carried out and the stability constants of the complexes were determined, completing the second main goal. A conclusion was drawn, that in general, quinoline-based compounds created higher stability complexes, in which the more sophisticated the side chains were, the higher the fluorescent intensity was. On the other hand, DPA-based molecules seemed to have higher fluorescent intensities. These parameters will be useful in future sensor-designs.

Evaluation of the results show, that four sensors can be applied in single-photon fluorescence microscopy, and 3 sensors are two-photon active. The sensors cover a wide-range of

concentration in their activity between 1 and 500 μM. We propose, that the stronger binding probes (**30**, **31**) could be used for studying signalling processes and protein interactions in cells, while the compounds forming less stable complexes (**29**, **33**) could be used in studying the brain, on fields of neuroscience and to detect cell proliferation.

In the course of the project, it was shown, that the fluorophore scaffold found in GFP can be successfully implemented in fluorescent sensor compounds, moreover, it is a fluorophore, that could take part in the chelation process, giving the possibility of fine-tuning selectivity and affinity.

Table 3. Summary of the research project.

Compound	Binding model	Synthesis	1P application	2P application	Proposed area of application
GFPHQ1(28)	✓	✓	✗	✗	-
GFPAQ1(29)	✓	✓	✓	✓	Gray matter, brain studies, CNS, cell proliferation (20-500 μM)
GFPAQ2(30)	✓	✓	✓	✓	Signalling, protein interaction (1-100 μM)
GFPAQ3(31)	✓	✓	✓	✓	Signalling, protein interaction (1-30 μM)
GFPDPA1(32)	✓	✗	✗	✗	-
GFPDPA2(33)	✓	✓	✓	✗	Gray matter, brain studies, CNS, cell proliferation (100-500 μM)
GFPDPA3(34)	✓	✗	-	-	-

The outcome of the project is summarized in *Table 3*. In one word, a rational fluorescent sensor design was carried out employing a radically new scaffold based on available knowledge. The goal to synthetize the compounds with this new scaffold was reached and analytical studies confirm, that the designed sensors indeed perform well in their planned field of application. In general, the project confirmed the usability of these compounds, which in itself is an exciting scientific results. I feel, that my main goals were reached and the research presented in this assay was successful.

Obviously, the project is not finished, and there is a lot to do. My future plan is to design a successful synthesis for **GFPDPA3(34)**, to carry out analytical measurements on a reference compound (**TSQ**, **11a**) and compare the results to it. Another important goal in the future is to carry out measurements on selectivity, determine the ligand to metal ratio and measure water-solubility and pH titration. Of course, the current results gave a variety of ideas for other sensor designs based on the chromophore of GFP. These include other side-chains, designs for other metal-ions, implementing double ionophores, or implementing quinolines in 2nd, 3rd and 4th generation GFP-chromophore derivatives. All of these plans however lead to an extensive research field covering a large amount of scientific work in the future years. Hopefully, the society will somehow make profit from the results of the project in the future.

6. Materials and methods

6.1. Methods and software used for quantumchemical computations

All calculations were carried out using Gaussian 09 on our own server.[67] DFT method M06-2X/6-31(d,p) level of theory was used with a standard IEF-PCM (integral Equation formalism polarizable continuum medium) method.[68] After optimization of geometry, energy of vibrational levels were calculated with the same method. The optimized structures were proven to be in a minimum of the potential energy surface (PES). This method was successfully employed before in calculations of the transition-field elements.

6.2. Methods and materials used in the synthetic preparation.

6.2.1. Chemicals

All chemicals and dry solvents used were purchased from *Merck* (*Aldrich, Sigma-Aldrich*) and *Fluorochem* in reagent grade. Solvents were from *Molar chemicals*. All chemicals were used without further purification. NMR solvents were from *Eurisotop* and *Merck*. HPLC solvents were purchased from *Merck.* For thin layer chromatography, *Kieselgel 60 F254* type plates were used from *Merck*. Production of the plates were carried out by UV, iodine bath and heating after a spray of aqueous solution of 10 % Cerium (IV) sulphate and 15% sulfuric acid.

6.2.2. Monitoring reactions and analysis with HPLC-MS.

Reactions were routinely monitored with HPLC-MS. UV-VIS and MS was used as a detection method. Conditions of the measurements and paraneters of the instrument:

Type: Shimadzu LCMS-2020 equipped with Shimadzu LC-20AD paralell pump, Shimadzu DG-20AS degasser, Shimadzu SIL-20A HT autosampler and a Shimadzu CTO-20A thermostate and a Shimadzu SPD-M20A 190-800 nm PDA detector. The used column was always Supelco 5μm, 50 x 4.6 mm, C18 column thermostated to 40 °C. A 1:1 split was employed between the PDA and MS detectors. MS: ionisator: ESI 10000 V, N_2 flow 14 L / min, 250 °C.

Two elution programs were used:

- LCMS method A: gradient elution, flow rate 1 ml / min. Eluent A: 0.1% TFA in H_2O. Eluent B: 0.1% TFA in MeCN. Elution program: B concentration 0→100% linearly in 10 min.

- LCMS method B: gradient elution, flow rate 1 ml / min. Eluent A: NH_4HCO_3 in H_2O. Eluent B:MeCN. Elution program: B concentration 0→100% linearly in 10 min.

6.2.3. Purification with preparative HPLC.

In order to achieve the highest purity with the least effort, preparative HPLC purifications were employed. Parameters of the instrument:

Type: Armen Spot Prep II system. Column: Phenomenex, Gemini 250x50,00 mm; 10 μm, C18, 110 Å loading. Flow rate: 250 ml/min, 300 bar. Injection: manual, 10 ml loop. Detector: PDA, 4 ch., scan mode, 200-600 nm.

Gradient elution with unique gradient for each compounds were used. Two main methods were used based on the eluents:

- method A: eluent A: 0.2 % TFA in H_2O →eluent B: MeCN

- method B: eluent A: 0.1 % NH_4HCO_3 in H_2O →eluent B: MeCN

6.2.4. Column chromatography

For column chromatography an Interchim puriFlash® XS520Plus instrument was used with dry loading (25g RediSep Solid Load Cartridge) and Puriflash SILICA HP 15UM F0040 flash column. Flow rate: 02 ml / min.

6.2.5. NMR spectroscopy

Structure and final purity determination was done with NMR spectroscopy. Samples were prepared by dissolving 7-15 mg of the compounds in 550 μl of DMSO-*d6*.

Designation of multiplicities: s (singlet), d (doublet), t (triplet), q (quartet), quin (quintet), m (multiplet), dd (double of doublets), td (triplet of doublets), ddd(doublet of doublet of doublets), bs (broad singlet), bs (broad doublet).

The used instrument was at *Varian 400 MHz, 500 MHz* and 6*00 MHz* spectrometers.

6.2.6. Microwave reactor

For MW reactions a CEM Discover System 908005 MW reactor was used.

6.3. Methods and materials used in the analytical experiments.

Fluorescent spectra were recorded on an Edinburgh Instrument FLS920 spectrofluorometer. A quartz cuvette with 3 ml volume and 1 cm length was used. Absorption spectra were recorded on a ThermoFisher NanoDrop 1000 spectrophotometer. Chemicals used in the analysis were all purchased from Sigma-Aldrich in analytical quality. The two-photon measurements were performed on the custom Femtonics Dobos Dual system using a water immersion lens, a Mai Tai High-Power laser operated at 50 mW. For processing the images, ImageJ software was used.

7. Detailed description of the synthetic procedures

7.1. Synthetic procedures for quinoline-based sensors

7.1.1. Preparation of common precursor 2-(phenylamino)-3,5-dihydro-4*H*-imidazol-4-one (**36**)

A three-necked round-bottom flask was equipped with a reflux condenser and a bubbler on top. The outlet of the bubbler was introduced into the vent of the fume hood. 1.89 g (47 mmol, 1.1 eq.) of NaH (60%, susp. in min. oil) was suspended in 10 ml abs. DMF in the flask. The suspension was cooled to 0°C. 5.00 g (43 mmol, 1 eq.) 2-thiohydantoin was dissolved in 10 ml abs. DMF chilled to 0 °C. The necks of the flask were sealed with septa and the system was flushed with nitrogen. The 2-thiohydantoin solution was added dropwise to the initial suspension during stirring and cooling. After the addition, the flask was let to room temperature, while stirring for 15 minutes. The mixture became a rose-coloured suspension. After the stoppage of gas evolution, the solution was cooled again to 0 °C. 2.6 ml (5.8 g, 41 mmol, 0.95 eq.) of MeI was added dropwise over the course of 30 minutes under vigorous stirring. The rose-coloured suspension slowly turned into a dark green coloured suspension. 5 ml DMF was added to promote stirring of the suspension. The mixture was stirred for 1 hour on room temperature. Then, while stirring 4.3 ml (4.41 g, 47 mmol, 1.1 eq.) aniline was added. The reaction mixture was heated to 110 °C and stirred overnight. The suspension turned into a dark green solution and small grey particles were floating in it. According to LCMS, the mixture contains the product and small amounts of dimethyl side-product, but no more reactants. The solution was cooled and poured onto 400 ml of stirred water mixed with curshed ice. Large amounts of grey precipitate was observable in the brown solution. The process is done in a well-ventilated fume hood with great care. After 5 minutes of stirring, the precipitate was filtered out and washed with ice-cold water until the washing liquor had no colour. The product was dried for 5 days of drying in vacuum drying oven at 40°C. The glassware used were washed with 30% H_2O_2, the septa were discarded due to absorption of mercaptomethanol.

Product: 4.75 g of gray powder. **Yield:** 63% **LCMS purity**: 100% (traces of DMF)

^{1}H NMR (400 MHz, DMSO-*d6*) δ 10.10 – 9.66 (m, 1H), 7.57 (s, 1H), 7.46 (d, J = 8.0 Hz, 2H), 7.30 (t, J = 7.9 Hz, 2H), 7.05 (t, J = 7.4 Hz, 1H), 3.70 (s, 2H).

^{13}C{1H} NMR (101 MHz, DMSO-*d6*) δ 139.25, 129.34, 123.84, 120.85, 94.66, 49.41

MS: [M+H^{+}] 176 m/z

7.1.2. Synthetic procedures for the preparation a GFPHQ1 (**28**)

7.1.2.1. Preparation of (*Z*)-5-((8-hydroxyquinolin-2-yl)methylene)-2-(phenylamino)-3,5-dihydro-4*H*-imidazol-4-one (**GFPHQ1**, **28**)

175 mg (1 mmol, 1 eq.) of **36** was dissolved in 3 ml of AcOH while stirring. 182 mg (1.05 mmol, 1.05 eq.) of solid 8-hydroxyquinoline-2-carbaldehyde (**37**) and 20 µl of catalytic piperidine (0.2 eq.) was added. The mixture was heated to 110°C and stirred for 2 hours in a closed tube. After 2 hours, the reaction mixture was a red solution containing the desired product. Solvents were removed on rotary evaporator and the solid residue was dissolved in a 10 ml mixture of methanol, acetonitrile and water (1:1:0.1), then injected onto prep. HPLC (method A). Acetonitrile from the pure fractions was evaporated and the aqueous residue was lyophilized after freezing.

Product: 225 mg of bright orange powder. **Yield:** 68% **LCMS purity**: 99% (contains TFA)

^{1}H NMR (400 MHz, DMSO-*d6*) δ 11.46 (s, 1H), 8.69 (s, 1H), 8.05 (s, 1H), 7.89 – 7.41 (m, 6H), 7.36 (s, 1H), 7.20 (t, *J* = 7.4 Hz, 1H), 6.68 (s, 1H).

The signals are broadened, ^{13}C spectrum could not be recorded on this instrument. The signals match the structure.

MS: [M+H^{+}] 331 m/z, [M+Na^{+}] 353 m/z

7.1.3. Synthetic procedures for the preparation a GFPAQ1 (**29**)

7.1.3.1. Preparation of *N,N*,2-trimethylquinolin-8-amine (**43**)

500 mg (3,65 mmol, 1 eq.) of 2-(N,N-Dimethylamino)-aniline (**38**) was dissolved in 6M HCl (6.6 ml) 510 mg crotonaldehyde (**39**) (7.3 mmol,2 eq., mixture of *E* and *Z*) in toluene (5 ml) was added to it. After stirring at RT for 1 hour 5 ml of toluene was added and the mixture was heated to 110 °C and refluxed for 4 h. The mixture was cooled and the organic layer was removed. NaOH was added to the aqueous phase until the pH was 7, then the mixture was

extracted with 3x20 ml DCM. After drying on MgSO₄, the solvent was evaporated and the crude product was purified with flash chromatography (DCM / cyclohexane 1/1).

Product: 270 mg of yellow oil. **Yield:** 40% **LCMS purity**: 95%

¹H NMR (400 MHz, DMSO-d_6): δ 7.97 (d, J = 8.0 Hz, 1H), 7.48 – 7.40 (m, J = 10.0 Hz, J = 6.0 Hz, J = 3.0 Hz, 2H), 7.56 (d, J = 7.4 Hz, 1H), 7.12 (dd, J = 6.3 Hz, J = 3.0 Hz, 1H), 3.18 (s, 6H), 2.70 (s, 3H).

¹³C{1H} NMR (101 MHz, DMSO-d_6): δ 156.8, 147.7, 140.6, 134.8, 126.9, 126.0, 120.8, 120.1, 110.1, 43.9, 27.5

MS: [M+H⁺] 187 m/z

7.1.3.2. Preparation of 8-(dimethylamino)quinoline-2-carbaldehyde (**46**)

190 mg (1.7 mmol, 1.3 eq.) of selenium dioxide was suspended in 10 ml dioxane and 0.1 ml H₂O. The mixture was stirred heated to 80 °C and 250 mg (1.34 mmol, 1 eq.) of **43** was added. After 3 hours, the reaction was completed and the mixture was cooled, filtered trough a pad of celite eluted with dioxane and the solvents were evaporated under reduced pressure. Flash chromatography on silica gel was performed. (DCM/yclohexane 1:1). The pure fractions were united and solvents were removed.

Product: 245 mg of yellow oil. **Yield:** 90% **LCMS purity**: 97%

¹H NMR (400 MHz, DMSO-d_6): δ 10.32 (s, 1H), 8.15 (d, J = 8.2 Hz, 1H), 8.10 (d, J = 8.3 Hz, 1H), 7.58 (d, J = 8.6 Hz, 1H), 7.16 (d, J = 8.4 Hz, 1H), 2.86 (s, 6H).

¹³C{1H} NMR (101 MHz, DMSO-d_6): δ 193.4, 151.6, 151.0, 142.6, 138.0, 130.4, 129.8, 119.7, 117.2, 116.0, 44.4.

7.1.3.3. Preparation of (*Z*)-5-((8-(dimethylamino)quinolin-2-yl)methylene)-2-(phenylamino)-3,5-dihydro-4*H*-imidazol-4-one (**GFPAQ1**, **29**)

180 mg (1.03 mmol, 1 eq.) of **36** was dissolved in 3 ml of AcOH while stirring. 216 mg (1.08 mmol, 1.05 eq.) of the oil 8-(dimethylamino)quinoline-2-carbaldehyde (**46**) and 20 µl of catalytic piperidine (0.2 eq.) was added. The mixture was heated to 110°C and stirred for 3 hours in a closed tube. After 3 hours, the reaction mixture was a red solution containing the desired product. Solvents were removed on rotary evaporator and the solid residue was dissolved in a 10 ml mixture of methanol, acetonitrile and water (1:1:0.1), then injected onto

prep. HPLC (method A). Pure fractions were collected and united, then acetonitrile was evaporated and the aqueous residue was lyophilized after freezing.

Product: 330 mg of intense red powder. **Yield:** 90% **LCMS purity**: 100% (contains TFA)

^{1}H NMR (400 MHz, DMSO-d_6) δ 8.61 (d, J = 8.6 Hz, 1H), 8.40 (s, 1H), 7.89 (d, J = 8.0 Hz, 1H), 7.80 (s, 1H), 7.67 (t, J = 7.9 Hz, 1H), 7.61 (s, 1H), 7.46 (t, J = 7.9 Hz, 2H), 7.23 (t, J = 7.4 Hz, 1H), 6.75 (s, 1H), 3.01 (s, 6H).

The signals are broadened, ^{13}C spectrum could not be recorded on this instrument. The signals match the structure.

MS: [M+H$^+$] 358 m/z, [M+Na$^+$] 381 m/z

7.1.4. Synthetic procedures for the preparation a GFPAQ2 (**30**)

7.1.4.1. Preparation of *N1,N1,N2*-trimethyl-*N2*-(2-methylquinolin-8-yl)ethane-1,2-diamine (**44**)

In a 10 ml microwave pressure vial 500 mg (2.251 mmol, 1 eq.) 8-bromo-2-methylquinoline (**40**) was dissolved in 7.5 ml toluene. 440 μl (344 mg, 3.38 mmol, 1.5 eq.) *N1,N1,N2*-trimethylethane-1,2-diamine (**41**) was added. 320 mg (3.38 mmol, 1.5 eq.) NaOtBu, 70 mg (0.11 mmol, 0.05 eq.) rac-BINAP, Palladium(0) bis(dibenzylideneacetone) (0.09 mmol, 0.04 eq.) was also added. The vial was flushed with argon and capped. In 20 minutes the mixture was heated to 120 °C by MW and was irradiated while stirring for 4 hours. LCMS has shown a conversion of 85% and several decomposition signs, so work-up was initiated. The mixture was filtered trough a pad of celite eluted with 30 ml DCM, then the filtrate was concentrated under reduced pressure. 528 mg of crude product was achieved. Based on TLC, no elution of the product was observable even by methanol. The crude product was dissolved in DCM and 2 g of Al$_2$O$_3$ was added, then the solvent was removed *in vacuo*. The product was absorbed onto the alumina. This dry load was put onto the top of an alumina plug and washed with 5 CV hexane, 5 CV DCM. Elution with 5 CV DCM/MeOH 3:2 gave the desired product.

Product: 320 mg of brown oil. **Yield:** 60% **LCMS purity**: 90%

^{1}H NMR (400 MHz, DMSO-d_6) δ 8.19 (d, J = 8.4 Hz, 1H), 7.42 – 7.38 (m, 3H), 7.13 (dd, J = 7.2, 1.9 Hz, 1H), 3.64 (t, J = 7.1 Hz, 2H), 3.15 (d, J = 5.8 Hz, 2H), 2.93 (s, 3H), 2.69 (s, 3H), 2.61 (s, 6H).

^{13}C spectrum was not recorded, as due to impurities it would contain no additional information

MS: [M+H$^+$] 244 m/z

7.1.4.2. Preparation of 8-((2-(dimethylamino)ethyl)(methyl)amino)quinoline-2-carbaldehyde (**47**)

160 mg (1.44 mmol, 1.3 eq.) of selenium dioxide was suspended in 10 ml dioxane and 0.1 ml H$_2$O. The mixture was stirred heated to 80 °C and 270 mg (1.11 mmol, 1 eq.) of **43** was added. After 1 hour, LCMS analysis of the reaction mixture shows a complete conversion, but two products are present. The main product (~60%) is the desired product. The side-product was identified based on mass spectrum in HPLC-MS and it was confirmed to be 8-((2-(dimethylamino)ethyl)(methyl)amino)quinoline-2-carboxylic acid, basically an overoxidated derivative containing carboxylic acid function instead of aldehyde. After evaporation of the solvents, the mixture was deposited onto the surface of 2 grams of alumina and was washed over an alumina plug with 5 CV hexane. Elution with 5 CV DCM/MeOH 4:1 washed the desired product from the column, but the fraction contained new minor impurities. Stronger solvents eluted fractions of the carboxylic acid only. The fraction, which had a purity of ~60% was concentrated and dissolved in in a 10 ml mixture of methanol, acetonitrile and water (1:1:0.1), then injected onto prep. HPLC (method A). Pure fractions were collected and united, then acetonitrile was evaporated and the aqueous residue was lyophilized after freezing.

Product: 45 mg of dark brown solid. **Yield:** 15% **LCMS purity**: 97%

The NMR sample decomposed upon waiting for measurement. A new sample will be made and measured in the future. (20% decomposition confirmed by LCMS)

MS: 258 m/z

7.1.4.3. (*Z*)-5-((8-((2-(dimethylamino)ethyl)(methyl)amino)quinolin-2-yl)methylene)-2-(phenylamino)-3,5-dihydro-4*H*-imidazol-4-one (**GFPAQ2**, **30**)

22 mg (0.131 mmol, 1.05 eq.) of **36** was dissolved in 1 ml of AcOH while stirring. 32 mg (0.124 mmol, 1 eq.) of **47** and 3 μl of catalytic piperidine (0.2 eq.) was added. The mixture was heated to 110°C and stirred for 3 hours in a closed tube. After 3 hours, the reaction mixture was a dark red solution containing the desired product. Solvents were removed on rotary evaporator and the solid residue was dissolved in a 10 ml mixture of methanol, acetonitrile and water (1:1:0.1), then injected onto prep. HPLC (method A). Pure fractions were collected and united, then acetonitrile was evaporated and the aqueous residue was lyophilized after freezing.

Product: 17 mg of brown powder. **Yield:** 33% **LCMS purity**: 100% (contains TFA)

The signals were highly broadened, and a high amount of the compound decomposed in the NMR sample, while waiting for measurement. The spectrums cannot be normally evaluated, but I will reproduce the compound and retake the NMR. (30% decomposition confirmed by LCMS)

MS: [M+H$^+$] 415 m/z, [M+Na$^+$] 437 m/z

7.1.5. Synthetic procedures for the preparation a GFPAQ3 (**31**)

7.1.5.1. Preparation of *N1,N1,N2*-trimethyl-*N2*-(2-methylquinolin-8-yl)ethane-1,2-diamine (**45**)

In a 10 ml microwave pressure vial 333 mg (1.5 mmol, 1.25 eq.) 8-bromo-2-methylquinoline (**40**) was dissolved in 5 ml toluene. 140 μl (147 mg, 1.20 mmol, 1 eq.) 2-(Methylamino)pyridine (**42**) was added. 216 mg (2.25 mmol, 1.9 eq.) NaOtBu, 47 mg (0.08 mmol, 0.05 eq.) rac-BINAP, 28 mg Pddba$_2$ (0.05 mmol, 0.04 eq.) was also added. The vial was flushed with argon and capped. In 20 minutes the mixture was heated to 120 °C by MW and was irradiated while stirring for 4 hours. After cooling, the mixture was diluted with DCM/water (15+15 ml) and the aqueous phase was extracted with DCM (2x15 ml) The organic phases were dried on MgSO4 and concentrated. The product was purified with flash chromatography (Hex/EtOAc 4/1 7M NH$_3$ (competing base)→EtOAc/MeOH 9/1).

Product: 221 mg of yellow oil. **Yield:** 70% **LCMS purity**: 92%

^{1}H NMR (400 MHz, Chloroform-*d*) δ 8.55 (ddd, *J* = 5.0, 1.9, 0.9 Hz, 1H), 7.94 (d, *J* = 8.4 Hz, 1H), 7.70 (dt, *J* = 7.9, 1.1 Hz, 1H), 7.59 (td, *J* = 7.6, 1.8 Hz, 1H), 7.33 – 7.27 (m, 2H), 7.19 (d, *J* = 8.4 Hz, 1H), 7.12 (ddd, *J* = 7.4, 4.9, 1.3 Hz, 1H), 7.05 (dd, *J* = 7.1, 1.9 Hz, 1H), 4.95 (s, 2H), 2.99 (s, 3H), 2.60 (s, 3H).

^{13}C{1H} NMR (101 MHz, Chloroform-*d*) δ 160.15, 155.82, 148.33, 147.96, 141.49, 136.28, 135.94, 127.53, 125.45, 122.69, 121.53, 121.33, 119.82, 115.38, 62.52, 40.01, 25.15.

7.1.5.2. Preparation of 8-((2-(dimethylamino)ethyl)(methyl)amino)quinoline-2-carbaldehyde (**48**)

121 mg (1.09 mmol, 1.3 eq.) of selenium dioxide was suspended in 5 ml dioxane and 0.1 ml H$_2$O. The mixture was stirred heated to 80 °C and 232 mg (0.80 mmol, 1 eq.) of **45** was added. After 3 hours, LCMS analysis of the reaction mixture shows a complete conversion. The

mixture was filtered trough celite and washed with DCM. Solvents were removed *in vacuo*, and the crude product was purified on column chromatography on silica gel. (Hex/EtOAc 7M NH$_3$ in MeOH 7/1/0.5).

Product: 198 mg of orange oil. **Yield:** 85% **LCMS purity**: 94%

^{1}H NMR (400 MHz, Chloroform-*d*) δ 9.68 (d, *J* = 0.9 Hz, 1H), 8.61 – 8.54 (m, 1H), 8.21 (dd, *J* = 8.5, 1.0 Hz, 1H), 7.94 (d, *J* = 8.5 Hz, 1H), 7.74 – 7.65 (m, 2H), 7.56 (t, *J* = 7.9 Hz, 1H), 7.37 (dd, *J* = 8.1, 1.3 Hz, 1H), 7.26 (s, 0H), 7.20 (ddd, *J* = 6.8, 5.0, 1.5 Hz, 1H), 7.14 (dd, *J* = 7.8, 1.3 Hz, 1H), 5.04 (s, 2H), 3.12 (s, 3H).

^{13}C{1H} NMR (101 MHz, Chloroform-*d*) δ 193.53, 160.26, 149.73, 149.50, 148.88, 137.55, 136.40, 131.82, 129.88, 122.12, 121.92, 118.87, 116.96, 115.02, 67.07, 62.85, 40.42.

MS: 278 m/z

7.1.5.3. (*Z*)-5-((8-(methyl(pyridin-2-ylmethyl)amino)quinolin-2-yl)methylene)-2-(phenylamino)-3,5-dihydro-4*H*-imidazol-4-one (**GFPAQ3**, **31**)

105 mg (0.6 mmol, 1 eq.) of **36** was dissolved in 2 ml of AcOH while stirring. 175 mg (0.630 mmol, 1.05 eq.) of **48** and 14 μl of catalytic piperidine (0.2 eq.) was added. The mixture was heated to 110°C and stirred for 3 hours in a closed tube. After 3 hours, the reaction mixture was an orange solution containing the desired product. Solvents were removed on rotary evaporator and the solid residue was dissolved in a 10 ml mixture of methanol, acetonitrile and water (1:1:0.1), then injected onto prep. HPLC (method A). Pure fractions were collected and united, then acetonitrile was evaporated and the aqueous residue was lyophilized after freezing.

Product: 130 mg of orange powder. **Yield:** 50% **LCMS purity**: 100% (contains TFA)

^{1}H NMR (400 MHz, DMSO-*d*$_6$) δ 11.16 (s, 1H), 8.72 (d, *J* = 4.8 Hz, 1H), 8.52 (bs, 1H), 8.47 (d, *J* = 8.4 Hz, 1H), 8.17 (s, 1H), 7.70-7.58 (m, 4H), 7.52 (dt, *J* = 15.4, 7.6 Hz, 2H), 7.41 (t, *J* = 7.9 Hz, 2H), 7.29 (d, *J* = 7.0 Hz, 1H), 7.15 (t, *J* = 7.4 Hz, 1H), 6.15 (s, 1H), 4.77 (s, 2H), 2.93 (s, 3H).

^{13}C{1H} NMR (101 MHz, DMSO-*d*$_6$) δ 158.59, 158.26, 157.37, 151.82, 146.09, 139.25, 138.43, 129.16, 127.64, 127.15, 123.93, 123.86, 122.41, 120.77, 120.55, 117.23, 59.44, 40.56.

MS: [M+H$^+$] 435 m/z, [M+Na$^+$] 457 m/z

7.2. Synthetic procedures for DPA-based sensors

7.2.1. Preparation of common 2-(bis(pyridin-2-ylmethyl)amino)-1,5-dihydro-4*H*-imidazol-4-one (**50**)

The same procedure was followed as in case of the preparation of **36** until the addition of the amine. The used quantities were 0.25 g (6.2 mmol, 1.1 eq.) of NaH (60%, susp. in min. oil) suspended in 2 ml abs. DMF, 0.65 g (5.6 mmol, 1 eq.) 2-thiohydantoin dissolved in 2 ml abs. DMF and 0.33 ml (0.75 g, 5.3 mmol, 0.95 eq.) MeI. After the methylation step, 1.11 ml (1.23 g, 6.2 mmol, 1.1 eq.) Bis(2-pyridylmethyl)amine (**DPA**, **49**) was added. The reaction mixture was heated to 110 °C and stirred overnight. The suspension turned into a dark green solution, but no particles precipitated. According to LCMS, the mixture contained the product and small amounts of dimethyl side-product, but no more reactants. The solution was cooled and a small part was poured onto small amount of stirred water mixed with crushed ice. Since no precipitation was observable, the DMF solvent was removed very carefully on a rotary evaporator. The solid residue was dissolved in 10 ml mixture of methanol, acetonitrile and water (1:1:0.1), then injected onto prep. HPLC. Method B was used, as in this case, separation on analytical HPLC was more efficient in neutral buffer. The glassware used were washed with 30% H_2O_2, the septa were discarded due to absorption of mercaptomethanol. The pure fractions were collected and unified, then acetonitrile was removed *in vacuo*. The aqueous solution of pure **50** was freeze-dried.

Product: 484 mg of sticky black powder. **Yield:** 30% **LCMS purity**: 100%

^{1}H NMR (400 MHz, DMSO-*d6*) δ 8.63 (bs, 2H), 8.41 (bs, 1H), 7.91 (bs, 2H), 7.34 (bs, 4H), 4.82 – 4.63 (bd, J = 8 Hz, 4H), 3.85 (s, 2H)

The signals are broadened, ^{13}C spectrum could not be recorded on this instrument. The signals match the structure.

MS: [M+H$^+$] 282 m/z

7.2.2. Synthetic procedures for the reparation of N^6,N^6-diethyl-N^2,N^2-bis(pyridin-2-ylmethyl)chromeno[2,3-d]imidazole-2,6-diamine (**GFPDPA1**, **32**)

7.2.2.1. First attempt to preparation of N^6,N^6-diethyl-N^2,N^2-bis(pyridin-2-ylmethyl)chromeno[2,3-d]imidazole-2,6-diamine (**GFPDPA1**, **32**)

190 mg (0.67 mmol, 0.95 eq.) of **50** was dissolved in 2 ml of AcOH while stirring. 137 mg (0.71 mmol, 1 eq.) of **48** and 14 μl of catalytic piperidine (0.2 eq.) was added. The mixture was heated to 110°C and stirred for 2 hours in a closed tube. After 3 hours, the reaction mixture was a dark red solution. The reactants were completely converted, however, instead of the expected signal ([M+H$^+$] 457 m/z) of the intermediate (**54**), LCMS was showing the molar weight of an oxidized product **57** (([M+H$^+$] 455 m/z). I was not able to further convert this product. In my future plans, I will isolate it and test it as a Zn^{2+} sensor as well.

7.2.2.2. Synthetic procedure for the preparation of N^6,N^6-diethyl-N^2,N^2-bis(pyridin-2-ylmethyl)chromeno[2,3-d]imidazole-2,6-diamine (**GFPDPA1**, **32**)

190 mg (0.67 mmol, 0.95 eq.) of **50** was dissolved in 2 ml of AcOH while stirring. 137 mg (0.71 mmol, 1 eq.) of **48** and 14 μl of catalytic piperidine (0.2 eq.) was added. The mixture was heated to 110°C and stirred for 3 hours in a closed tube flushed with nitrogen. After 3 hours, the reaction mixture was a blood-coloured solution. The reactants were mostly converted into intermediate **54** based on LCMS. ([M+H$^+$] 457 m/z, t_R = 6.24 min, method A). Heating and stirring was continued for four more days with daily LCMS sampling of the mixture. The formation of a new peak belonging to target compound **32** was observable ([M+H$^+$] 439 m/z, t_R = 7.12 min, method A). After four days the ratio **32**:**57** was 2:1, but due to the increase in the amount of decomposition products, the reaction was quenched by evaporating the solvents under reduced pressure. The solid residue was dissolved in 10 ml mixture of methanol, acetonitrile and water (1:1:0.1), then injected onto prep. HPLC (method A, since LCMS provided good results in similar buffer). The pure fractions of both products were collected and acetonitrile was removed under reduced pressure. The aqueous solutions were frozen and lyophilized. Although, LCMS confirmed a 100% purity of **32** in the collected fractions, the 90 mg of lyophilized product contained 20% **57** as impurity. I suggested, that in the aqueous acidic media the product (**32**) hydrolyses, when the solvent was removed.

Purification with column chromatography was also tried. TLC has shown only two components with different eluents, thus an elution trough a plug of silica seemed a good idea (5% MeOH in DCM). However, only an 85% purity was achieved with this method. Purification was tried on a flash chromatograph (DCM → 3% MeOH in DCM, 10 CV), but purity was still not more, than 90%. Finally, an LCMS method B run was tried out, and a good separation was observed. Moreover, several other minor impurities were separated from the main peak. A preparative HPLC on method B was carried out. The collected pure fractions were concentrated with care under higher vacuum and lower temperature (25 °C). Then the remaining solution was frozen and lyophilized. The resulting product was 100% pure according to both HPLC-MS methods. The compound was stored at -20°C. NMR spectrum was measured on 80°C and 2D measurements confirmed the structure.

Product: 18 mg of orange powder, yellow in solution with bright green fluorescence. **Yield:** 6% **LCMS purity**: 100%

^{1}H NMR (600 MHz, DMSO-*d6*, 80°C) δ 8.53 – 8.46 (m, 2H), 7.74 (td, J = 7.7, 1.9 Hz, 2H), 7.60 – 7.52 (m, 2H), 7.32 (s, 2H), 7.27 (dd, J = 7.5, 4.9 Hz, 2H), 6.90 – 6.83 (m, 2H), 4.97 (s, 4H), 3.45 (d, J = 7.1 Hz, 4H), 1.14 (t, J = 7.0 Hz, 6H).

^{13}C{1H} NMR (151 MHz, DMSO-*d6*, 80°C) δ 170.30, 169.02, 157.67, 151.27, 149.08, 148.24, 136.79, 129.01, 122.33, 121.61, 118.78, 110.64, 110.48, 97.52, 69.76, 53.39, 52.66, 43.99, 12.33.

MS: [M+H$^+$] 438 m/z

7.2.3. Synthetic procedure for the preparation of 3-(bis(pyridin-2-ylmethyl)amino)-5-hydroxybenzo[c]imidazo[5,1-*f*][1,2]azaborinin-1(5*H*)-one (GFPDPA2, 33)

131 mg (0.47 mmol, 1 eq.) of **50** was dissolved in 2 ml of AcOH while stirring. 70 mg (0.47 mmol, 1 eq.) of **52** and 10 μl of catalytic piperidine (0.2 eq.) was added. The mixture was heated to 110°C and stirred for 1 hour in a closed tube. The brown reaction mixture was analysed with LCMS to find a main peak representing the expected product **33** (LCMS method A, t_R = 6.15 min, [M+H$^+$] 396 m/z). Solvents were removed on rotary evaporator and the solid residue was dissolved in a 10 ml mixture of methanol, acetonitrile and water (1:1:0.1), then injected onto prep. HPLC (method A). Pure fractions were collected and united, then acetonitrile was evaporated and the aqueous residue was lyophilized after freezing. A slightly

beige coloured powder was isolated, which had one LCMS peak. A strong binding to the column was observed, the compound elutes with large tailing present in both PDA and MS detectors. The product stays on the column for 3 more consecutive runs. However, NMR confirmed, that the product was impure, making structure determination impossible. As quite strange NMR signals were achieved, I had to purify the product in order to confirm its final structure. LCMS on method B has shown several minor impurities, thus a run on prep. HPLC (method B) was also carried out and the product was isolated in the usual way. NMR spectrum was measured on 80°C and 2D measurements confirmed the structure.

Product: 74 mg of beige powder. Water-soluble, colourless solution, no fluorescence. Bright blue fluorescence upon addition of Zn. **Yield:** 40% **LCMS purity**: 95%

^{1}H NMR (600 MHz, DMSO-d_6) δ 8.55 – 8.50 (m, 1H), 8.32 (d, J = 5.9 Hz, 1H), 8.26 (d, J = 9.1 Hz, 1H), 7.79 (d, J = 8.0 Hz, 2H), 7.73 – 7.66 (m, 2H), 7.42 – 7.26 (m, 6H), 6.44 (s, 1H), 5.80 (s, 2H), 5.14 (s, 2H), 4.99 (d, J = 1.5 Hz, 1H).

^{13}C{1H} NMR (151 MHz, DMSO-d_6) δ 176.83, 170.02, 156.71, 152.36, 149.09, 144.70, 142.66, 139.87, 136.92, 136.51, 136.41, 134.22, 129.07, 127.74, 127.62, 127.17, 125.63, 122.65, 121.74, 107.43, 56.01.

MS: [M+H^{+}] 396 m/z (LCMS method A)

MS: [M+H^{+}] 395 m/z, [M+NH4HCO3] 474 m/z (LCMS method B, negative mode)

7.2.4. Synthetic procedure for the preparation of 3-(bis(pyridin-2-ylmethyl)amino)-5,5-difluoro-1-oxo-1,5-dihydrobenzo[c]imidazo[5,1-f][1,2]azaborinin-5-uide (GFPDPA3, 34)

7.2.4.1. Attempt to preparation of potassium trifluoro(2-formylphenyl)borate (53)

500 mg (3.33 mmol, 1 eq.) of (2-formylphenyl)boronic acid (62) was dissolved in 5 ml of water/MeOH 1:1 mixture. 1.04 g (13.33 mmol, 4 eq.) of potassium bifluoride was added to the mixture. LCMS method B was choosen to monitor the reaction in order to observe the anions in negative ionization mode. In 10 minutes a total conversion was observed with a single peak with [M[-]] 173 m/z in negative ionization mode belonging to the expected product (53). However, the purification of the product was unsuccessful. Extractions with acetone yielded only small amount of product. A new method will be tried in the future to produce the pure material. However, the solvents were removed and a white cristalline powder was earned,

which contains the product and inorganic impurities (KOH, KF, KHF$_2$). The glassware employed was etched by HF produced *in situ*, therefore, care must be applied when performing the procedure.

7.2.4.2. Attempt to preparation of 3-(bis(pyridin-2-ylmethyl)amino)-5,5-difluoro-1-oxo-1,5-dihydrobenzo[*c*]imidazo[5,1-*f*][1,2]azaborinin-5-uide (GFPDPA3, 34) from potassium trifluoro(2-formylphenyl)borate

4.9 mg (0.017 mmol, 1 eq.) of **50** was dissolved in 0.5 ml of AcOH while stirring. 6 mg (0.035 mmol, 2 eq.) **53** contaminated with inorganic salts and 1 μl of catalytic piperidine (0.2 eq.) was added. The mixture was heated to 110°C and stirred for 1 hour in a closed tube. Conversion was shown, however, the new peak on HPLC-MS (method B) had the same retention time and mass spectrum as **GFPDPA2** (**33**). Perhaps, due to the impurities, the hydrolized product is formed. The experiment will be reproduced with pure **53**.

7.2.4.3. Attempt to preparation of 3-(bis(pyridin-2-ylmethyl)amino)-5,5-difluoro-1-oxo-1,5-dihydrobenzo[*c*]imidazo[5,1-*f*][1,2]azaborinin-5-uide (GFPDPA3, 34) from GFPDPA2, 33

20 mg (0.05 mmol, 1 eq.) of **GFPDPA2**, **33** was dissolved in different solvents (MeCN and water was tried) and 17 mg (0,053 mmol, 1.05 eq.) of KHF$_2$ was added to the mixture. The reaction was tried with different conditions (RT and 90°C), but no conversion was observable in 3 days.

8. Bibliography

(1)   Bellion, E. *J. Chem. Educ.* **1992**, *69* (12), A326.
        https://doi.org/10.1021/ed069pA326.1.

(2)   Gumienna-Kontecka, E.; Rowińska-Żyrek, M.; Łuczkowski, M. *Recent Advances in
        Trace Elements*. April 3, 2018, pp 177–206.
        https://doi.org/https://doi.org/10.1002/9781119133780.ch9.

(3)   Doboszewska, U.; Wlaź, P.; Nowak, G.; Młyniec, K. *Br. J. Pharmacol.* **2020**, *177*
        (21), 4887–4898. https://doi.org/10.1111/bph.15199.

(4)   Levaot, N.; Hershfinkel, M. *Cell Calcium* **2018**, *75*, 53–63.
        https://doi.org/https://doi.org/10.1016/j.ceca.2018.08.004.

(5)   Maret, W. *Adv. Nutr.* **2013**, *4* (1), 82–91. https://doi.org/10.3945/an.112.003038.

(6)   Johnson, A. D.; Curtis, R. M.; Wallace, K. J. *Chemosensors* **2019**, *7* (2).
        https://doi.org/10.3390/chemosensors7020022.

(7)   De Silva, A. P.; Moody, T. S.; Wright, G. D. *Analyst* **2009**, *134* (12), 2385–2393.
        https://doi.org/10.1039/b912527m.

(8)   Hecel, A.; Miller, A.; Matera-witkiewicz, A.; Dudek, D.; Dominguez-martin, A.
        2020, No. II, 1–29.

(9)   Shittu, M. O.; Afolami, O. I. *Infez. Med.* **2020**, *28* (2), 192–197.

(10)   Jancsó, A.; Kovács, E.; Cseri, L.; Rózsa, B. J.; Galbács, G.; Csizmadia, I. G.; Mucsi,
        Z. *Spectrochim. Acta Part A Mol. Biomol. Spectrosc.* **2019**, *218*, 161–170.
        https://doi.org/https://doi.org/10.1016/j.saa.2019.03.111.

(11)   PRASAD, A. S.; HALSTED, J. A.; NADIMI, M. *Am. J. Med.* **1961**, *31*, 532–546.
        https://doi.org/10.1016/0002-9343(61)90137-1.

(12)   Mayor-Ibarguren, A.; Busca-Arenzana, C.; Robles-Marhuenda, Á. *Front. Immunol.*
        2020, *11* (July), 1–8. https://doi.org/10.3389/fimmu.2020.01736.

(13)   Maret, W.; Sandstead, H. H. *J. Trace Elem. Med. Biol.* **2006**, *20* (1), 3–18.
        https://doi.org/10.1016/j.jtemb.2006.01.006.

(14)   Assaf, S. Y.; Chung, S. H. *Nature* **1984**, *308* (5961), 734–736.

https://doi.org/10.1038/308734a0.

(15) Zhang, L.; Clark, R. J.; Zhu, L. *Chem. - A Eur. J.* **2008**, *14* (9), 2894–2903. https://doi.org/10.1002/chem.200701419.

(16) Palmer, A. E.; Miranda, J. G.; Carter, K. P. *Encycl. Inorg. Bioinorg. Chem.* **2004**, No. Ii, 1–14. https://doi.org/10.1002/9781119951438.eibc2109.

(17) Chang, C. J.; Lippard, S. J. *Zinc Metalloneurochemistry: Physiology, Pathology, and Probes*; 2006; Vol. 1. https://doi.org/10.1002/0470028114.ch12.

(18) Ayman A. A. Aziz; Amir E. Aboelhasan; Mostafa A. Sayed. *J. Braz. Chem. Soc.* **2020**, *31* (8), 1635–1647. https://doi.org/10.21577/0103-5053.20200049 J.

(19) Frederickson, C. J.; Koh, J. Y.; Bush, A. I. *Nat. Rev. Neurosci.* **2005**, *6* (6), 449–462. https://doi.org/10.1038/nrn1671.

(20) Valeur, B.; Leray, I. *Coord. Chem. Rev.* **2000**, *205* (1), 3–40. https://doi.org/10.1016/s0010-8545(00)00246-0.

(21) Skalny, A. V.; Rink, L.; Ajsuvakova, O. P.; Aschner, M.; Gritsenko, V. A.; Alekseenko, S. I.; Svistunov, A. A.; Petrakis, D.; Spandidos, D. A.; Aaseth, J.; Tsatsakis, A.; Tinkov, A. A. *Int. J. Mol. Med.* **2020**, *46* (1), 17–26. https://doi.org/10.3892/ijmm.2020.4575.

(22) Einstein, A. *Ann. Phys.* **1905**, *322* (6), 132–148. https://doi.org/10.1002/andp.19053220607.

(23) Mayer, J. G.-. *Ann. Phys.* **1928**, *401*, 273–294. https://doi.org/10.1002/andp.19314010303.

(24) Katona, G.; Szalay, G.; Maák, P.; Kaszás, A.; Veress, M.; Hillier, D.; Chiovini, B.; Vizi, E. S.; Roska, B.; Rózsa, B. *Nat. Methods* **2012**, *9*, 201. http://10.0.4.14/nmeth.1851

(25) Szalay, G.; Judák, L.; Katona, G.; Ócsai, K.; Juhász, G.; Veress, M.; Szadai, Z.; Fehér, A.; Tompa, T.; Chiovini, B.; Maák, P.; Rózsa, B. *Neuron* **2016**, *92* (4), 723–738. https://doi.org/10.1016/j.neuron.2016.10.002.

(26) Helmchen, F.; Denk, W. *Nat. Methods* **2005**, *2* (12), 932–940. https://doi.org/10.1038/nmeth818.

(27) Grienberger, C.; Konnerth, A. *Neuron* **2012**, *73* (5), 862–885.
https://doi.org/10.1016/j.neuron.2012.02.011.

(28) Ashley, C. C.; Ridgway, E. B. *Nature* **1968**, *219* (5159), 1168–1169.
https://doi.org/10.1038/2191168a0.

(29) Shimomura, O.; Johnson, F. H.; Saiga, Y. *J. Cell. Comp. Physiol.* **1962**, *59* (3), 223–239. https://doi.org/10.1002/jcp.1030590302.

(30) *IUPAC Compend. Chem. Terminol.* **1994**, *1077*, 2014.
https://doi.org/10.1351/goldbook.C01012.

(31) Schwarzenbach, G. *Helv. Chim. Acta* **1952**, *35* (7), 2344–2359.
https://doi.org/10.1002/hlca.19520350721.

(32) Richey, W. D. *Stud. Conserv.* **1975**, *20* (sup1), 229–234.
https://doi.org/10.1179/sic.1975.s1.038.

(33) Montavon, G.; Le Du, A.; Champion, J.; Rabung, T.; Morgenstern, A. *Dalt. Trans.* **2012**, *41* (28), 8615–8623. https://doi.org/10.1039/c2dt30230f.

(34) Twedt, D. C. *Canine Feline Gastroenterol.* **2013**, 489–493.
https://doi.org/10.1016/B978-1-4160-3661-6.00043-2.

(35) Crea, F.; De Stefano, C.; Gianguzza, A.; Piazzese, D.; Sammartano, S. *Chem. Speciat. Bioavailab.* **2003**, *15* (3), 75–86. https://doi.org/10.3184/095422903782775190.

(36) Pinto, I. S. S.; Neto, I. F. F.; Soares, H. M. V. M. *Environ. Sci. Pollut. Res.* **2014**, *21* (20), 11893–11906. https://doi.org/10.1007/s11356-014-2592-6.

(37) Mihucz, V. G.; Csog, Á.; Fodor, F.; Tatár, E.; Szoboszlai, N.; Silaghi-Dumitrescu, L.; Záray, G. *J. Plant Physiol.* **2012**, *169* (6), 561–566.
https://doi.org/10.1016/j.jplph.2011.12.012.

(38) Evangelou, M. W. H.; Ebel, M.; Schaeffer, A. *Chemosphere* **2007**, *68* (6), 989–1003.
https://doi.org/10.1016/j.chemosphere.2007.01.062.

(39) Wandell, R. J.; Younes, A. H.; Zhu, L. *New J. Chem.* **2010**, *34* (10), 2176–2182.
https://doi.org/10.1039/c0nj00241k.

(40) Lakowicz, J. R.; Masters, B. R. *Principles of Fluorescence Spectroscopy, Third Edition*; 2008. https://doi.org/10.1117/1.2904580.

(41)   Feng, G.; Du, Y. *Anal. Lett.* **2020**, *53* (1), 40–52.
         https://doi.org/10.1080/00032719.2019.1636258.

(42)   Förster, T. *Ann. Phys.* **1948**, *437* (1–2), 55–75.
         https://doi.org/https://doi.org/10.1002/andp.19484370105.

(43)   Marx, V. *Nat. Methods* **2017**, *14* (10), 949–953. https://doi.org/10.1038/nmeth.4434.

(44)   FLETCHER, A. N. *Photochem. Photobiol.* **1969**, *9* (5), 439–444.
         https://doi.org/10.1111/j.1751-1097.1969.tb07311.x.

(45)   Kim, A.; Lee, H.; Yun, D.; Jung, U.; Kim, K. T.; Kim, C. *Spectrochim. Acta - Part A
         Mol. Biomol. Spectrosc.* **2020**, *241*, 118652.
         https://doi.org/10.1016/j.saa.2020.118652.

(46)   Zhou, X.; Yu, B.; Guo, Y.; Tang, X.; Zhang, H.; Liu, W. *Inorg. Chem.* **2010**, *49* (9),
         4002–4007. https://doi.org/10.1021/ic901354x.

(47)   Fu, H.; Liu, H.; Zhao, L.; Xiao, B.; Fan, T.; Jiang, Y. *Tetrahedron* **2019**, *75* (49),
         130710. https://doi.org/10.1016/j.tet.2019.130710.

(48)   Zhang, Y.; Guo, X.; Si, W.; Jia, L.; Qian, X. *Org. Lett.* **2008**, *10* (3), 473–476.
         https://doi.org/10.1021/ol702869w.

(49)   Nolan, E. M.; Jaworski, J.; Okamoto, K. I.; Hayashi, Y.; Sheng, M.; Lippard, S. J. *J.
         Am. Chem. Soc.* **2005**, *127* (48), 16812–16823. https://doi.org/10.1021/ja052184t.

(50)   *United States Pharmacopeia XIX, p. 203.*

(51)   Prachayasittikul, V.; Prachayasittikul, S.; Ruchirawat, S.; Prachayasittikul, V. *Drug
         Des. Devel. Ther.* **2013**, *7*, 1157–1178. https://doi.org/10.2147/DDDT.S49763.

(52)   Pearce, D. A.; Jotterand, N.; Carrico, I. S.; Imperiali, B. **2001**, 5160–5161.

(53)   Xu, Z.; Yoon, J.; Spring, D. R. *Chem. Soc. Rev.* **2010**, *39* (6), 1996–2006.
         https://doi.org/10.1039/b916287a.

(54)   Nolan, E. M.; Lippard, S. J. *Acc. Chem. Res.* **2009**, *42* (1), 193–203.
         https://doi.org/10.1002/chin.200917278.

(55)   Burdette, S. C.; Walkup, G. K.; Spingler, B.; Tsien, R. Y.; Lippard, S. J. *J. Am. Chem.
         Soc.* **2001**, *123* (32), 7831–7841. https://doi.org/10.1021/ja010059l.

(56)   Walkup, G. K.; Burdette, S. C.; Lippard, S. J.; Tsien, R. Y. *J. Am. Chem. Soc.* **2000**, *122* (23), 5644–5645. https://doi.org/10.1021/ja000868p.

(57)   Tsien, R. Y. *Biochemistry* **1980**, *19* (11), 2396–2404.

http://doi.org/10.1021/bi00552a018

(58)   Stability constants of metal chelates https://www.dojindo.com/Images/Product Photo/Chelate_Table_of_Stability_Constants.pdf.

(59)   Xu, Y.; Zhou, Y.; Ma, W.; Wang, S. *J. Nanomater.* **2013**, *2013*. https://doi.org/10.1155/2013/178138.

(60)   Liu, T.; Liu, S. *Anal. Chem.* **2011**, *83* (7), 2775–2785. https://doi.org/10.1021/ac200095f.

(61)   Prendergast, F. G.; Mann, K. G. *Biochemistry* **1978**, *17* (17), 3448–3453. https://doi.org/10.1021/bi00610a004.

(62)   Tsien, R. Y. *Annu. Rev. Biochem.* **1998**, *67*, 509–544. https://doi.org/10.1146/annurev.biochem.67.1.509.

(63)   Phillips, G. J. *FEMS Microbiol. Lett.* **2001**, *204* (1), 9–18. https://doi.org/10.1016/S0378-1097(01)00358-5.

(64)   Scott, D. J.; Gunn, N. J.; Yong, K. J.; Wimmer, V. C.; Veldhuis, N. A.; Challis, L. M.; Haidar, M.; Petrou, S.; Bathgate, R. A. D.; Griffin, M. D. W. *Sci. Rep.* **2018**, *8* (1), 1–15. https://doi.org/10.1038/s41598-017-18045-y.

(65)   Kadry, A. M. *J. Heterocycl. Chem.* **1985**, *22* (1), 155–157. https://doi.org/10.1002/jhet.5570220138.

(66)   Daboun, H. A.; Ibrahim, Y. A. *J. Heterocycl. Chem.* **1982**, *19* (1), 41–43. https://doi.org/10.1002/jhet.5570190105.

(67)   Gaussian 16, Revision C.01, M. J. Frisch, G. W. Trucks, H. B. Schlegel, G. E. Scuseria, M. A. Robb, J. R. Cheeseman, G. Scalmani, V. Barone, G. A. Petersson, H. Nakatsuji, X. Li, M. Caricato, A. V. Marenich, J. Bloino, B. G. Janesko, R. Gomperts, B. Mennucci, H. P. Hratchian, J. V. Ortiz, A. F. Izmaylov, J. L. Sonnenberg, D. Williams-Young, F. Ding, F. Lipparini, F. Egidi, J. Goings, B. Peng, A. Petrone, T. Henderson, D. Ranasinghe, V. G. Zakrzewski, J. Gao, N. Rega, G. Zheng, W. Liang,

M. Hada, M. Ehara, K. Toyota, R. Fukuda, J. Hasegawa, M. Ishida, T. Nakajima, Y. Honda, O. Kitao, H. Nakai, T. Vreven, K. Throssell, J. A. Montgomery, Jr., J. E. Peralta, F. Ogliaro, M. J. Bearpark, J. J. Heyd, E. N. Brothers, K. N. Kudin, V. N. Staroverov, T. A. Keith, R. Kobayashi, J. Normand, K. Raghavachari, A. P. Rendell, J. C. Burant, S. S. Iyengar, J. Tomasi, M. Cossi, J. M. Millam, M. Klene, C. Adamo, R. Cammi, J. W. Ochterski, R. L. Martin, K. Morokuma, O. Farkas, J. B. Foresman, and D. J. Fox, Gaussian, Inc., Wallingford CT, 2016.

(68)   Zhao, Y.; Truhlar, D. G. *Theor. Chem. Acc.* **2008**, *120* (1–3), 215–241. https://doi.org/10.1007/s00214-007-0310-x.

(69)   Petit, M.; Tran, C.; Roger, T.; Gallavardin, T.; Dhimane, H.; Palma-Cerda, F.; Blanchard-Desce, M.; Acher, F. C.; Ogden, D.; Dalko, P. I. *Org. Lett.* **2012**, *14* (24), 6366–6369. https://doi.org/10.1021/ol3031704.

(70)   Thierig, D.; Umland, F. *Naturwissenschaften* **1967**, *54* (21), 563. https://doi.org/10.1007/BF00602336.

(71)   Lennox, A. J. J. In *Organotrifluoroborate Preparation, Coupling and Hydrolysis*; 2013; pp 11–36. https://doi.org/10.1007/978-3-319-01134-9_2.

(72)   Kim, H. M.; Seo, M. S.; An, M. J.; Hong, J. H.; Tian, Y. S.; Choi, J. H.; Kwon, O.; Lee, K. J.; Cho, B. R. *Angew. Chemie Int. Ed.* **2008**, *47* (28), 5167–5170. https://doi.org/https://doi.org/10.1002/anie.200800929.